Quality assurance of CT scanning for industrial applications

Angel, Jais Andreas Breusch

Publication date:
2014

Document Version
Publisher's PDF, also known as Version of record

Quality assurance of CT scanning for industrial applications

by

Jais Andreas Breusch Angel

For fulfillment of the degree

Philosophiae Doctor

Department of Mechanical Engineering

Technical University of Denmark

March 2014

This Ph.D. thesis is dedicated to my family, friends and colleagues.

Preface and acknowledgements

This thesis has been completed as one of the requirements of the Ph.D. degree.

This Ph.D. thesis was financed by the Technical University of Denmark (DTU) and the Danish project CIA-CT: Centre for Industrial Application of CT scanning. The work was carried out from August 2010 to March 2014 at the Department of Mechanical Engineering (DTU MEK) under the supervision of Professor Leonardo De Chiffre, Professor Hans Nørgaard Hansen and Dr. Angela Cantatore. Three months, September-December 2012, were spent at the Katholieke Universiteit Leuven (KUL), Belgium under the supervision of Professor Jean-Pierre Kruth and Professor Wim Dewulf.

First of all, I would like to thank all my supervisors for the possibility to work with this project. The discussions, contributions, work and support from the supervisors are gratefully acknowledged.

The participation of the following organisations is gratefully acknowledged in the ”Interlaboratory comparisons on CT scanners for industrial applications in the manufacturing industry”: 3D-CT A/S (DK), BAM Federal institute for materials research and testing (DE), Braun GmbH (DE), Carl Zeiss IMT GmbH (DE), Danish Technological Institute (DK), Fraunhofer Development Center for X-ray Technology (DE), Zebicon A/S (DK), GRUNDFOS A/S (DK), Hexagon Metrology Inc. (US), Huddersfield University (UK), FMT Institute of Manufacturing Metrology Friedrich-Alexander-University Erlangen-Nuremberg (DE), Katholieke Universiteit Leuven (BE), LEGO System A/S (DK), AIST National Institute of Advanced Industrial Science and Technology (JP), NPL National Physical Laboratory (UK), Nikon Metrology (UK), Novo Nordisk A/S Device R&D (DK), Novo Nordisk A/S DMS Metrology & Calibration (DK), SGS Institut Fregenius GmbH (DE), SIMTech (SGP), UNCC Center for Precision Metrology (USA), University of Padova (IT), University of Southampton (UK), Wenzel Volumetrik GmbH (DE), Werth Messtechnik GmbH (DE), IPK Fraunhofer-Institut für Produktionsanlagen und Konstruktionstechnik (DE), YXLON International GmbH (DE).

The participation of the following organisations is gratefully acknowledged in the ”Interlaboratory comparison on CT scanners for industrial applications in the meat processing industry”: DMRI Danish Meat Research Institute (DK), IFIP-Institut du Porc (FR), MRI - Department of Safety and Quality of Meat (DE), SIC Egészségügyi Centruma (HU).

Then, I want to thank the staff at DTU MEK and IPU, namely Mr. Jakob Rasmussen, Mr. Erik Larsen and Mr. René Sobiecki in connection with all kinds of dimensional measurements and for valuable discussions on metrological topics. My colleagues at the

department, Chris Valentin Nielsen, Ermanno Ceron, Alessandro Godi, Pavel Müller, Peter Søe Nielsen and Alessandro Stolfi, are also acknowledged for their friendship.

I would like to thank all the partners of the CIA-CT project, mainly IPU, Danish Meat Research Institute (DMRI), Niels Bohr Institute (NBI), Novo Nordisk A/S, LEGO System A/S and Danish Technological Institute (DTI) for their support. In particular I thank Dr. Lars Bager Christensen, Mr. Peder Pedersen, Mr. Torsten Lauridsen, Professor Robert Feidenhans'l and Mr. Mikkel S. Nielsen for their valuable contributions and discussions.

Furthermore, I would like to express my gratitude to the colleagues at KUL. Especially to Mr. Frank Welkenhuyzen, Ms. Kim Kiekens, Mr. Tan Ye and Mr. Bart Boeckmans for their hospitality and inspiration to my research activities. A chapter of this Ph.D. thesis with the title: "Performance enhancement and characterization on a CT system using step gauges" has been carried out in collaboration with KUL. Special thanks go to Mr. Christophe Vandenhoeck and Mr. Karel Deputter for carrying out the CT scans.

I would like to thank Lyngby Taarbæk Kommune and Tegnsprogstolken.dk for their support and the possibility to bring along interpreters abroad during the Ph.D. progress.

I will thank following foundations for their financial contributions for traveling: Myhrwolds Fond, Fabrikant P.A.Fiskers Fond, and H. P. Christensens Fond.

Last I will thank my family and my friends for their support throughout my Ph.D. work at DTU.

Kongens Lyngby, March 2014

Jais Andreas Breusch Angel

Abstract

X-ray computed tomography (CT) gives major possibilities by looking through the industrial parts with complex geometries, but one of the largest challenges is the quality assurance of measurements. This Ph.D. project at DTU Mechanical Engineering deals with the development of procedures for quality assurance of CT for industrial measurements both in the manufacturing and in the meat processing industries. Various methods and reference objects have been developed in this project to establish metrological traceability of measurements. Moreover investigations as well as international comparisons in the field of application on the two different areas have been carried out.

Different reference objects have been developed and introduced for the manufacturing industry: step gauge, step cylinder and a cylindrical multi-material assembly. These objects can be used for correction of measurement errors in the CT model. Moreover, two reference objects are calibrated objects from the manufacturing industry: a threaded tube from the medical industry and a LEGO brick from the toy industry. Establishment of traceability for all objects is performed using coordinate measuring machines (CMMs) with known uncertainty. The stability has been documented for all reference objects except for the step cylinder and the cylindrical multi-material assembly.

A design of experiment (DOE) was performed on measuring errors arising in a CT, in terms of material density and orientation of scanned step gauges. An analysis of variance (ANOVA) shows that all main factors and their interactions are significant. The maximum deviation from the reference value can be reduced by compensating for systematic errors, but it is more complicated to correct for vertical orientations in high density materials.

In an interlaboratory comparison involving 27 laboratories from 8 countries, measurements were carried out using CT on two common objects from the manufacturing industry, a threaded tube and a LEGO brick. The comparison has shown that CT measurements on the industrial parts used lie in the range 6-53 µm, with maximum values up to 158 µm, compared to average uncertainties below 5.5 µm using CMMs.

A test was performed to check if X-ray contrast modalities can be applied for metrological purposes. Traditionally, segmentation between multi-materials in CT scanning is done by using different edge detection techniques and threshold algorithms, but these are only available for multi-materials where the densities are not close to each other. X-ray contrast modalities overcome this problem by constructing dark field, phase contrast and transmission images. Measurement results show that further development related to stability issues on the used CT is needed to create a metrological tool using X-ray contrast modalities.

Two synthetic reference phantoms have been developed by Danish Meat Research Institute (DMRI) and introduced for the meat processing industry. The phantoms represent real pig carcasses and are made of several polymer components, representing tissue types such as lean meat, fat, and bone. Establishment of traceable volume measurements for the phantoms is performed using the gravimetric method (also called water displacement). The stability has been documented for the two phantoms.

For the meat processing industry concerned, a similar interlaboratory comparison using two reference phantoms from the meat processing industry was carried out using CT, and involved four laboratories from 4 countries. The comparison has shown that CT measurements on the phantoms used lie in the range 1-1090 mL, with maximum values up to 1348 mL, compared to average uncertainties below 10 mL using the gravimetric method.

DMRI and DTU Compute have previously developed advanced image analysis software (PigClassWeb) which performs virtual dissections in pig carcasses. A DOE was carried out to document the performance of PigClassWeb through volume comparisons to real dissections of pig carcasses. For the real dissections, volumes of tissue types such as bone, lean meat and fat, are estimated using commercial VolumeGraphics software. It is detected that the ANOVA and the residuals from the virtual dissection fail the normality test. The reason can be that the simulation data has special problems and challenges which are difficult to overcome by using current regression software.

Resumé (DANSK)

Røntgen computer-tomografi (CT) giver store muligheder, ved at se igennem industrielle emner med komplekse geometrier, men en af de største udfordringer er kvalitetssikringen af målingerne. Dette ph.d. projekt ved DTU Mekanik omhandler udvikling af procedurer for kvalitetssikring af CT til industrielle målinger i fremstillings- og kødforarbejdningsindustrien. Forskellige metoder og reference objekter er blevet udviklet i dette projekt for at etablere måleteknisk sporbarhed af målinger. Endvidere er undersøgelser og internationale sammenligninger udført indenfor de to forskellige anvendelsesområder.

Forskellige reference objekter er blevet udviklet til brug i fremstillingsindustrien: trin sporvidde, trin cylinder og en cylindrisk multi-materiale forsamling. Disse objekter kan bruges til korrektion af målefejl i CT modellen. Desuden er to reference objekter kalibrerede objekter fra fremstillingsindustrien: et gevind rør fra medicinindustrien og en LEGO klods fra legetøjsindustrien. Etablering af sporbarhed for alle objekter er udført ved hjælp af koordinat målemaskiner (KMM) med kendt usikkerhed. Stabiliteten er blevet dokumenteret for alle referenceobjekter, bortset fra trin cylinderen og den cylindriske multi-materiale forsamling.

Et design af eksperiment (DOE) er udført på målefejl, der opstår i et CT system i form af massefylde og placering af scannede trin gauges. Variansanalysen (ANOVA) viser, at alle de vigtigste faktorer og deres samspil er væsentlige. Den maksimale afvigelse fra referenceværdien kan reduceres ved at kompensere for systematiske fejl, såsom skala fejlkorrektion og tærskel forskydninger, men det er mere kompliceret at korrigere for lodrette positioner i materialer med en høj massefylde.

I en præstationsprøvning, der involverer 27 laboratorier fra 8 lande, blev målingerne foretaget ved hjælp af CT på to almindelige genstande fra fremstillingsindustrien, et rør med gevind og en LEGO klods. Sammenligningen har vist, at CT måleusikkerheder på de industrielle dele, der anvendes ligger i intervallet 6-53 µm, med maksimale værdier op til 158 µm, sammenlignet med gennemsnitsusikkerheder under 5,5 µm ved hjælp af KMM.

En test er udført for at kontrollere, om røntgen kontrast modaliteter kan anvendes til metrologiske formål. Traditionelt foretages segmentering mellem multi-materialer i CT skanning ved hjælp af forskellige kant sporingsteknikker og tærskel algoritmer, men disse er kun tilgængelig for multi-materialer, hvor massefylderne ikke ligger tæt op ad hinanden. Røntgenkontrast modaliteter overvinder dette problem ved at konstruere mørke felt, fasekontrast og transmission billeder. Måleresultaterne viser, at der er behov for yderligere udvikling relateret til stabiliteten på den anvendte CT skanner for at skabe et metrologisk værktøj ved hjælp af røntgenkontrast modaliteter.

To syntetiske fantomer er udviklet af Slagteriernes Forskningsinstitut (DMRI) til brug i kødforarbejdningsindustrien. Fantomerne repræsenterer reelle svinekroppe og er lavet af flere polymerkomponenter, der repræsenterer vævstyper såsom magert kød, fedt og knogler. Etablering af sporbare volumen målinger for fantomerne udføres ved hjælp af den gravimetriske metode (også kaldet fortrængningsmetoden af vand). Stabiliteten er blevet dokumenteret for de to fantomer.

For kødforarbejdningsindustriens vedkommende blev en lignende præstationsprøvning vha. CT udfærdiget på to fantomer fra kødforarbejdningsindustrien, og involverede 4 laboratorier fra 4 lande. Sammenligningen har vist, at CT måleusikkerheder på de fantomer, der anvendes ligger i intervallet 1-1090 mL, med maksimale værdier op til 1348 mL, sammenlignet med gennemsnitsusikkerheder under 10 mL ved hjælp af den gravimetriske metode.

DMRI og DTU Compute har tidligere udviklet avanceret billedanalyse software (PigClassWeb), som udfører virtuelle dissekeringer i svinekroppe. En DOE blev udført for at dokumentere kvaliteten af PigClassWeb via volumen sammenligninger med reelle dissekeringer af slagtede svin. For de reelle dissekeringer, er volumen skøn over vævstyper såsom knogle, magert kød og fedt, estimeret ved hjælp af kommercielt VolumeGraphics software. Det er registreret, at ANOVA'en og residualerne fra den virtuelle dissekering dumpede normalitetstesten. Årsagen kan være, at simulering af data har særlige problemer og udfordringer, der er vanskelige at overvinde ved hjælp af nuværende regression software.

Contents

Nomenclature

Some of the most commonly used abbreviations and interchangeable terms are listed below.

AD	Anderson-Darling statistic (lower AD values indicate a better fit)
ANOVA	Analysis of variance
CGM	Centre for Geometrical Metrology
CIA-CT	Center for Industrial Application of CT scanning
CMM	Coordinate Measuring Machine
CT	Computed Tomography
df	Degree of freedom
DMRI	Danish Meat Research Institute
DOE	Design of experiment
DTI	Danish Technological Institute
DTU	Technical University of Denmark
F-value	Ratio of two mean squares (treatment mean square/error mean square)
G_0	Source grating
G_1	Phase grating
G_2	Analyzer absorption grating
GBI	Grating-interferometer Based Imaging
GUM	Guide to the expression of uncertainty in measurement
ID	Inner diameter
KUL	Katholieke Universiteit Leuven
MCE	Minimum Circumscribed Element
Mean	Average
MIE	Maximum Inscribed Element
MPE	Maximum Permissible Error
MS	Mean square
N	Sample size
NBI	Niels Bohr Institute
NDT	Non-destructive-testing

NPL	National Physical Laboratory
OD	Outer diameter
PA	Polyamide
PEEK	Polyetheretherketone
PMMA	Poly methyl methacrylate
POM	Polyoxymethylene
PPS	Polyp-phenylenesulphide
PUMA	Procedure for uncertainty management
P-value	Statistically significant value
PVC	Polyvinyl chloride
RND	Number of measurement round
SC	Step cylinder
SG	Step gauge
SS	Sum of squares
StDev	Standard deviation
STL	STereoLithography surface geometry of a three dimensional object

Explanation of symbols

Some of the most commonly used symbols are listed below.

a	Linear regression coefficient
b	Edge correction offset
d	The m^{th} fractional Talbot
E_n	E_n value normalised with respect to the estimated uncertainty, computed according to ISO 17043 guidelines
G_0	Source grating
G_1	Phase grating
G_2	Analyzer absorption grating
I	Current
k	Coverage factor (k=2 for a coverage probability of 95 %)
L	The distance between G_0 and G_1
L_{CMM}	Distance measured by traceable instruments such as tactile CMMs
L_{CTcor}	CT data after correction
$L_{CTuncor}$	CT data before correction
m	Geometrical magnification
M	The selected Talbot number
p	Detector pixel size
P	Power
Ra	Arithmetical mean deviation
Rz	Max height
s	Voxel size
s_{vox}	Correction factor
SDD	Source-detector distance
SOD	Source-object distance
U	Expanded uncertainty
U	Voltage
u_a	Uncertainty, water absorption for object
U_{after}	Uncertainty obtained after
U_{before}	Uncertainty obtained before

u_c	Combined standard uncertainty
u_e	Uncertainty, temperature effects
$u_{e(1)}$	Temperature difference between workpiece and instrument
$u_{e(2)}$	Temperature deviation from standard reference temperature for instrument
$u_{e(3)}$	Temperature deviation from standard reference temperature for workpiece
$u_{e(4)}$	Workpiece expansion coefficient uncertainty
$u_{e(5)}$	Component from measuring force
u_m	Uncertainty, MPE
u_p	Uncertainty, reproducibility
u_r	Uncertainty, reference artefact
u_r	Uncertainty, measuring weights
u_{rep}	Repeatability on reference artefact
u_{t1}	Temperature difference for instrument
u_{t2}	Temperature difference for artefact
u_{t3}	Temperature deviation from the standard reference temperature
u_w	Uncertainty, workpiece form error
u_w	Uncertainty, technical weight
x_{after}	Measurement obtained after
x_{before}	Measurement obtained before
$\bar{y}$	Actual value
Y	Measurement result
δ	Other error sources such as physical phenomenons and/or reconstruction algorithms
λ	Wavelength

Chapter 1 Introduction

This chapter presents the need for X-ray Computed Tomography (CT) in the industry in which CT gives major possibilities by looking through the industrial parts with complex geometries. This non-destructive-testing (NDT) technique is becoming widely used for industrial measurements in the manufacturing industry and the meat processing industry although the field of application in the manufacturing industry is different compared to the one in the meat processing industry. But the evaluation of the measurement uncertainty with assessment of all influential contributors and error sources constitutes a challenge with respect to the establishment of traceability and quality assurance of industrial measurements. Additionally a short description is carried out of the CIA-CT project of which this Ph.D. project was a part, and then the chapter is completed with a problem identification and project structure.

1.1 Background and need of CT scanning for industrial applications

Originally X-ray Computed Tomography (CT) was developed for medical imaging by Hounsfield in 1969 [1] and is mostly known from the hospitals, where it acts as a clinical CT. This technique makes it possible for the doctor to scan the patient and inspect the organs. Since 1980, CT became popular for material analysis and non-destructive-testing (NDT), such as inspecting inner material structures and detecting material defects [2]. The first dedicated dimensional CT machine came in 2005, and has an unique advantage compared to other NDT measuring methods, since it is possible for the engineer or scientist to inspect and measure inner geometries, which consist of high geometrical complexity [3]. An overview of the application area in relation to the location of defects of the different NDT techniques, as well as the application area in relation to the geometrical complexity can be seen in Figure 1.1.

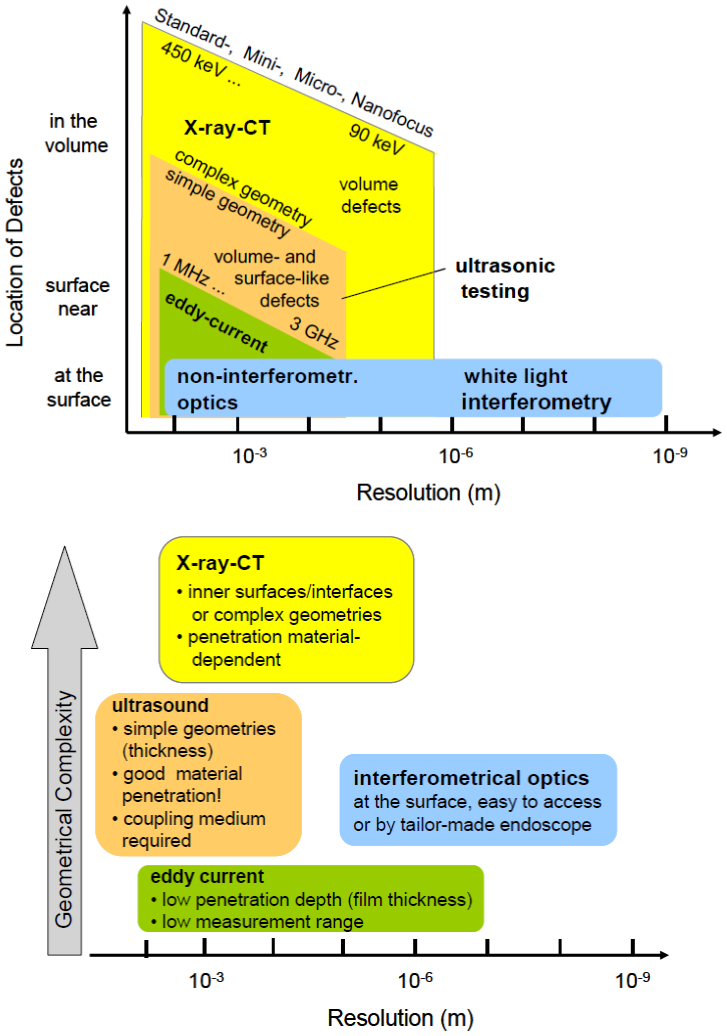

Figure 1.1. Top: Classification and comparison of the different NDT techniques depending on the location of defects. Bottom: Classification and comparison of the different NDT techniques depending on the geometrical complexity **[3]**.

At present CT is becoming widely used for industrial measurements in the industry, but the evaluation of the measurement uncertainty with assessment of all influential contributors and error sources constitutes a challenge with respect to the establishment of traceability and quality assurance of industrial measurements. Additionally many standardized procedures are still under development which means that the traceability of CT cannot be ensured. This Ph.D. project deals with the development of procedures for quality assurance of CT for industrial measurements both in the manufacturing and in the meat processing industries although the field of application in the manufacturing industry is different compared to the one in the meat processing industry. These differences in the fields of the two scopes have been divided into following subtopics: the background, principles and construction of used CT systems, and need of CT scanning.

In general a CT for industrial applications in the manufacturing industry consists of the following components: a X-ray source, a X-ray detector, kinematic systems, reconstruction software, edge detection software and analysis software. The basic construction of a CT for dimensional metrology used in the manufacturing industry is shown in Figure 1.2 where the scanned object is fixed on a rotary table. There are two generations of CT which consists of either 1) a fan beam and a single slice detector or 2) a cone beam and a flat panel detector, in which the last one is most applied [4].

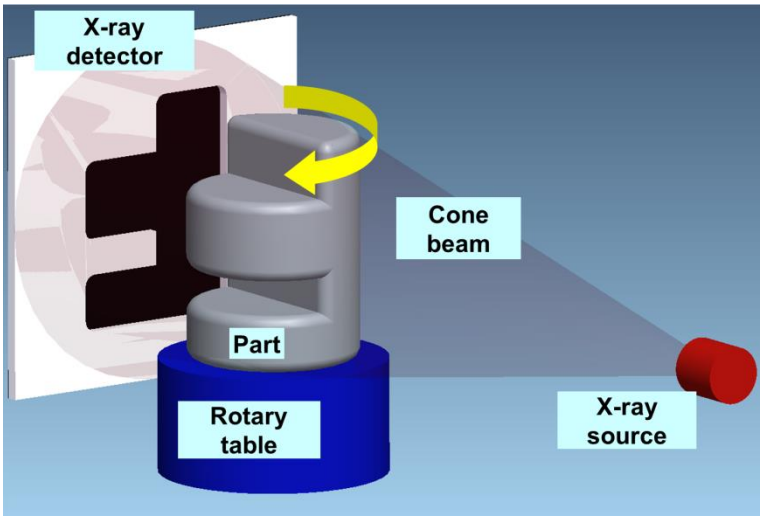

Figure 1.2. The construction of a dimensional metrology CT used in the manufacturing industry, where the table is rotating. Sizes are not to scale.

The process chain in CT is as follows in which the CT uses the ability of X-rays to penetrate the scanned object, where the X-rays attenuate when they penetrate the object. The amount of attenuation depends on material density and geometry in which a higher degree of attenuation of the X-rays is obtained with increasing thickness and higher density. In the attenuation phase some of the X-rays are scattered, absorbed or transmitted and thereafter a detector registers the X-rays and creates a 2D grey image. This process is repeated several times using kinematic systems which results in a stack of images which is transferred to a reconstructed 3D model using reconstruction software. Subsequently the segmentation between object and background is carried out using the threshold value (also called surface determination). This reconstructed 3D model can be exported in two ways: 1) as volume data (voxels also called 3D pixels) or 2) triangulated surface data (STL), but converting files to STL results in voxel information being lost [5]. And finally the CT measurements and analyses can be achieved and compared to nominal data or reference measurements. A flow chart which sums up the process chain is shown in Figure 1.3.

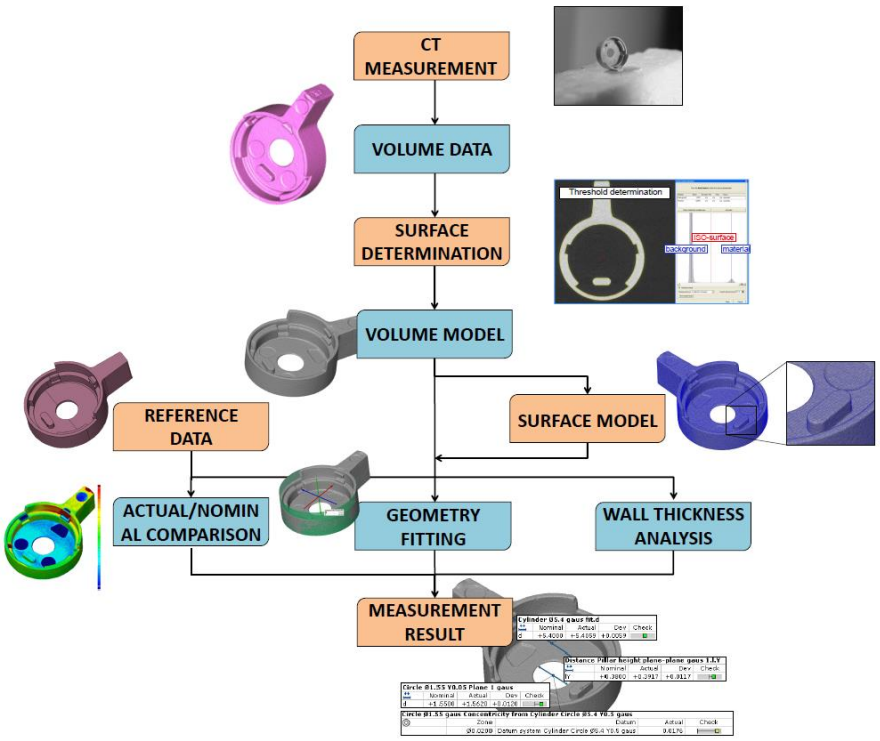

Figure 1.3. A flow chart of a typical dimensional CT measurement process in the manufacturing industry **[6]**.

Today, the manufacturing of a product has largely become an automated process in the manufacturing industry. In the production chain, quality assurance is a key parameter and demands for a high and automated quality check are more and more pressing. In-line analysis, inspection and quality assurance close to the process based on an automated in-line control is a way to ensure fast and efficient feedback during the manufacturing process, which results in cost savings and improved competitiveness. CT is considered as a solution to be implemented in the automated in-line control. This technology is well suited to perform tolerance verification on components which are often complex or to carry out inspection of assemblies. The advantage of using CT in the manufacturing industry is that it can inspect faults (e.g. assemblies, sink marks, cracks and inner defects) and measure complex inner geometries. But the evaluation of the measurement uncertainty with assessment of all influential contributors and error sources constitutes a challenge with respect to the establishment of traceability and quality assurance of CT measurements. Examples of CT scanners for industrial applications in the manufacturing industry can be seen in Figure 1.4. An overview of some CT applications in the manufacturing industry is shown in Figure 1.5, and an example of an in-line CT system for inspection of castings in the manufacturing industry is shown in Figure 1.6.

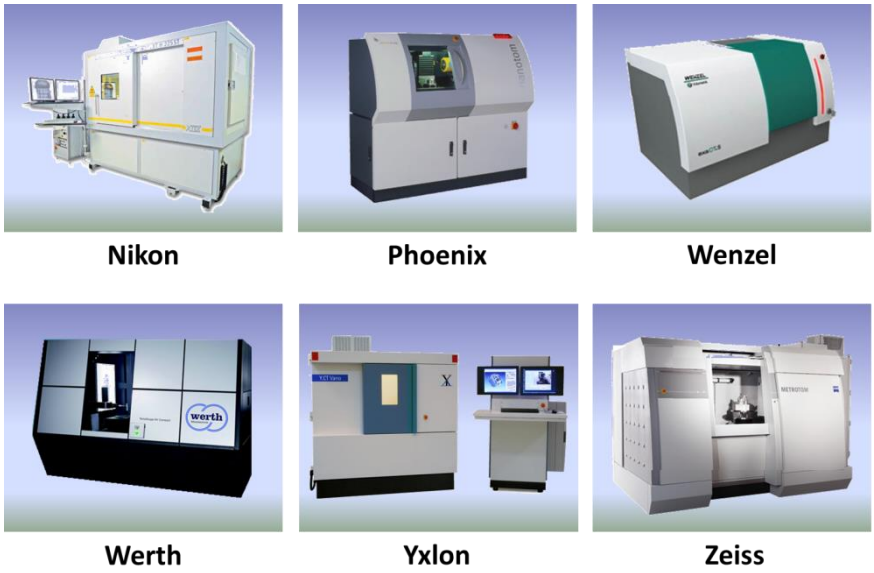

Figure 1.4. Examples of some CT scanners for industrial applications in the manufacturing industry. Sizes are not to scale.

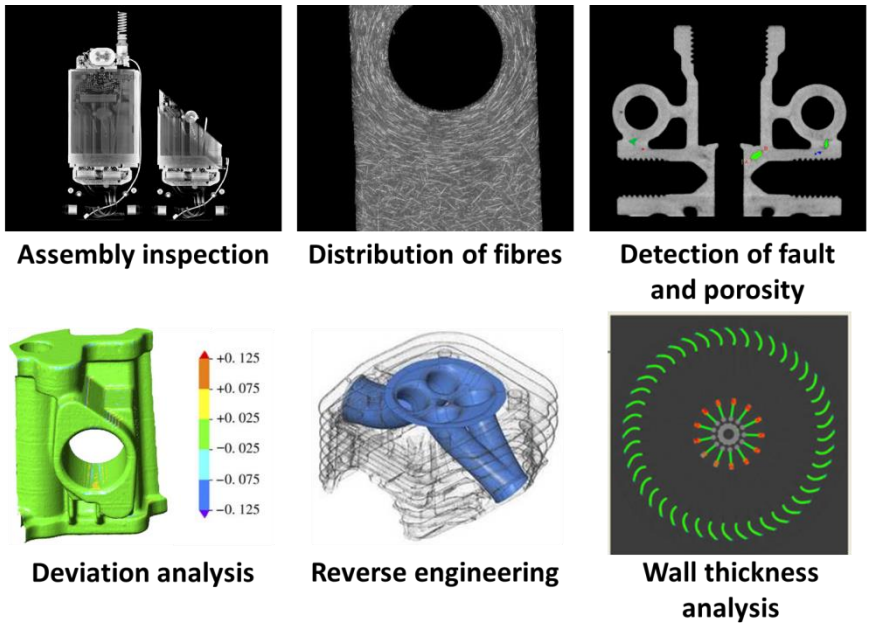

Figure 1.5. An overview of some CT applications in the manufacturing industry. Sizes are not to scale. From top left to right bottom: Assembly inspection of Mobile Phone **[7]**, visualization of the distribution of fibres in glass-fibre reinforced injection molded parts **[8]**, detection of fault and porosity in an aluminium casted part **[9]**, deviation analysis of an industrial test object **[10]**, reverse engineering of cylinder head **[11]**, and wall thickness analysis of a car inlet fan **[2]**.

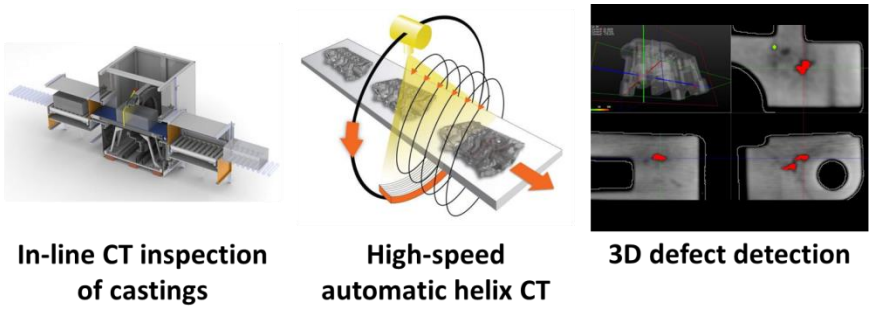

Figure 1.6. Example of fast in-line CT inspection of castings **[12]**. From left to right: In-line CT scanner is fitted with automatic conveyor equipment and encased in a radiation protection cabinet for industrial use, a gantry with an X-ray tube and corresponding multi-line detector rotates around the workpieces on a conveyor belt, for 3D defect detection and evaluation analysis.

The field of the meat processing industry differs from the one in the manufacturing industry. The applied CT scanners in the meat processing industry are similar to the ones from the hospitals (so-called clinical CT). This is due to the size, shape and density of the scanned biological artefacts, in which the main focus is set on volume estimations of the biological products. The basic construction of a clinical CT used in the meat processing industry is shown in Figure 1.7 where the detector and X-ray source are continuously rotated around the object to obtain tomographic images representing slices of the scanned object. The measurement process and considered challenges with respect to the establishment of traceability and quality assurance of CT measurements are more or less the same as the one used for dimensional metrology, only for volumes instead of geometrical measurands. Examples of some CT scanners for industrial applications in the meat processing industry are shown in Figure 1.8.

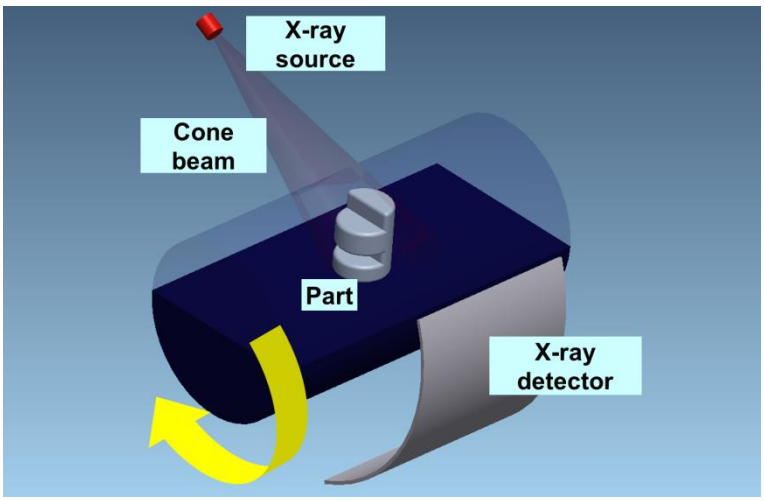

Figure 1.7. The construction of a clinical CT used in the meat processing industry, where the X-ray source and detector are rotating. Sizes are not to scale.

Figure 1.8. Examples of some CT scanners for industrial applications in the meat processing industry. Sizes are not to scale.

The meat industry recognizes that a more efficient use of the raw materials is one of the largest and most important challenges. Today the dissection is made through an expensive manual dissection of a large batch of carcasses. CT is considered as an online system for measuring lean meat and fat distribution in pig carcasses. Using CT scanning, it would be possible to make the dissection process automated (an example of an automated cutting line in the slaughterhouses is shown in Figure 1.9), with reduction of time and costs, in which precise dissections can be performed due to the contents of the expensive meat. Overviews of some CT applications in the meat processing industry are shown in Figure 1.10.

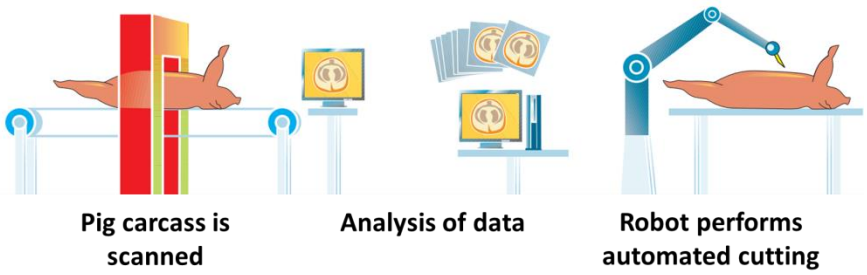

Figure 1.9. Example of an automated cutting line of pig carcasses in the meat processing industry. From left to right: The pig carcass is scanned, analysis of data and an optimal cutting is calculated, and based on the calculations a robot will perform the automated cutting of the pig carcass **[13]**.

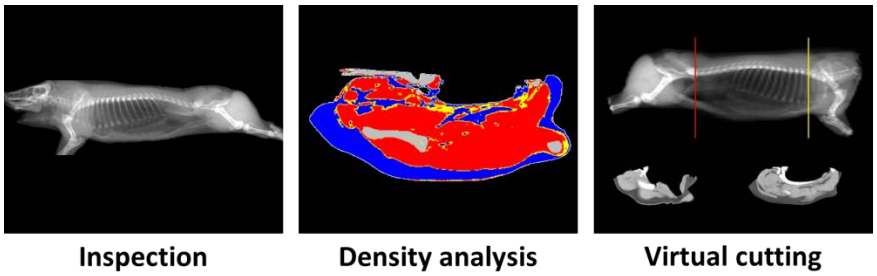

Figure 1.10. An overview of some CT applications in the meat processing industry. Sizes are not to scale. From left to right: Inspection of 2D-view of half a pig carcass generated from a 3D CT volume **[14]**, density analysis of different materials in a shoulder from a pig carcass (yellow = PVE, grey = bone, red = meat, blue = fat, and black = background) **[15]**, and virtual cutting of scanned pig carcass **[16]**.

1.2 Center for Industrial Application of CT scanning (CIA-CT project)

This Ph.D. project at Department of Mechanical Engineering, Technical University of Denmark (DTU MEK) was a part of the project "Center for Industrial Application of CT scanning - CIA-CT" (http://www.cia-ct.mek.dtu.dk/), co-financed by the Danish Ministry of Science, Technology and Innovation. The main activities focused on industrial applications of CT scanning, quality assurance and product development. The project started in September 2009 and finished in August 2013, and consisted of five major research projects: 1) CT scanning for coordinate metrology, 2) Data processing for high speed scanning, 3) New beam sources and signal conditioning, 4) Equipment with high stability beam source, and 5) Quality assurance and automation. This Ph.D. project was a part of subproject 1 and 5 carried out in collaboration with IPU, DMRI, NBI, Novo Nordisk A/S, LEGO System A/S, DTI and KUL.

1.3 Problem statement

Evaluation of measurement uncertainty in CT with assessment of all influential contributors and error sources has become a most important challenge related to the establishment of traceability, because many standardized procedures are still under development. It means that the traceability of CT cannot be ensured. Based on these challenges, there is a need for developing procedures for quality assurance of CT scanning for industrial measurements, and evaluating the metrological compatibility using CT scanning on components in the manufacturing industry and in the meat processing industry. In general it is more challenging to test industrial parts compared to reference objects dependent on precision, stability, form error, reproducibility, uncertainty and traceability. This Ph.D. thesis deals with quality assurance of CT scanning for industrial applications, and the work can be summarized as follows:

1. Development and testing of reference objects.
2. Test of the applicability of measurement on objects, commonly measured in the industry, which are more representative than conventional reference objects.
3. Establish metrological traceability of measurements, which can be achieved by documenting the reference measurements using instruments with known measurement uncertainty.
4. Accomplishment of comparisons that has aimed to collect information about measurement performance in state-of-the-art CT.
5. Evaluation of the impact of instrument settings and operator decisions.
6. Document and evaluate the performance of existing image analysis software used in CT.

1.4 Project structure

The structure of the Ph.D. thesis involves two parts according to the application field of CT: 1) the manufacturing industry and 2) the meat processing industry. The manufacturing industry is covered in Chapter 2-5, and the meat processing industry is presented in chapter 6-8.

Chapter 2 presents a brief state-of-the-art about reference objects, standards and guidelines relevant for CT used in manufacturing industry. Furthermore, a short description is given on some error sources in CT scanning such as scale errors, threshold offsets, beam hardening, cone beam artifacts and scattered radiation. The development of new reference objects and calibrated objects from manufacturing industry is presented. The calibrated objects are considered more relevant for industrial measurements, in terms of materials, dimensions and geometrical properties, but their use poses a number of challenges. Some of these challenges taken into consideration are form errors, temperature sensitivity, and lower material stability over time which degrade the metrological compatibility and increase the measurement uncertainty. A key issue has been to document that the objects mentioned are stable and controllable, and useful as reference objects for evaluating dimensional measurements from CT scanning, in terms of detecting systematic errors and estimated uncertainties.

Chapter 3 presents a method for evaluating measurement errors arising in a CT system used in manufacturing industry in terms of material density and orientation of the scanned reference objects.

Chapter 4 presents a comparison that has aimed to collect information about measurement performance in state-of-the-art industrial CT in the manufacturing industry. A previous international comparison has involved a number of objects typically used for CT performance testing featuring easy X-ray penetration and well defined geometries with low form errors. In the present comparison, two common industrial items have been used that are relevant for industrial measurements in terms of material, dimensions and geometrical properties.

In Chapter 5 it is tested if grating based X-ray contrast modalities can be applied for metrological purposes. Traditionally, segmentation between multi-materials in X-ray CT is only possible for objects where material densities are not close to each other. A novel method called Grating-interferometer Based Imaging offers a new possibility to overcome this problem. The method is evaluated with respect to its metrological compatibility by comparing it to traceable measurements.

Chapter 6 presents a brief state-of-the-art about reference objects, standards and guidelines relevant for CT used in the meat processing industry. Two new reference phantoms are developed by DMRI and consist of different polymers representing tissue

materials such as lean meat, fat and bone. These phantoms are considered more relevant for industrial measurements, in terms of materials, dimensions and volumetric properties, but their use poses a number of challenges. Some of these challenges taken into consideration are temperature sensitivity and lower material stability over time which degrade the volumetric compatibility and increase the measurement uncertainty. A key issue has been to document that the phantoms mentioned are stable and controllable, and useful as reference objects for evaluating volume measurements from CT scanning in the meat processing industry, in terms of detecting systematic errors and estimated uncertainties.

Chapter 7 presents a comparison that has aimed to collect information about measurement performance in state-of-the-art CT in the meat processing industry. In the present comparison, two reference phantoms from the meat industry have been used that are relevant for industrial measurements in terms of material, dimensions and geometrical properties. The uncertainty considerations and challenges are very similar to the one from the comparison on CT for industrial applications in manufacturing industry in Chapter 4. The main differences between this comparison and the comparison in Chapter 4 are the following: 1) clinical CT are applied, 2) volumes are investigated, and 3) multi-materials are applied.

In chapter 8, experiments are prepared and accomplished to document the performance of advanced image analysis software PigClassWeb (previously developed by DMRI and DTU Compute) through volume comparisons to real dissections of pig carcasses. For the real dissections, volume estimations of tissue types such as bone, lean meat and fat, are estimated using VolumeGraphics software.

Chapter 9 summarizes the most important findings and achievements of this work. Suggestions for future work in the field of CT based on this Ph.D. project are provided too.

1.5 Chapter conclusion

This chapter presents the need for CT in the industry. The application field in two areas has been presented: 1) the manufacturing industry and 2) the meat processing industry, although the field of application in the manufacturing industry is different compared to the one in the meat processing industry.

The manufacturing of a product has largely become an automated process in the manufacturing industry today and CT is considered as a solution to be implemented in automated in-line control. The CT technology is well suited to perform tolerance verification on components which are often complex or to carry out inspection of assemblies. The manufacturing industry is concerned with geometrical measurements

such as lengths, diameters and roundness. The CT in the manufacturing industry is of the classification dimensional metrology CT.

The field of the meat processing industry differs from the one in the manufacturing industry. Here, a more efficient use of the raw materials is one of the largest and most important challenges. Today the dissection is made through an expensive manual dissection of a large batch of carcasses. This dissection can be made automated by using CT as an online system for measuring lean meat and fat distribution in pig carcasses in which it is possible to adapt the dissection according to current costs and demands. In the meat processing industry a clinical CT is used for volume estimations of lean meat and fat distribution in pig carcasses.

Commonly for the two industries is that the evaluation of the measurement uncertainty with assessment of all influential contributors and error sources constitutes a challenge with respect to the establishment of traceability and quality assurance of CT measurements.

Additionally a short description is given of the CIA-CT project of which this Ph.D. project was a part. And then the chapter is completed with a problem statement and project structure, where the main focus is to develop methods for quality assurance of CT scanning for industrial measurements in both application areas.

Chapter 2 Reference objects for applications in the manufacturing industry

This chapter presents a brief state-of-the-art about reference objects, standards and guidelines relevant for CT used in manufacturing industry. Furthermore, a short description is given on some error sources in CT scanning such as scale errors, threshold offsets, beam hardening, cone beam artifacts and scattered radiation. The development of new reference objects for CT is presented. Three kinds of reference objects are introduced: *step gauge*, *step cylinder* and a c*ylindrical multi-material assembly*, developed by the author at the laboratories of DTU. Moreover, two reference objects are calibrated objects from the manufacturing industry: a *threaded tube* from the medical industry and a *LEGO brick* from the toy industry. The threaded tube and the LEGO brick are considered more relevant for industrial measurements, in terms of materials, dimensions and geometrical properties, but their use poses a number of challenges. Some of these challenges taken into consideration are form errors, temperature sensitivity, and lower material stability over time which degrade the metrological compatibilities and increase measurement uncertainty. A key issue has been to document that the objects mentioned are stable and controllable, and useful as reference objects for evaluating dimensional measurements from CT scanning, in terms of detecting systematic errors and estimated uncertainties.

2.1 Traceability of CT measurements

The work in this Ph.D. project was composed in parallel with another Ph.D. project [6] which describes the detailed work on existing methods, standards, measurement uncertainty and guidelines for generating traceability of CT measurements. Therefore these topics are briefly presented in this Ph.D. thesis.

2.1.1 Standards and guide lines

Currently many standardized procedures are still under development which means that the traceability of CT cannot be ensured. One of them is the German guideline VDI/VDE 2617-13 which is currently considered as a fundamental one for specification and verification of CT systems used for coordinate metrology in the manufacturing industry [17]. But the evaluation of the measurement uncertainty with assessment of all influential contributors and error sources constitutes a challenge with respect to the establishment of traceability and quality assurance of industrial measurements. For this purpose, reference objects can be applied corresponding as used in conventional

coordinate metrology. This means that measurement traceability can be implemented in CT by the use of other instruments with known uncertainty. The uncertainty estimate for this case can be achieved by the substitution approach ISO 15530-3, which transforms traceability from reference objects to real parts [18]. This approach can be applied if the reference object is close to the real part in terms of material characteristics, size and shape. The use of the substitution approach in CT metrology is more critical compared to the one in e.g. CMM metrology [2]. A critical aspect to the application of the substitution approach to CT is the missing guidance in dealing with CT specific effects. Consequently, CT effects must be taken in account for particular measurement tasks such as the influence of material characteristics and roughness of the scanned object [6]. But it is important to underline that there is not only one method for uncertainty estimation of CT measurements in which a full description of the other models for uncertainty estimation can be achieved in another Ph.D. project such as simulation, ISO 14253-2 (procedure for uncertainty management, PUMA) and ISO/DTS 15530-2 [6].

2.1.2 Influence factors

There are several influence factors, which affect the overall performance of the CT measurements. The influence factors can in general be divided into five main categories as shown in Figure 2.1. The German guideline VDI/VDE 2630-1.2 [19] gives a full overview of all the influence factors in CT metrology.

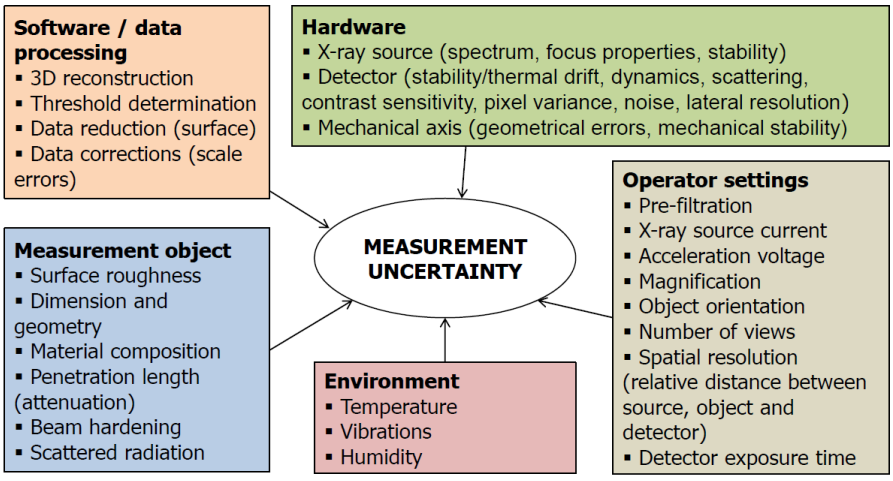

Figure 2.1. An overview of influence factors in CT metrology **[6]**.

2.1.3 Measurement uncertainty

According to GUM and PUMA [20; 21; 22], measurement results can only be compared to methods and/or equipment provided with documented traceability to the meter definition through a chain of calibrations with stated uncertainties. A complete statement of a measurement result can be expressed as specified in (2.1) [6], where *y* is a result of measurement and *U* is an expanded uncertainty of measurement.

$$Y = y \pm U \tag{2.1}$$

In cases where compensation of bias effects is not possible, or one want to point out the quantity of the bias, the measurement result can be expressed as in (2.2) [6].

$$Y = y - b \pm U \tag{2.2}$$

Hence *b* is the bias (systematic error), expressed in (2.2) [6].

$$b = \bar{y} - x_{cal} \tag{2.3}$$

Hence $\bar{y}$ is the actual value obtained by CT and x_{cal} is the true value obtained through calibration using a CMM.

2.1.4 State-of-the-art reference objects

The development and manufacturing of reference objects for CT metrology must follow the German standard VDI/VDE 2630 series (or VDI/VDE 2617-13) [2; 6]. Several existing reference objects have been developed for this purpose and these are shown in Figure 2.2.

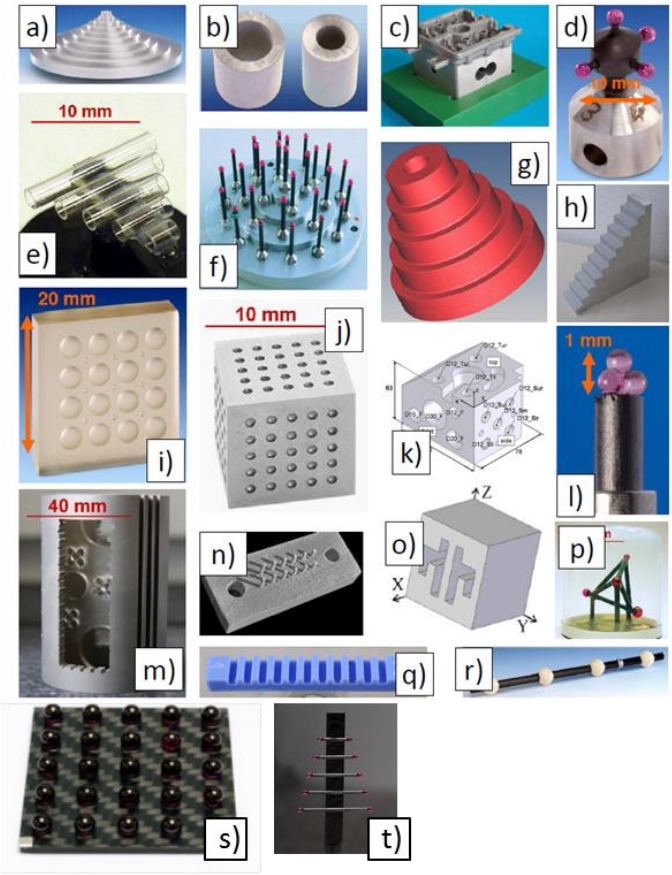

Figure 2.2. An overview of existing reference objects in CT metrology **[6]**.

2.1.5 Error sources

Each reference object is developed depending on its purpose to correct for eventual biases according to the GUM [20]. In CT there are several error sources which contribute to systematic errors such as image artifacts, scale errors, CT system limits and data evaluation strategy. In this Ph.D. thesis a brief description is given on some of these error sources such as scale errors, threshold offset, beam hardening artefacts, cone beam artifacts, and scattered radiation.

Scale errors occur in CT measurements because of instable temperature conditions during the scanning process and/or magnification errors. It is possible to correct for the scale error using threshold independent (also called unidirectional) distances in which the reference measurements are known using geometrical compensations. An example of an independent distance is the center distance between the spheres, assuming that form errors are neglected, as shown in Figure 2.3.

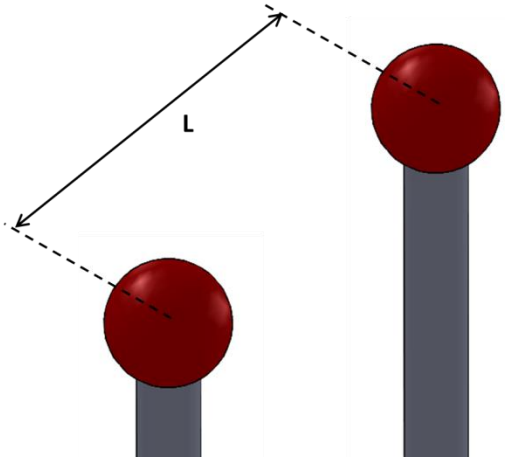

Figure 2.3. Example on an independent distance (center distance between spheres).

Independent distances are not affected by threshold determination. The scale error correction is obtained by using linear regression through the calculations presented in (2.4) and (2.5) [6].

$$L_{CT-cor} = L_{CT-uncor} - a \cdot L_{CMM} \tag{2.4}$$

$$a = \frac{1}{s_{vox}} - 1 = \frac{1}{\left(\frac{L_{CMM}}{L_{CT}}\right)} - 1 = \frac{L_{CT}}{L_{CMM}} - 1 \tag{2.5}$$

Hence s_{vox} is the correction factor, $L_{CT\text{-}cor}$ is the data after correction, L_{CT} is the distance measured by CT and L_{CMM} is the distance measured by traceable instruments such as the tactile CMM. The linear regression coefficient is defined by a which is determined by L_{CT} (another independent distance different from $L_{CT\text{-}uncor}$) and its appurtenant reference value L_{CMM}.

Threshold offsets occur in CT measurements because of wrong defined edge segmentation areas between the scanned object and the surrounding air. Traditionally segmentation between air and material is made using different principles and techniques of edge detection and threshold algorithms [23; 24; 25]. The most conventional principle is the global one (also called ISO 50%) which is used for surface determination [6]. It is possible to perform an edge correction by using threshold dependent (also called bidirectional) distances with known reference measurements and by the use of geometrical compensations. The method for edge correction offset b is obtained by using linear regression through the calculations presented in (2.6) and (2.7). Hence b acts on both sides of a threshold dependent measurand.

$$L_{CT-cor} = L_{CT-uncor} - a \cdot L_{CMM} + 2 \cdot b \tag{2.6}$$

$$b = \frac{L_{CMM} - \left(L_{CT} - a \cdot L_{CMM}\right)}{2} \tag{2.7}$$

If there is no access for a threshold independent distance on the scanned object, other methods must be considered. The linear regression coefficient *a* can also be obtained using threshold dependent geometrical features [26]. There are two different types of dependent features, in which a visual description is shown in Figure 2.4, based on a knob in this case. These are called type 1 and type 2 (also called internal and external measurements respectively according to ISO 10360-2 [27]). Type 1's offset is opposite type 2. This principle can also be transferred to inner and outer diameters, in which the inner diameters are type 1 and the outer diameters are type 2.

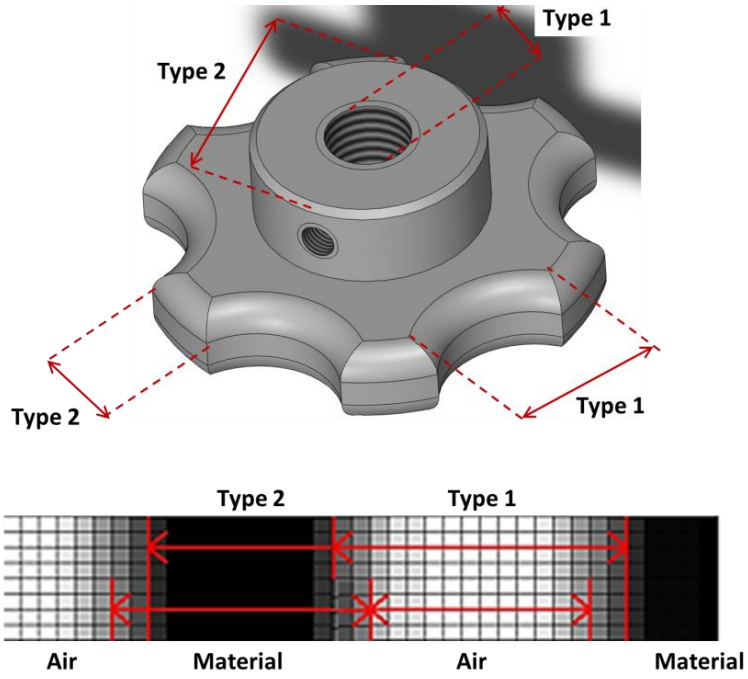

Figure 2.4. Two types of edge dependent distances on the step gauge. Theoretically, type 1 and 2 have opposite edge offsets **[26]**.

The linear regression coefficient *a* can be obtained based on one of the two following methods: method A and method B. Method A is valid for two edge dependent features of the same type (either type 1 or type 2) and is presented in (2.8).

$$a = \frac{1}{s_{vox}} - 1 = \frac{1}{\left(\frac{L_{CMM-2} - L_{CMM-1}}{L_{CT-2} - L_{CT-1}} \right)} - 1 = \frac{L_{CT-2} - L_{CT-1}}{L_{CMM-2} - L_{CMM-1}} - 1 \quad \textbf{(2.8)}$$

Method B is valid for two edge dependent features of the different types (one type 1 and one type 2) and is presented in (2.9). It is different compared to (2.8) because of the opposite edge offsets *b* for two different feature types.

$$a = \frac{1}{s_{vox}} - 1 = \frac{1}{\left(\frac{L_{CMM-2} + L_{CMM-1}}{L_{CT-2} + L_{CT-1}} \right)} - 1 = \frac{L_{CT-2} + L_{CT-1}}{L_{CMM-2} + L_{CMM-1}} - 1 \quad \textbf{(2.9)}$$

The edge correction size *b* can then be found as already stated (2.7). If the object features threshold independent features only *b* will equal to 0. Note that the stated equations above are valid for scanned objects which are not affected by other error sources such as physical phenomenons and/or reconstruction algorithms. These error sources are stated by the symbol δ and added in the equation for correction of scale errors and edge offsets in (2.10).

$$L_{CT-cor} = L_{CT-uncor} - a \cdot L_{CMM} + 2 \cdot b + \delta \quad \textbf{(2.10)}$$

The correction curve for beam hardening artifacts depends on the thickness and density of the scanned object and is not linear [6; 28]. The beam hardening artifacts influence the threshold values and this primarily occurs in high density materials. It is recommended to increase the energy of the X-ray depending on material density and thickness of the scanned object to ensure that the X-rays can penetrate the object [29]. If the amount of energy is dosed incorrectly it can result in beam hardening and blurred images which makes it difficult to distinguish between the scanned object and the surrounding air [30]. Beam hardening artifacts can be reduced or eliminated using methods and techniques such as pre-hardening using physical filters (aluminium, copper, brass, etc.) and/or correction before and during image processing [6]. The correction before and during image processing can be done based on a reference object (such as step wedges and step cylinders) or could be software based (also called the Iterative Artifact Reduction method) [6; 28; 31]. But it is challenging to correct for beam hardening artifacts in objects with varying wall thickness, or objects consisting of several materials. A case of non-corrected and corrected beam hardening artifacts on a ball calotte plate is shown in Figure 2.5.

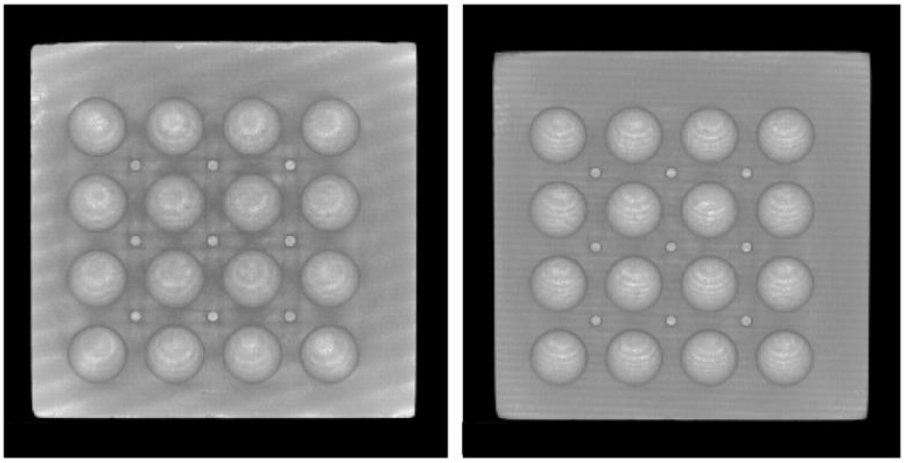

Figure 2.5. Reconstructed ball calotte plate. On the rendered surface dark stripes can be recognized which are beam hardening artifacts (left). The Iterative Artifact Reduction method reduces beam hardening effects visibly (right) **[31]**.

Cone beam artifacts are incomplete and blurred areas on the projection data at the top and bottom of the detector. In general it is not recommended to orientate the scanned object too close to the borders with the detector, in which errors due to cone beam artifacts are pronounced [6]. These can be avoided by 1) placing the scanned object more close to the detector, 2) reducing the limits of the vertical length by changing the position of the object, or 3) using a helical trajectory [2; 4]. A helical trajectory is shown in Figure 2.6 and an example of cone beam artifacts on a test phantom is shown in Figure 2.7.

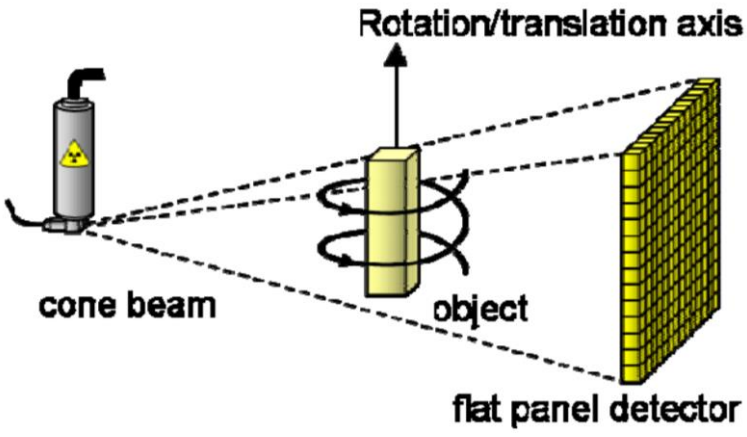

Figure 2.6. Sketch of the trajectory on a helical CT **[4]**.

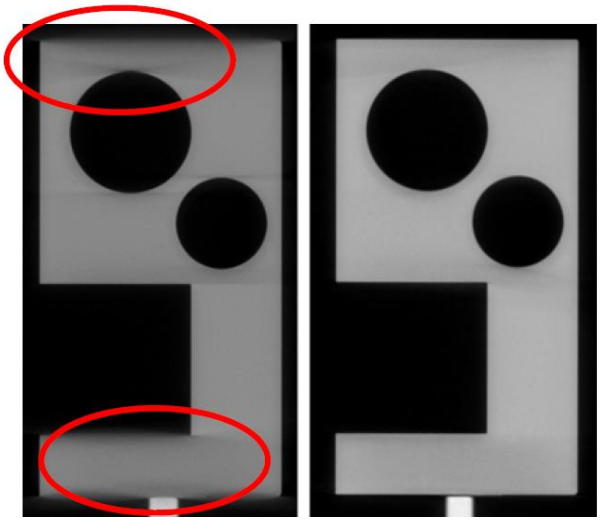

Figure 2.7. Reconstructions with standard (left) and with helical trajectory (right) of a test phantom **[4]**.

Scattered radiation occurs because of a photoelectric effect in the scanned object when the energy of an incoming X-ray photon is transferred to an electron, and subsequently are ejected and scattered (see Figure 2.8 and Figure 2.9) [32]. Scattered radiation represents a source of image degradation in CT which leads to the formation of scattered artifacts in the reconstructed 3D volume. These artifacts include streaks between contrast details and a general loss of contrast, which reduce qualitative and quantitative analysis in the reconstructed 3D volume and affect dimensional measurements [2]. Scattering artifacts can be avoided using methods and techniques such as Monte Carlo, anti-scatter grids and slit scans [33]. An example of non-corrected and corrected scattered artifacts on an aluminium motor block is shown in Figure 2.10.

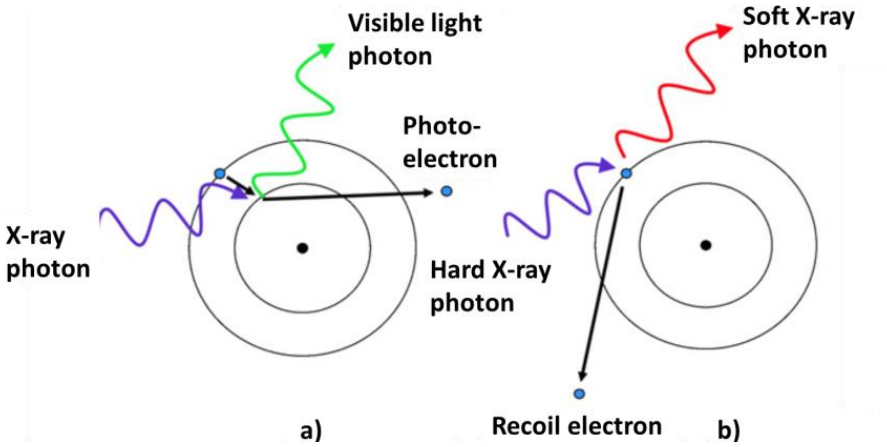

Figure 2.8. Photoelectric absorption (a) and scattering (b) **[2]**.

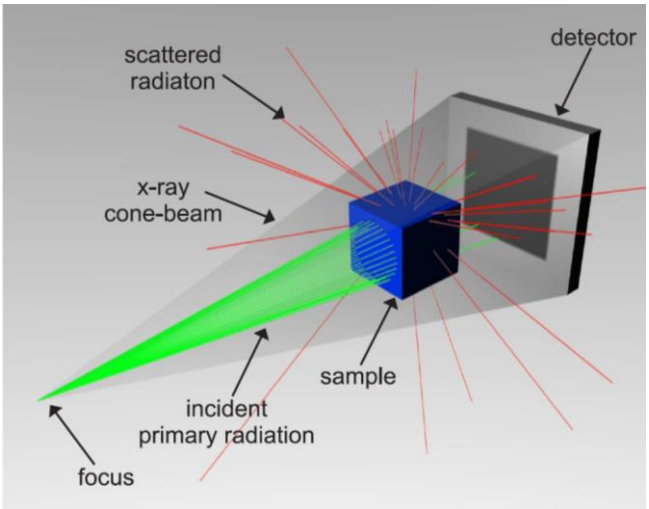

Figure 2.9. Schematic illustration of a cone beam CT setup where incident primary radiation (green) partially is scattered by the sample. A part of this scattered radiation (red) reaches the detector where it gives rise to scatter signals **[32]**.

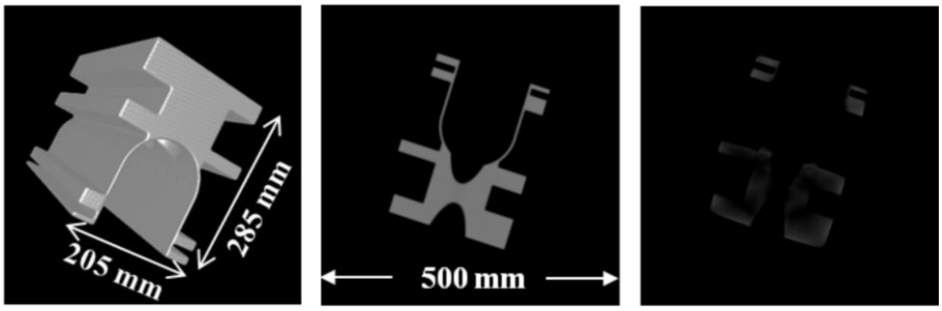

Figure 2.10. Left: volume rendering of aluminium motor block. Middle: a scatter free reference. Right: the uncorrected image containing scattered artifacts **[33]**.

2.2 Step gauge

Originally, a miniature step gauge made of a bisacryl material for dental applications (Luxabite) was developed and moulded at DTU in connection with development of reference objects for instrument verification in optical 3D scanning and CT [34; 35; 36]. Although the initial investigations had indicated a good metrological compatibility [37] of the material, a later stability investigation showed that the material was not strong and stable enough to be used for reference objects. It was due to problems with measurement repeatability with average deviations ranging from 3 µm to 27 µm for all distances with expanded uncertainties (confidence level = 95%) higher than 30 µm. These high values pointed out problems associated with repeatability and form errors, due to the occurrence of indentations in correspondence to the CMM probing points, see Figure 2.11 [38]. The manufacturing and replication of the objects did not allow them to reach sufficient surface properties (such as form errors and resistance to deformations). Because of material instability and bad resistance to deformations, an investigation on

better materials for manufacturing of reference step gauges for CT scanning applications was carried out. Low density materials such as polymers were advisedly better to use, since they do not produce any image artifacts in the reconstructed 3D volume compared to high density materials as lead [2]. Furthermore polymers are widely used in the industry and are of great interest in industrial CT scanning [2]. The selected polymers meet the requirements in terms of hardness, mechanical properties, surface cooperativeness and stability. These requirements had been divided into two parts, the first group involving the most important themes and the second one the less important themes, see Table 2.1. A literature investigation showed that the recommended polymers for a new step gauge could be polyoxymethylene (POM), polyetheretherketone (PEEK) or polyp-phenylenesulphide (PPS). These three polymers have been listed and evaluated in relation to the requirements described in Table 2.1 too, and PEEK and PPS were selected for further use. The two polymer materials are in the category known as: "valuable special polymers", and are mainly used in the automotive industry showing good mechanical properties at high temperatures [39]. PPS with 40% glass was selected instead of pure PPS, because the availability of pure PPS was limited. An advantage of the glass content is that it improves the stability and strength of the polymer material [39]. The material hardness results also improved and was measured using a Vickers hardness test, taking average and standard deviation of five repeated measurements. An increase of around 50% with PEEK and PPS with respect to Luxabite was detected [38]. Five PEEK step gauges (PEEK SG: #1 to #5) and five PPS step gauges (PPS SG: #6 to #10) were manufactured. Additionally, two aluminium step gauges (Aluminium SG: #1, #2) and two steel step gauges (Steel SG: #1, #2) were implemented to cover a broad range of materials. Examples of the manufactured step gauges are shown in Figure 2.12.

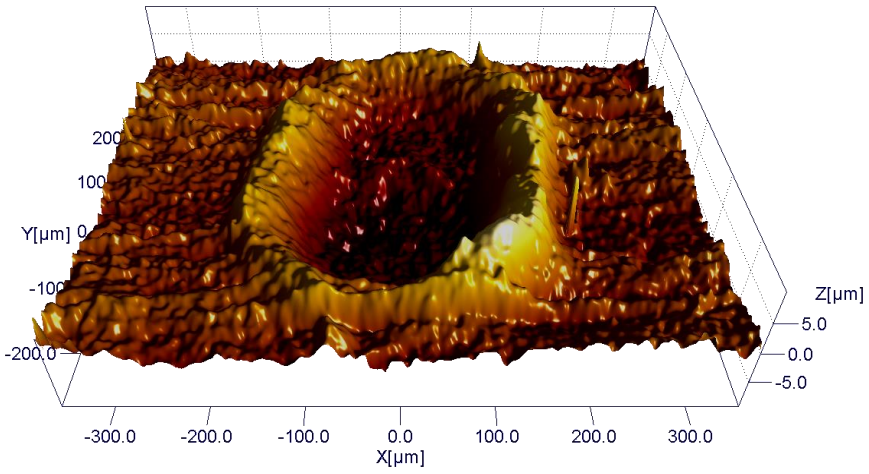

Figure 2.11. Example of indentation marks presented on the measurement surfaces of the Luxabite step gauge. Average peak to valley height = 17 µm and average maximum width = 345 µm, measured with an Infinite Focus microscope by Alicona **[38]**.

Table 2.1. Set-up of requirements for development of the new step gauges using **[39; 40; 41]**.

Importance	Description	POM	PEEK	PPS
High	High hardness and mechanical properties to avoid deflections and deformations.	Acceptable	Yes	Yes
	High surface cooperativeness. The surface should be smooth (it means a small form error) in order to use the probe from a tactile CMM in random positions on the surface.	Unknown	Unknown	Unknown
	Resistance to X-rays to avoid degradation or change of the structure.	Unknown	Yes	Yes
	High material stability. After a reasonable shrinkage, the material has to be reasonably stable.	Acceptable	Yes	Unknown
Medium	The material should be resistant to water and humidity.	Yes	Yes	Yes
	The designed features should be well defined.	Unknown	Unknown	Unknown
	It is not recommended to use conventional methods such as injection moulding and thermoforming. Tools are expensive to develop and manufacture. Furthermore the number of step gauges to be manufactured is quite small to injection moulding. Other considerable methods should be cutting methods. In this case it is very important that the polymer selected is very form stable in relation to the cutting process. Possible tolerances using milling are defined here.	≥ 0.05 mm	≥ 0.01 mm	≥ 0.01 mm
	Costs.	Low	High	Acceptable
	It is important that the polymer properties as amorphous and crystalline polymers. It is recommended to avoid amorphous polymers (they are transparent), since they cannot be used for e.g. optical CMMs if required.	Crystalline	Crystalline	Crystalline
	The glass transition temperature is important, because it is the temperature shift for a polymer, where it changes properties from hard to soft.	< 20°C	> 20°C	> 20°C
	The density of the selected polymer should be selected in relation to fixture materials available due to penetration of X-rays. From this it is assumed that the density should be higher than 1000 kg/m^3.	Yes	Yes	Yes

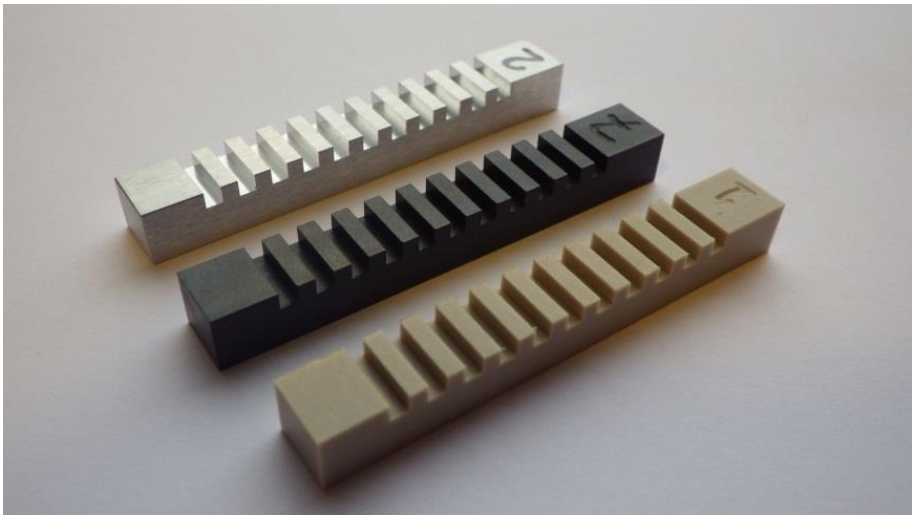

Figure 2.12. Examples of the step gauges. From left to right: aluminium, PPS, and PEEK.

2.2.1 Use

The step gauge can be used as a reference object for characterization of measurement errors in a CT system such as systematic errors. The step gauge features bidirectional and unidirectional lengths. Material characteristics as density and thermal expansion coefficient data are shown in Table 2.2. The step gauges are manufactured with a short (7 mm) and a long edge (9 mm) for identification of position and direction for the alignment, as shown in Figure 2.13.

Table 2.2. Material characteristics of the step gauges.

Material	Supplier	Grade	Density [g/cm³]	Thermal expansion coefficient [10^{-6} K^{-1}]
PEEK	Nordisk Plast A/S	PEEK Natur	1.310	50.0
PPS	Röchling High Performance Plastics	PPS GF 40	1.650	30.0
Aluminium	Alumeco A/S	AW 2011	2.830	22.9
Steel	Uddeholm A/S	UHB 11	7.800	11.0

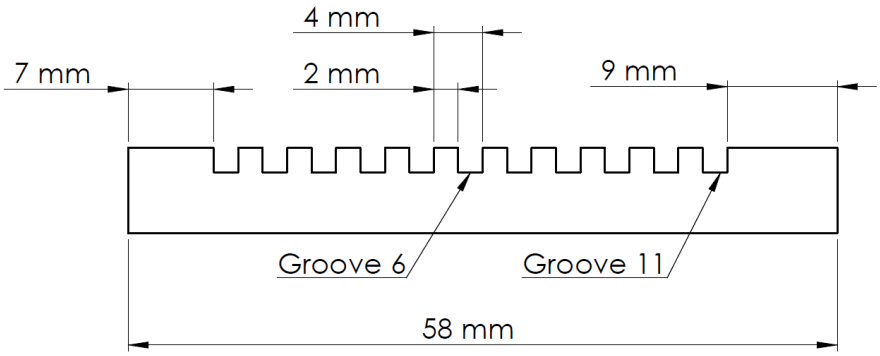

Figure 2.13. Step gauge with nominal dimensions.

2.2.2 Manufacture

The step gauges were manufactured using milling. Linear groove accuracies in the range ±1.3-1.9 µm were estimated from measurements on CMM, see Figure 2.14 and Figure 2.15. This milling process significantly improved the surface quality on the vertical sides of the grooves compared to step gauges in Luxabite [38], with form errors in the range of 5 µm for the PEEK step gauges and of 3 µm for the PPS step gauges. Form errors for aluminium and steel step gauges were similar to the ones for PPS step gauges (see section 2.2.3). Measurements of the depth of the eventual scratches on the vertical planes on the grooves was carried out using a stylus profilometer Taylor-Hobson RTH Talysurf 5-120 with Z resolution of 0.001 µm and based on roughness parameters as defined in the standard ISO 4287 [42]. A roughness standard was used as roughness reference to generate traceability. Roughness measurements were carried out on the left side of groove 1 and 6, and on the right side of groove 6 and 11. The definition of the positioning and tracing direction is shown in Figure 2.16 and Figure 2.17 and is based on the right sides of the grooves. The positioning and tracing direction was mirrored for the left sides of the grooves. Each tracing had a length of 5.1 mm. The second tracing direction was identical to one of the used areas for alignment of flatness using the CMM (see section 2.2.3). This was located at the horizontal area measured 0.7 mm from the edge. A short cut-off filter on 2.5 µm and a long cut-off filter on 0.80 mm were selected. All measurements were performed on the four different materials: aluminium, PEEK, PPS and steel. Maximum, average and minimum values based on 12 measurements are shown in Table 2.3 for the arithmetical mean deviation *Ra* and the max height *Rz*. Examples of roughness profiles are shown for all four materials in Figure 2.18. Aluminium and steel were smoother compared to PEEK and PPS with a difference up to 0.8 µm following the average of the arithmetical mean deviation *Ra*. The roughness is of high importance in CT, because the quality of the surface roughness can influence on the threshold determination [6].

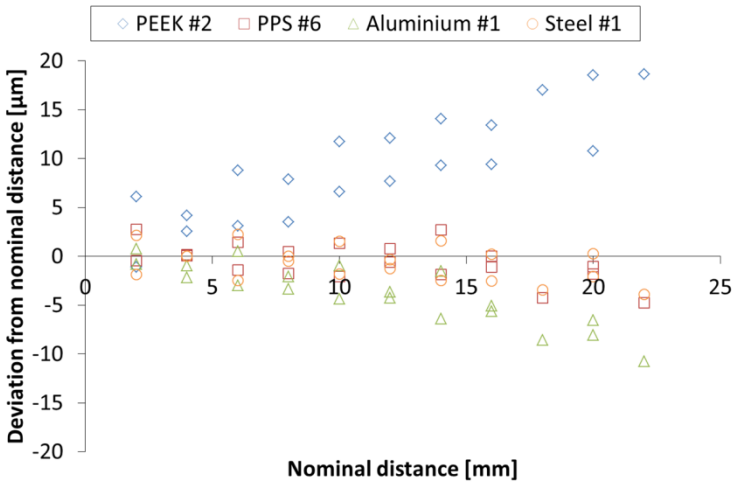

Figure 2.14. PEEK SG #2, PPS SG #6, Aluminum SG #1, and Steel SG #1 – Comparison example of the linear groove accuracies. Measured with the OMC.

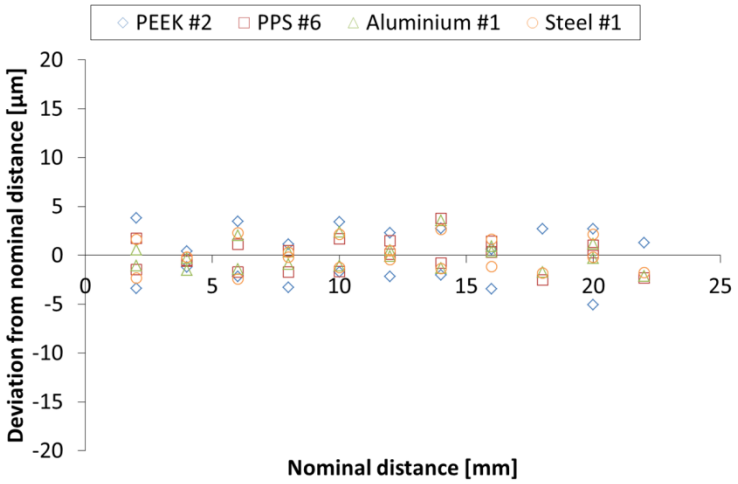

Figure 2.15. PEEK SG #2, PPS SG #6, Aluminum SG #1, and Steel SG #1 – Corrections of systematic errors are realized by applying linear regression.

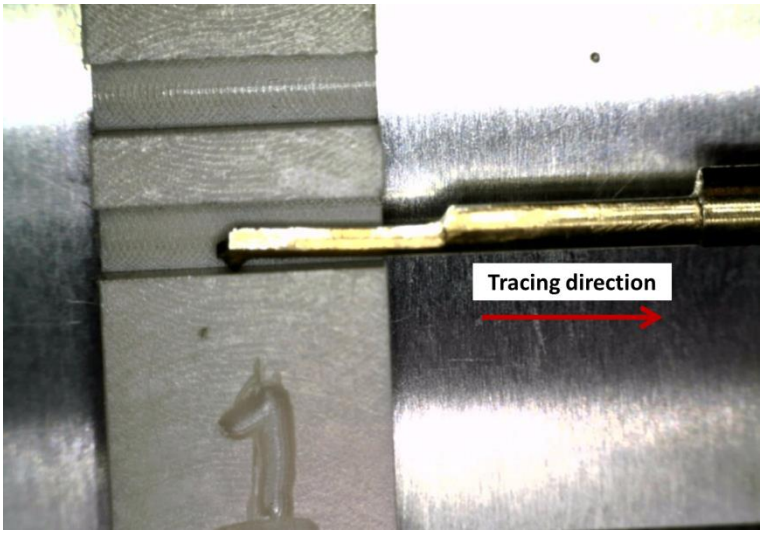

Figure 2.16. Tracking in progress on the right side of groove 11 on a step gauge.

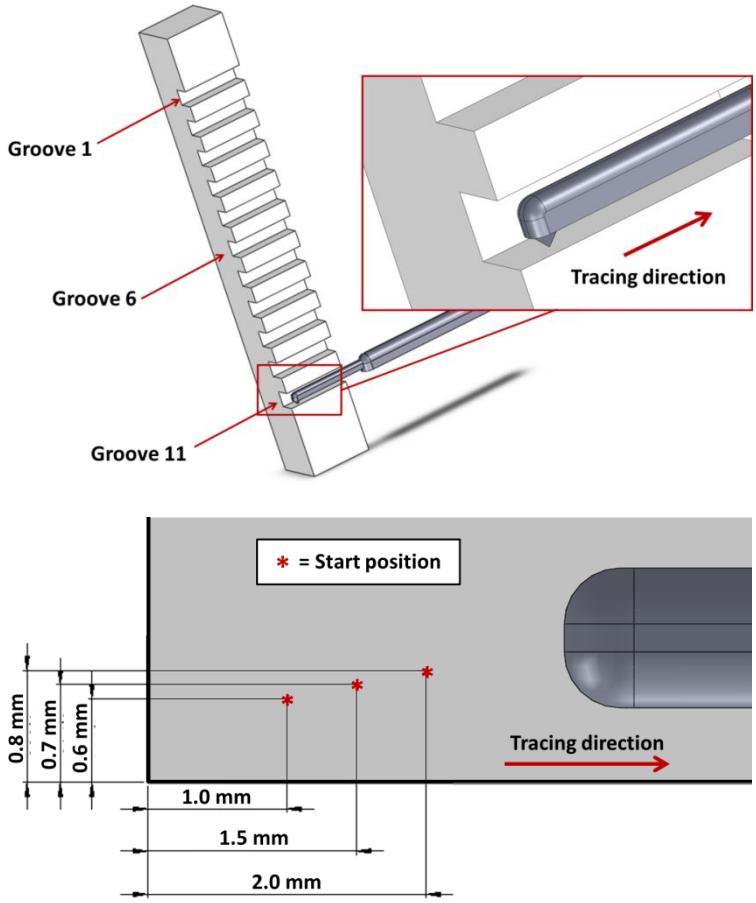

Figure 2.17. Positioning and tracing direction example on the right side of groove 11. The three red marks show the start positions before the tracing is achieved.

Table 2.3. Roughness on the vertical planes on the grooves. All values are in µm and based on 12 measurements for each material.

	PEEK # 1		PPS # 7		Aluminium # 2		Steel # 1	
	Ra	Rz	Ra	Rz	Ra	Rz	Ra	Rz
MAX	1.211	7.537	1.090	8.218	0.307	1.725	0.800	4.762
AVG	**1.014**	**5.905**	**0.820**	**6.191**	**0.204**	**1.326**	**0.449**	**2.821**
MIN	0.738	4.710	0.645	4.587	0.118	0.733	0.324	1.926

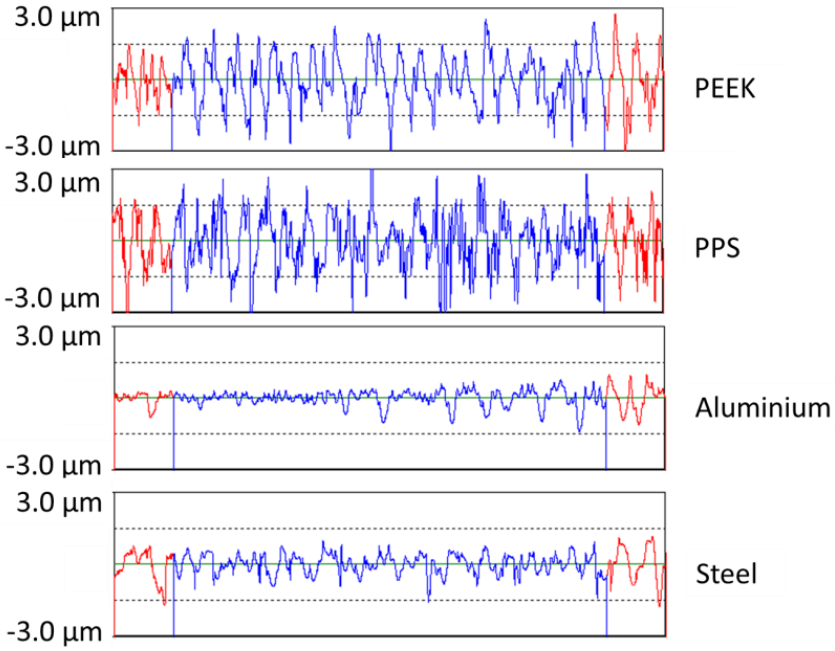

Figure 2.18. Examples of roughness profiles.

2.2.3 Calibration and transfer of traceability

The coordinate measuring machine used at DTU to calibrate the step gauges was a mechanical CMM equipped with a dynamic probe. The CMM is of the type Zeiss OMC 850 (Figure 2.19) with a maximum permissible error (MPE) of $MPE_{U3} = (3+L/250)$ µm (L in mm). A probe with a diameter of Ø0.8 mm with 20 mm long stylus was used, see Figure 2.20. The CMM is placed in a temperature controlled room where the temperature is 20.0±1.0°C. Grade I steel blocks were used as length references to generate traceability. Compensation of the results for temperature changes were made manually. Due to the dynamic probe, no force compensation was performed.

Figure 2.19. CMM of the type Zeiss OMC 850.

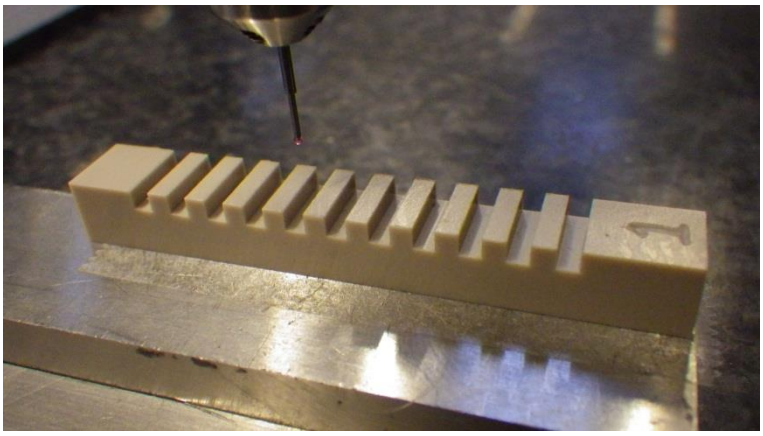

Figure 2.20. Measurement setup for calibration of step gauge using the OMC.

The definition of the coordinate system for the step gauge is performed using a "3-2-1 alignment". Plane Z is created through least square fitting of four teeth areas positioned on the top of the step gauge teeth between groove 4 and 8. Line X (plane Y) is defined as a symmetry line by using least square fitting of the two most extreme areas along the step gauge longitudinal length. These lines are created by the best fitting approach. Plane X is on the left side of the sixth groove and is created through a least square fitting. The reference axis is defined as follows (see Figure 2.21):

- Z: perpendicular to plane Z;
- Y: perpendicular to plane Y;

- O: intersection among plane X, Y and Z.

The measurement strategy of incremental lengths are computed indirectly as the distance between the center points of the corresponding groove planes obtained through a least square fitting of 8 points acquired on each groove side, as shown in Figure 2.22 on the one side. All distances are defined as the distance from a random side to the left side of groove 6 resulting in a total of ten unidirectional (ranging from 2 to 20 mm with 4 mm intervals) and ten bidirectional incremental distances (ranging from 4 to 22 mm with 4 mm intervals). Some of the distances have identical lengths.

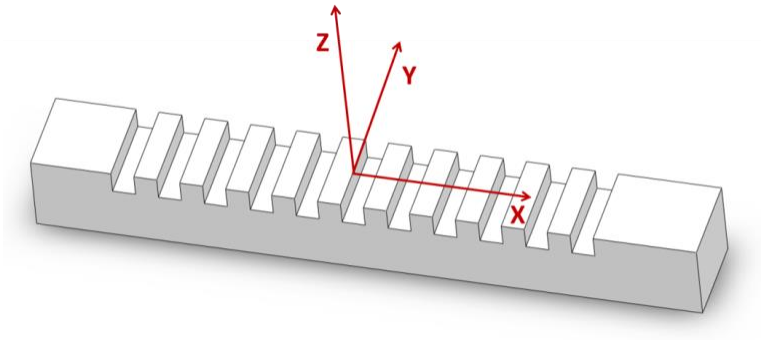

Figure 2.21. Definition of the reference system.

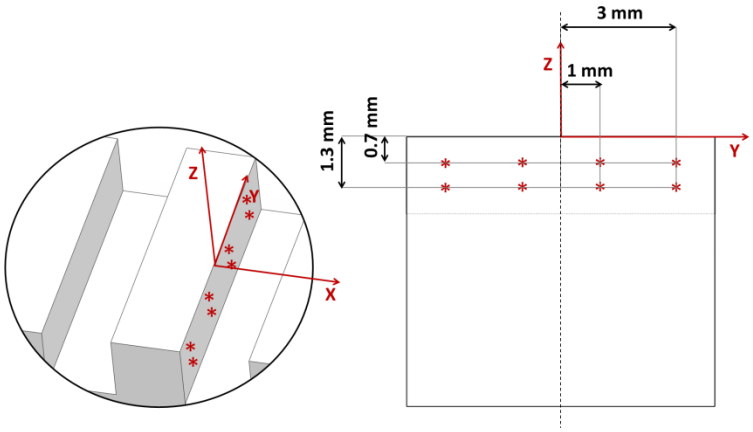

Figure 2.22. Measurement points example on the left side of groove 6.

A practical approach inspired by the PUMA method [21] was used for uncertainty estimation, as a simplification of the GUM approach [20]. The uncertainty contributors used were the following: 1) reference artefact u_r, 2) MPE u_m, 3) workpiece form error u_w, 4) temperature effects u_e, and 5) reproducibility u_p where the parts were repositioned and measured again five times. The temperature contribution was divided into three sub categories: 4.1) temperature difference for instrument $u_{e(1)}$, 4.2) temperature difference for artefact $u_{e(2)}$, and 4.3) deviation from the standard reference temperature $u_{e(3)}$. The models in (2.11) and (2.12) are used for uncertainty estimation.

$$U = k \cdot u_c \qquad (k = 2) \tag{2.11}$$

In this case U is the expanded uncertainty, u_c is the combined standard uncertainty and k is the coverage factor (k=2 for a coverage probability of 95 %). The considered uncertainty contributors are given in (2.12).

$$U = k \cdot \sqrt{u_r{}^2 + u_m{}^2 + u_w{}^2 + u_{e(1)}{}^2 + u_{e(2)}{}^2 + u_{e(3)}{}^2 + u_p{}^2} \tag{2.12}$$

An example of the distribution of uncertainty contributions is summarized in Figure 2.23 for the largest bidirectional (22 mm) distances of step gauges in all four different materials (PEEK SG #2, PPS SG #6, Aluminum SG #1, and Steel SG). The graph shows that the workpiece form error is larger for PEEK compared to the three other materials. PPS show form errors similar to aluminium and steel, which could be due to the glass content. It was detected too for polyamide (PA) in the literature where the addition of glass fibre into the polymer matrix increases stiffness, strength and thermal resistance [43]. These properties affect the machinability of the composites.

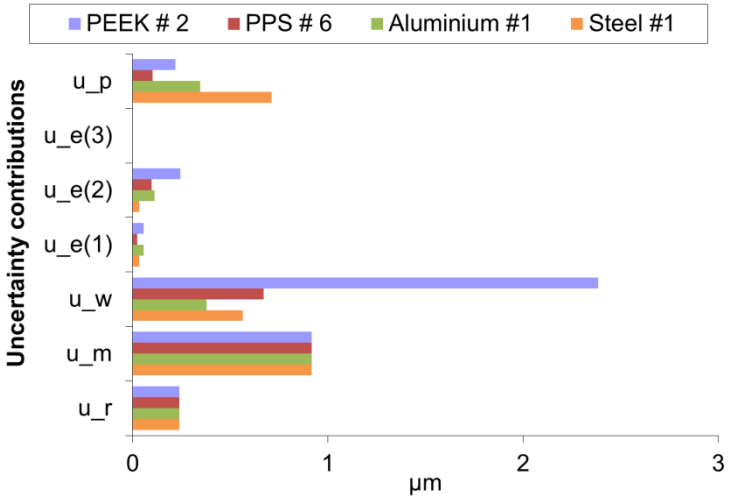

Figure 2.23. PEEK SG #2, PPS SG #6, Aluminum SG #1, and Steel SG #1 – Comparison example of the distribution of uncertainty contributions acquired from the last calibrations of a bidirectional distance (22 mm).

2.2.4 Stability investigation

It is important to test and document the stability of polymers over a period of time, since they are sensitive to environmental changes (such as humidity and shrinkage) [44; 45]. The stability was monitored for the polymer step gauges and performed through reproduced measurements carried out eight times over approximately one year (from November 2011 to September 2012). Figure 2.24 shows an investigation example on

the longest unidirectional (20 mm) and bidirectional (22 mm) distances on the stability of a PEEK step gauge. The deviations of the first measurements were computed with related uncertainties (k=2). Deviations (2σ) from the first calibrated values over one year based on 10 distances of each type can be seen in Table 2.4 for PEEK and Table 2.5 for PPS. The stability was significantly improved compared to Luxabite step gauges with maximum deviations below 6 µm for PEEK and limited expanded uncertainty (below 8 µm), see Table 2.6 . Improved results were obtained for PPS compared to PEEK and for all distances due to the glass fibre (see Table 2.7). In order to judge the agreement between reference values over a period, the E_n value normalised with respect to the estimated uncertainty was computed according to ISO 17043 guidelines [46], see (2.13). If $|E_n| < 1$ the quality of the measurement result is acceptable, while it is not acceptable if $|E_n| \geq 1$.

$$E_n = \frac{x_{after} - x_{before}}{\sqrt{U_{after}^{\ 2} + U_{before}^{\ 2}}} \tag{2.13}$$

Here, x_{after} is the measurement obtained at a given month after November 2011 and x_{before} is the reference value from November 2011, while U_{after} and U_{before} are the corresponding expanded uncertainties (k=2). The estimated $|E_n|$ values were almost in the accepted range for both polymer materials with a calculated average on $|E_n|$ = 0.2, and is based on the histogram shown in Figure 2.25. A test report on step gauges, including the average measured values is attached in the Appendix.

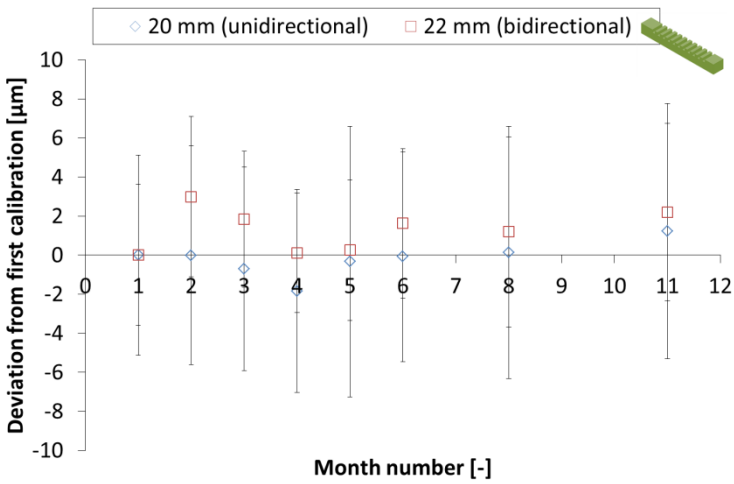

Figure 2.24. PEEK SG #2 – Calibration stability example of an unidirectional (20 mm) and a bidirectional distance (22 mm) over one year. Deviations with respect to the first measurements were computed with related uncertainties (k=2). Month number refers to first month, second month etc.

Table 2.4. PEEK step gauge – Average and maximum deviations (2σ) from first calibration values over one year. Values are based on 10 distances of each type (unidirectional and bidirectional distances), and are in µm.

CGM 	Deviations (2σ) from first calibration values over 1 year (values based on 10 distances of each type)			
	Unidirectional		Bidirectional	
	Mean value [µm]	Max value [µm]	Mean value [µm]	Max value [µm]
PEEK Step Gauge # 1	0.68	2.71	1.33	3.22
PEEK Step Gauge # 2	0.49	2.26	1.68	3.12
PEEK Step Gauge # 3	0.61	1.99	1.68	4.00
PEEK Step Gauge # 4	0.65	3.77	1.85	3.92
PEEK Step Gauge # 5	0.65	2.67	2.04	5.21
MAX	0.68	3.77	2.04	5.21
AVG	0.62	2.68	1.72	3.89
MIN	0.49	1.99	1.33	3.12

Table 2.5. PPS step gauge – Average and maximum deviations (2σ) from first calibration values over one year. Values are based on 10 distances of each type (unidirectional and bidirectional distances), and are in µm.

CGM 	Deviations (2σ) from first calibration values over 1 year (values based on 10 distances of each type)			
	Unidirectional		Bidirectional	
	Mean value [µm]	Max value [µm]	Mean value [µm]	Max value [µm]
PPS Step Gauge # 6	0.74	2.23	0.76	3.21
PPS Step Gauge # 7	0.82	2.12	1.11	3.02
PPS Step Gauge # 8	0.68	3.27	0.77	3.58
PPS Step Gauge # 9	0.77	3.59	0.71	2.29
PPS Step Gauge # 10	0.69	1.89	0.68	1.77
MAX	0.82	3.59	1.11	3.58
AVG	0.74	2.62	0.81	2.77
MIN	0.68	1.89	0.68	1.77

Table 2.6. PEEK step gauge – Calibration uncertainties (k=2) over one year. Values are based on 10 distances of each type (unidirectional and bidirectional distances), and are in µm.

CGM 	Calibration uncertainties (k=2) for PEEK over 1 year (values based on 10 distances of each type)					
	Unidirectional			Bidirectional		
	MIN [µm]	AVG [µm]	MAX [µm]	MIN [µm]	AVG [µm]	MAX [µm]
PEEK Step Gauge # 1	3.08	4.60	7.74	3.11	4.17	6.76
PEEK Step Gauge # 2	3.92	5.15	7.69	2.98	3.94	5.81
PEEK Step Gauge # 3	3.45	4.53	5.44	3.12	4.09	5.47
PEEK Step Gauge # 4	3.04	4.39	6.19	2.60	3.89	5.70
PEEK Step Gauge # 5	4.14	5.14	7.14	3.06	4.38	5.83
MAX	4.14	5.15	7.74	3.12	4.38	6.76
AVG	3.53	4.76	6.84	2.97	4.09	5.91
MIN	3.04	4.39	5.44	2.60	3.89	5.47

Table 2.7. PPS step gauge – Calibration uncertainties (k=2) over one year. Values are based on 10 distances of each type (unidirectional and bidirectional distances), and are in µm.

CGM 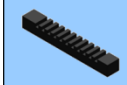	Calibration uncertainties (k=2) for PPS over 1 year (values based on 10 distances of each type)					
	Unidirectional			Bidirectional		
	MIN [µm]	AVG [µm]	MAX [µm]	MIN [µm]	AVG [µm]	MAX [µm]
PPS Step Gauge # 6	2.21	2.74	4.35	2.16	3.29	6.19
PPS Step Gauge # 7	2.30	2.95	4.72	2.25	3.10	4.56
PPS Step Gauge # 8	2.39	2.84	3.87	2.41	3.11	4.54
PPS Step Gauge # 9	2.12	2.63	3.67	2.17	3.09	4.34
PPS Step Gauge # 10	2.41	2.96	3.68	2.27	3.15	4.73
MAX	2.41	2.96	4.72	2.41	3.29	6.19
AVG	2.29	2.82	4.06	2.25	3.15	4.87
MIN	2.12	2.63	3.67	2.16	3.09	4.34

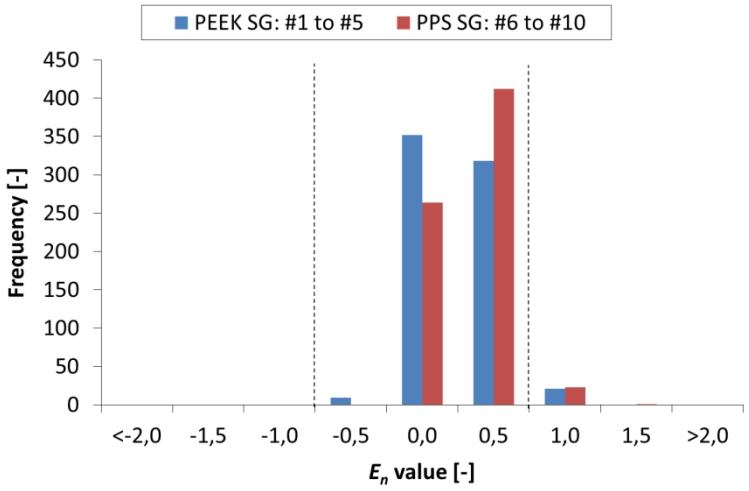

Figure 2.25. PEEK and PPS step gauges – Histogram of E_n values for all measurands.

2.3 Step cylinder

A miniature step cylinder was developed and made at DTU for instrument verification in grating based X-ray contrast modalities for metrology [47]. The parts were developed with dimensional limitations (field of view = 50 mm x 25 mm) and X-ray energy of the applied CT (atomic number of the object, Z < 20). The 15 mm high step cylinder was made by polyoxymethylene (POM) featuring five steps, as shown on Figure 2.26. The selected material POM is in the category known as: “technical thermo polymers”. It is mainly used in gears and screws in the industry and shows good mechanical properties as well as good stress relaxation resistance, good wear properties, and resistance to creep and organic solvents [39].

Figure 2.26. Example of the POM step cylinder.

2.3.1 Use

The step cylinder can be used as a reference object for determination of parametric errors, such as well inner and outer diameters. The main application of the object is similar to the ones for the step gauge but for grating based X-ray contrast modalities. Additionally it can be used to investigate error sources such as beam hardening on internal dimensions of a CT system [48]. Material characteristics such as density and thermal expansion coefficient data are shown in Table 2.8.

Table 2.8. Material characteristics of the step cylinder.

Material	Supplier	Grade	Density [g/cm³]	Thermal expansion coefficient [10^{-6} K^{-1}]
POM	Nordisk Plast A/S	POM-C	1.410	110.0

2.3.2 Manufacture

The step cylinders were manufactured using turning and drilling processes. Diameter accuracies in the range of ±1.1-4.1 µm were estimated from measurements on CMM, see Figure 2.27 and Figure 2.28. Detected form errors (roundness) were in the range of 1.7-2.8 µm. Normally roughness measurements should be performed to evaluate the surface on the object. Furthermore an evaluation of the flatness on the plane areas should be considered. These measurements were not carried out because of limited time.

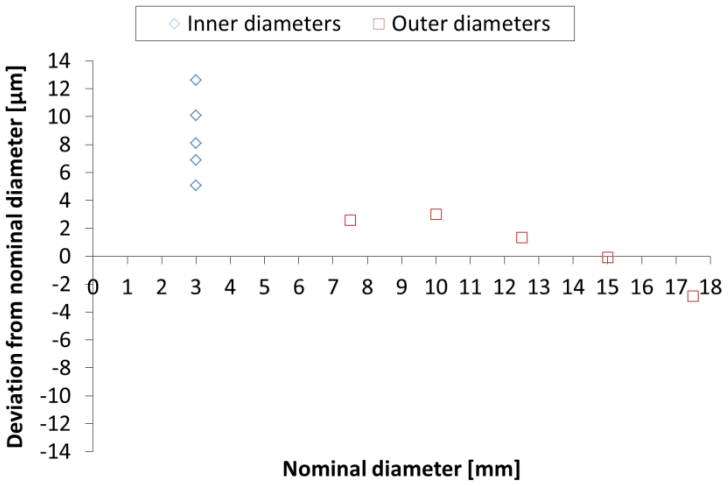

Figure 2.27. POM SC #2 – Comparison example of the diameter accuracies. Measured with the OMC.

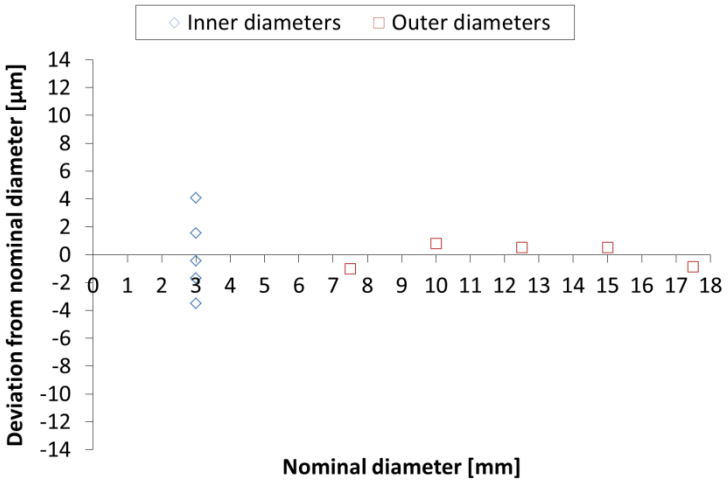

Figure 2.28. POM SC #2 – Corrections of systematic errors are obtained by applying linear regression for the step cylinder.

2.3.3 Calibration and transfer of traceability

Similar to the step gauges, the step cylinders were calibrated using the OMC. A probe with a diameter of Ø1.5 mm with 20 mm long stylus was used, see Figure 2.29. A ring gauge was used as diameter reference to generate traceability. Compensation of the results for temperature changes were made manually. Due to the dynamic probe, no force compensation was performed.

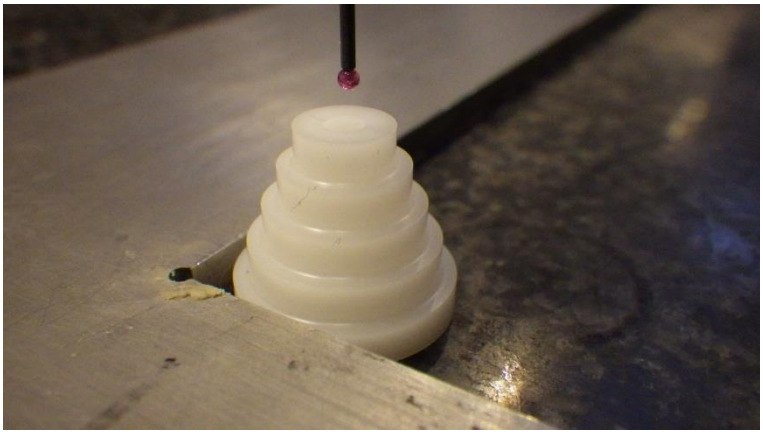

Figure 2.29. Measurement setup for calibration of step cylinder using the OMC.

The alignment on the step cylinder is performed by using a "3-2-1 alignment". Plane Z is created through least square fitting on the top on the plane of the step cylinder. The 4 points defining plane Z should be equally distributed. Plane Y can be created randomly perpendicular to plane Z, since only the diameter is of interest. The reference axis is defined as follows (see Figure 2.30):

- Z: perpendicular to plane Z;
- Y: perpendicular to plane Y;
- O: intersection between plane Z and axis of a cylindrical datum, which is performed by 20 points, which are equally distributed in the inner diameter of the step cylinder.

The selected geometrical features are five inner (ID) and five outer (OD) diameters (see Figure 2.31), and both are measured as circles. The step cylinder is measured from top to bottom at equidistant slices, where the first position (ID1 and OD1) refers to the top. The measurement strategy of the outer diameters is computed using the best fitting approach following the Minimum Circumscribed Element (MCE). The MCE is performed by 20 points, which are equally distributed. The inner diameters are found using best fitting approach following the Maximum Inscribed Element (MIE) and are performed by 20 points, which are equally distributed.

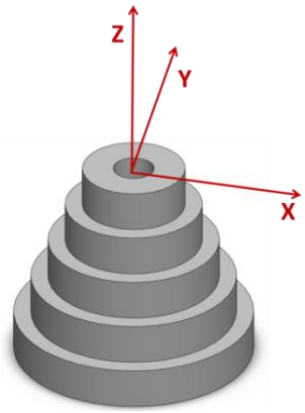

Figure 2.30. Definition of the reference system.

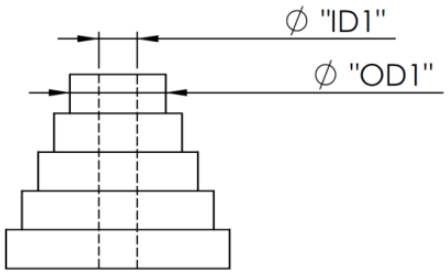

Figure 2.31. Step cylinder with measurands.

PUMA approach [21] was used for the uncertainty assessment, and uncertainty contributions were similar to the ones for the step gauges, see section 2.2.3. One difference was that the estimated form error for the step cylinder was the roundness. An example of the distribution of uncertainty contributions is summarized in Figure 2.32 for the largest outer diameter (OD5 = Ø17.5 mm) and one inner diameter (ID1 = Ø3 mm) of a step cylinder. The graph shows that the uncertainty contribution is scattered. No reproduced measurements were performed for the step cylinders, because they were scheduled to be CT scanned immediately after the calibrations were performed in September 2011. Average uncertainties (k=2) were in the range of 2.4-4.3 µm for all 3 step cylinders.

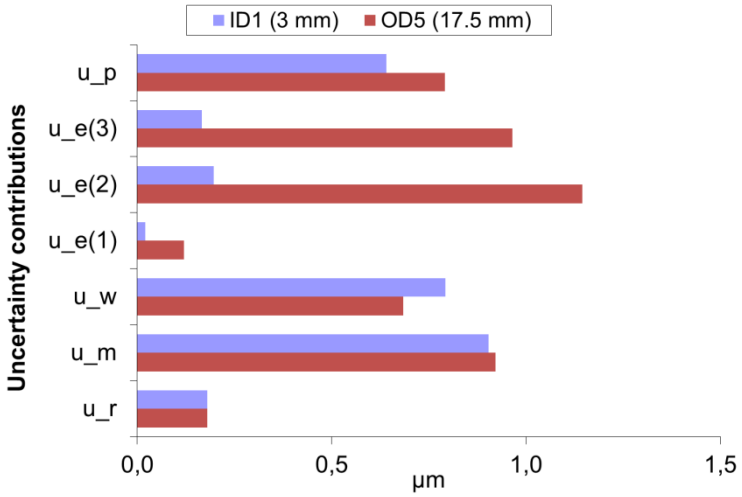

Figure 2.32. POM SC #2 – Comparison example of the distribution of uncertainty contributions acquired from the calibrations of the longest outer diameter (OD5 = Ø17.5 mm) and one inner diameter (ID1 = Ø3 mm).

2.4 Cylindrical multi-material assembly

Three series of three cylindrical multi-material assemblies (one series for each combination of multi-materials) were developed and made at DTU for instrument verification in grating based X-ray contrast modalities for metrology [47]. The cylindrical multi-material assembly can be used for the parameterisation of a CT system and is inspired by another design for assemblies in CT [23]. The parts were developed with dimensional limitations as described for the step cylinder. Furthermore the combinations should be as follows due to segmentation challenges in CT: two identical materials, two different materials with different density, and two different materials with the same density. From these requirements, a 10 mm high cylindrical multi-material assembly was made featuring a male and a female part. The male part was made by polypropylene (PP). The three series of female parts were made by polyoxymethylene (POM), PP, and polyethylene (PE). A cylindrical multi-material assembly in the combination PP-PE is shown in Figure 2.33. PP was selected because of good dimensional stability at high temperature and humid conditions [39]. PE was selected, because its density is close to the one for PP. And POM was selected, because its density is different from PP. A further advantage of POM has already been described for the step cylinder.

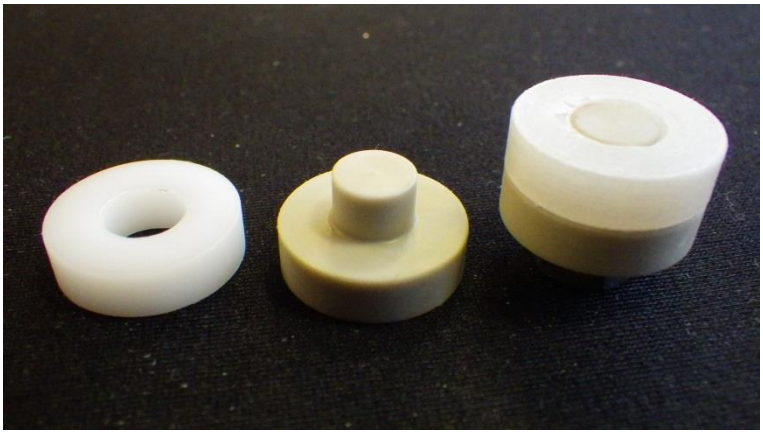

Figure 2.33. Pictures of cylindrical multi-material assembly in the combination PP-PE. From left to right: PE female part, PP male part, and assembled view in the combination PP-PE.

2.4.1 Use

The cylindrical multi-material object can be used as a reference object for determination of parametric errors, as well as assembly inspection, and inner and outer diameters. The main application of the object is similar to the ones for the step cylinder. Additionally it can be used to inspect assemblies consisting of multi-materials in grating based X-ray contrast modalities, and how it affects the measurements. Material characteristics as density and thermal expansion coefficient data are shown in Table 2.9.

Table 2.9. Material characteristics of the cylindrical multi-material assemblies.

Material	Supplier	Grade	Density [g/cm³]	Thermal expansion coefficient [10^{-6} K^{-1}]
PP	Nordisk Plast A/S	PP-H	0.905	155.0
PE	Nordisk Plast A/S	PEHD 500 Natur	0.955	190.0
POM	Nordisk Plast A/S	POM-C	1.410	110.0

2.4.2 Manufacture

The machining processes for the cylindrical multi-material assemblies were similar to the one for the step cylinder. For assembling the parts an engineering tolerance of H7 was used for the hole (inner diameter named ID), and h7 was used for the shaft (outer diameter labelled OD) to ensure a sliding fit [49]. For the measurements in real there will occur small deformations, when assembling the parts depending on the quality of surface roughness [50]. This Ph.D. thesis does not take the deformations into consideration. The manufactured shaft was bigger compared to the drilled holes with a deviation of 0.9 µm, see Figure 2.34. Detected form errors (roundness) were in the range of 5.9-18.1 µm. Normally roughness measurements should be performed to evaluate the surface on the object. Furthermore an evaluation of the flatness on the plane areas should be considered. These measurements were not carried out because of limited time.

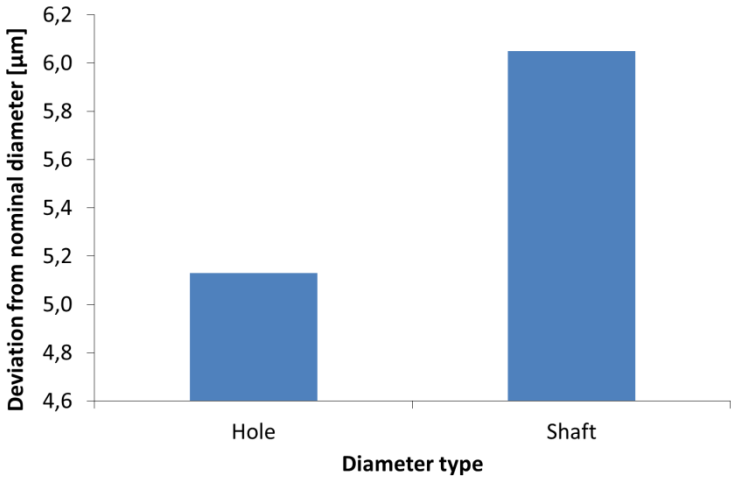

Figure 2.34. Assembly parts – Comparison example of the diameter accuracies (deviations from a nominal diameter of Ø7.5 mm are stated). Measured with the OMC.

2.4.3 Calibration and transfer of traceability

Similar to the step cylinders, the cylindrical multi-material assemblies were calibrated using the OMC, where a ring gauge was used as diameter reference to generate traceability. A probe with a diameter of Ø1.5 mm with 20 mm long stylus was used, see Figure 2.35. The systematic compensations were similar to the one used for the step cylinders.

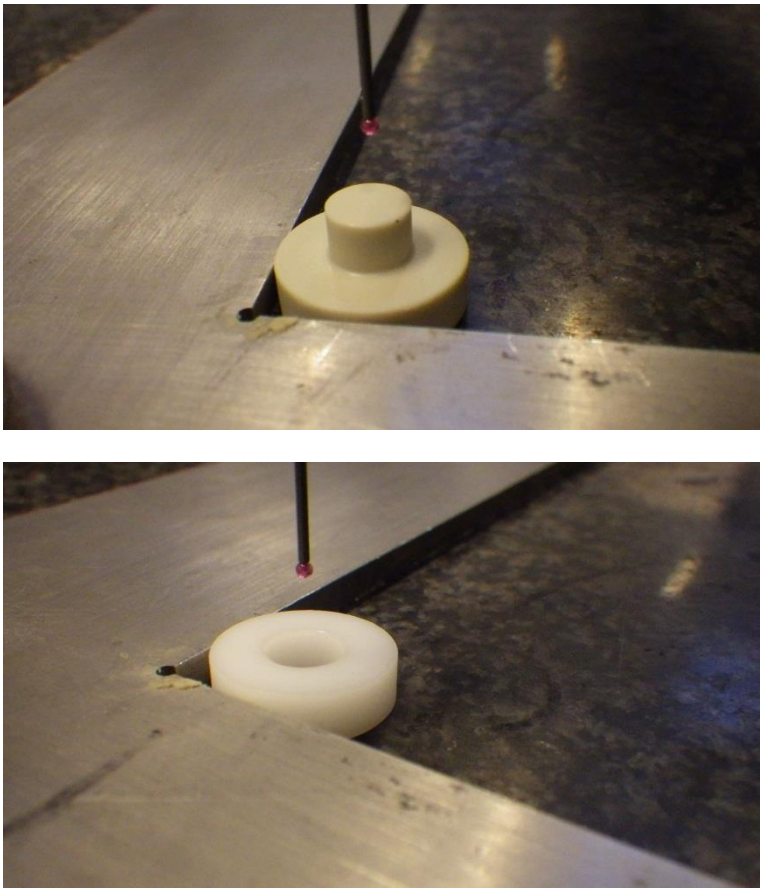

Figure 2.35. Measurement setup for calibration of male part (top) and female part (bottom) from the cylindrical multi-material assembly using the OMC.

The male and female parts were disassembled during the calibrations and measurement process using CMM. The alignment on the male part is performed by using a "3-2-1 alignment". Plane Z is created through least square fitting on the middle plane. The points defining plane Z should be equally distributed by 12 points. Plane Y can be created randomly perpendicular to plane Z, since only the diameter is of interest. The reference axis is defined as follows (see Figure 2.36):

- Z: perpendicular to plane Z;
- Y: perpendicular to plane Y;
- O: intersection between plane Z and axis of a cylindrical datum, which is performed by 50 points, which are equally distributed on the small outer diameter of the male part.

The outer diameter is measured as a circle and the measurement strategy of the outer diameter is computed using the best fitting approach following the Minimum Circumscribed Element (MCE). The MCE is performed by 50 points, which are equally distributed.

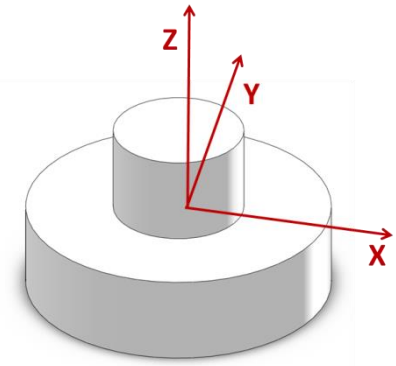

Figure 2.36. Definition of the reference system.

The alignment on the female part is performed by using a "3-2-1 alignment". Plane Z is created through least square fitting on the flat plane. The points defining plane Z should be equally distributed by 12 points. Plane Y can be created randomly perpendicular to plane Z, since only the diameter is of interest. The reference axis is defined as follows (see Figure 2.37):

- Z: perpendicular to plane Z;
- Y: perpendicular to plane Y;
- O: intersection between plane Z and axis of a cylindrical datum, which is performed by 50 points, which are equally distributed in the inner diameter of the female part.

The inner diameter is measured as a circle and the measurement strategy of the inner diameter is computed using the best fitting approach following the Maximum Inscribed Element (MIE). The MIE is performed by 50 points, which are equally distributed.

The selected geometrical features were inner (ID) and outer (OD) diameters (see Figure 2.38), and both were measured from circles.

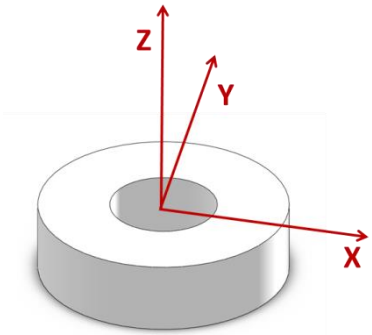

Figure 2.37. Definition of the reference system.

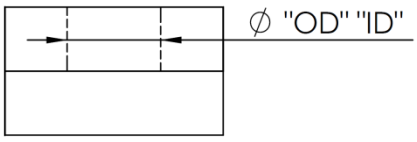

Figure 2.38. Assembly sketch with measurands.

PUMA approach [21] was used for the uncertainty assessment, and estimated uncertainty contributions were similar to the ones for the step gauges, see section 2.2.3. One difference was that the estimated form errors for the assemblies were the roundness. An example of the distribution of uncertainty contributions is summarized in Figure 2.39 for a PP male part and a PE female part. The graph shows that the workpiece form error (roundness) is much larger compared to the other contributions. It documents that the selected polymer materials for the assemblies are ill-suited for milling and drilling processes. No reproduced measurements were performed for on assemblies, because they were scheduled to be CT scanned immediately after the calibrations were completed in September 2011. Average uncertainties (k=2) were in the range of 7.7-22.2 µm for all parts.

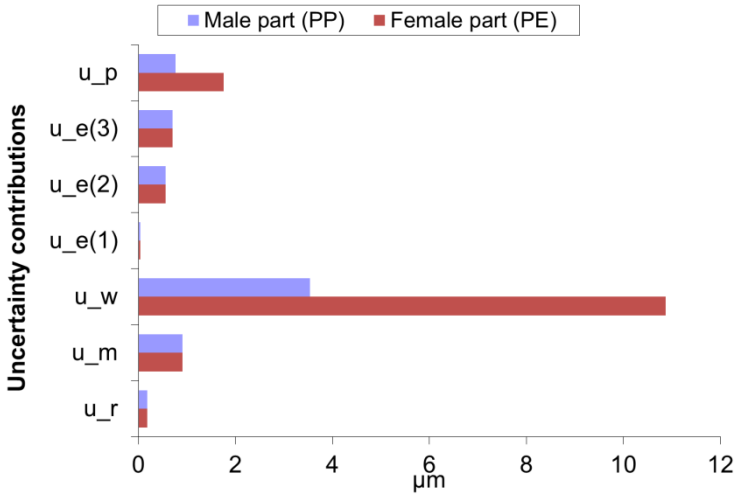

Figure 2.39. Assembly in combination PP-PE – Comparison example of the distribution of uncertainty contributions (k=2) acquired from the calibrations of the male and female parts.

2.5 Threaded tube from the medical industry

The industrial part was a 47 mm length metallic threaded tube tubular component from an insulin pen produced by the Danish medical company Novo Nordisk A/S, see Figure 2.40. The part is manufactured in brass and coated with nickel [6]. For purposes of this thesis, this component is used in connection with an interlaboratory comparison on CT for industrial applications in the manufacturing industry. Altogether, 29 threaded tubes (with each their ID no.) were selected by the author for this issue. Material characteristics as density and thermal expansion coefficient data are shown in Table 2.10.

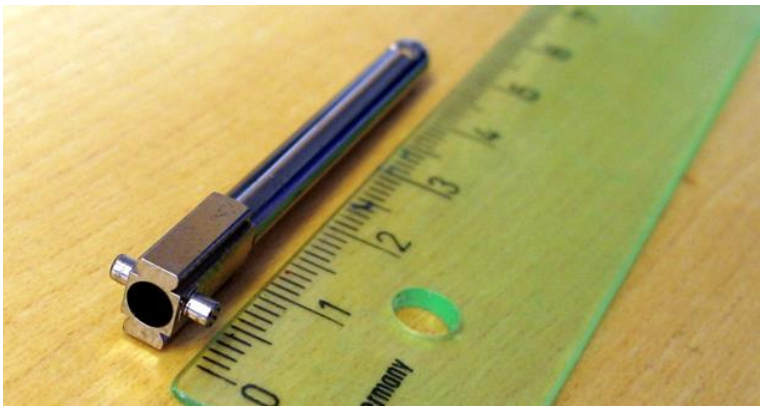

Figure 2.40. Threaded tube from the medical industry.

Table 2.10. Density and thermal expansion coefficient of the threaded tube.

Density [g/cm³]	Thermal expansion coefficient [10^{-6} K^{-1}]
8.500	20±1

2.5.1 Calibration and transfer of traceability

Similar to the step gauges, the metal part was calibrated using the OMC. The probe configuration consisted of three probes: one vertical (probe of Ø2 mm and stylus length of 20 mm) and two horizontal (probe diameters of respectively Ø2 mm with stylus length of 20 mm, and Ø5 mm with stylus length of 50 mm), see Figure 2.41. A ring gauge and gauge block were used as diameter/roundness references and length references to generate traceability. Compensation of the results for temperature changes were made manually. Due to the dynamic probe, no force compensation was performed. Compensation of systematic deviation due to the reference object was carried out.

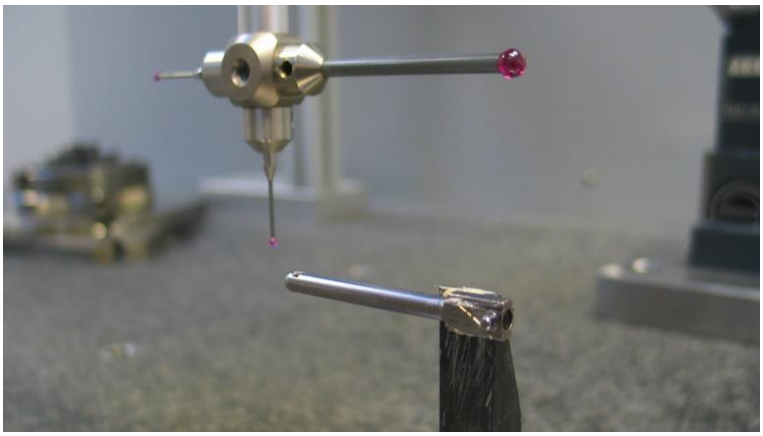

Figure 2.41. Measurement setup for calibration of threaded tube using the OMC.

The coordinate system in Figure 2.42 is defined as follows:

- The primary/spatial alignment is performed using the axis of the outside cylinder, which is created by a least square fitting between the center of circle datums positioned 18 mm and 40 mm from the edge with the pins.
- The secondary/plane alignment is defined as the symmetry line based on two lines using least square elements, 1 mm from the edge with the pins.

- The tertiary alignment to generate the zero point in the third axis is defined as the intersection point between the plane defined from the spatial alignment and the edge with the pins.

The threaded tube features five measurands, identified as D1, R1, D2, R2 and L1. The measurands are illustrated in Figure 2.43.

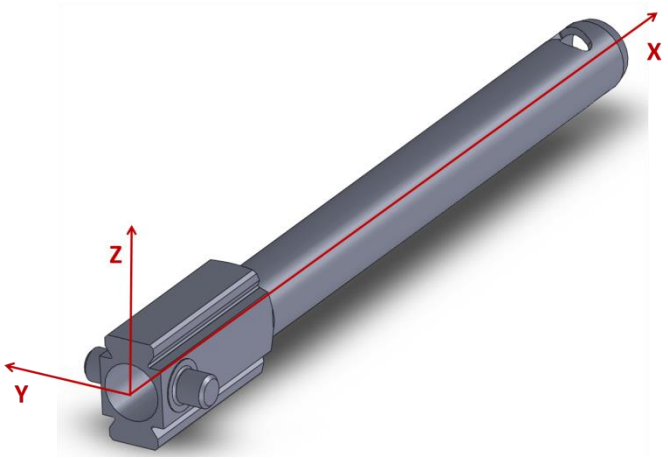

Figure 2.42. Definition of the reference system.

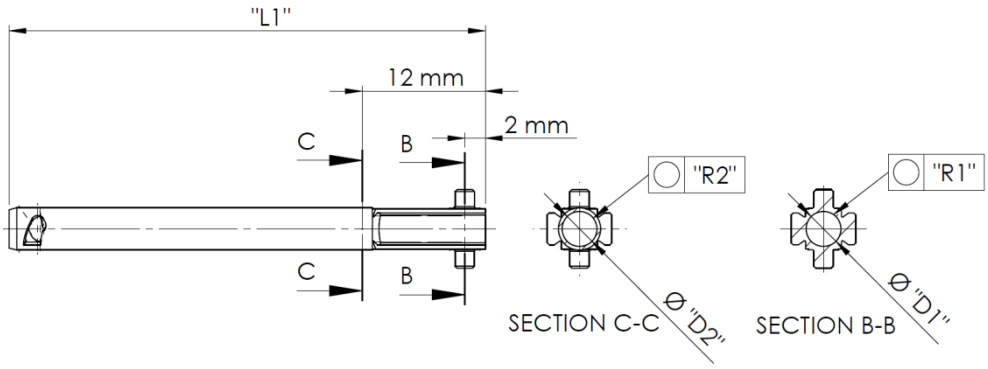

Figure 2.43. Definition of measurands.

A practical approach inspired by the PUMA method [21] was used for uncertainty estimation, as a simplification of the GUM approach [20]. The uncertainty contributors used were the following: 1) reference artefact u_r, 2) repeatability on reference artefact u_{rep}, 3) workpiece u_w, 4) temperature effects u_e, and 5) reproducibility u_p where the parts were repositioned and measured again five times. The temperature contribution was divided into four sub categories: 4.1) difference between workpiece and instrument $u_{e(1)}$, 4.2) deviation from standard reference temperature for instrument $u_{e(2)}$, 4.3) deviation

from standard reference temperature for workpiece $u_{e(3)}$, and 4.4) workpiece expansion coefficient uncertainty $u_{e(4)}$. The models in (2.14) and (2.15) are used for uncertainty estimation.

$$U = k \cdot u_c \qquad (k = 2) \tag{2.14}$$

In this case U is the expanded uncertainty, u_c is the combined standard uncertainty and k is the coverage factor (k=2 for a coverage probability of 95 %). The considered uncertainty contributors are given in (2.15).

$$U = k \cdot \sqrt{u_r{}^2 + u_{rep}{}^2 + u_w{}^2 + u_{e(1)}{}^2 + u_{e(2)}{}^2 + u_{e(3)}{}^2 + u_{e(4)}{}^2 + u_p{}^2} \tag{2.15}$$

An example of the distribution of uncertainty contributions is summarized in Figure 2.44 for the threaded tube in December 2012 (ID no. 2). The graph shows that the contributions from workpiece and reproducibility regarding the measurement process are larger compared to the others.

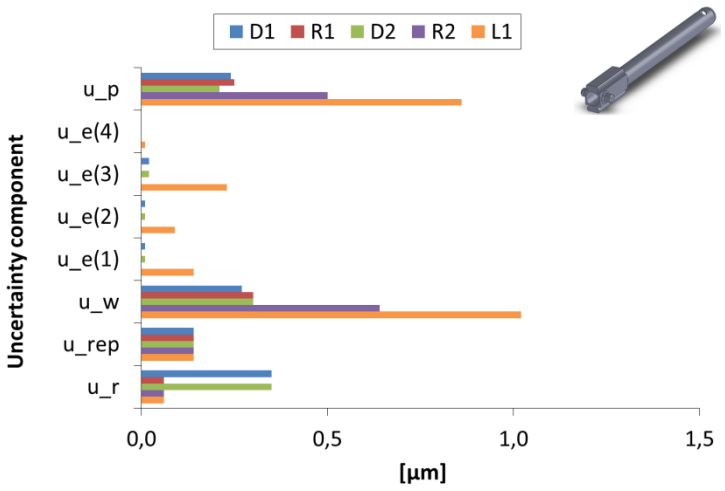

Figure 2.44. Threaded tube ID no. 2 – Comparison example of the distribution of uncertainty contributions acquired from the calibrations in December 2012.

2.5.2 Stability investigation

In order to judge the agreement between reference values, the E_n value normalised with respect to the estimated uncertainty was computed according to ISO 17043 guidelines [46]. If $|E_n| < 1$ the quality of the measurement result is acceptable, while it is not acceptable if $|E_n| \geq 1$. The threaded tube was measured two times (in December 2012 and August 2013, respectively). The months indicated refer to a subset of items: see [51] for the precise time periods. The expanded uncertainties (k=2) from the

measurement rounds are shown in Table 2.11, and are based on all the respective 29 samples. The reproducibility of uncertainty values, as well as that of these and similar other plots, obtained in two different measurements rounds with up to six months difference in-between, is very clear. As a general conclusion, the threaded tube has shown a good stability over the 6 months (see the distribution of E_n values in Figure 2.45). Only R2 is the exception in some cases. It was probably due to the lower wall thickness compared to R1, which made it more sensitive to deformation. Examples of form plots of the roundness R1 and R2 are shown in Figure 2.46. Depending on item and measurand, average reference expanded measurement uncertainties (k=2) ranging from 1.5 µm to 2.5 µm were estimated, see Table 2.12. All reference values and uncertainties for each single item are reported in [51].

Table 2.11. Threaded tube – Average, minimum and maximum expanded uncertainties (k=2). Average values based on 29 samples. Values are in µm. Number of measurement round (RND) as indicated.

	D1		R1		D2		R2		L1	
RND	1st	2nd	1st	2nd	1st	2nd	1st	2nd	1st	2nd
MAX	2.6	1.9	4.4	6.4	3.4	1.2	3.4	3.2	5.2	2.8
AVG	**1.4**	**0.9**	**1.7**	**1.3**	**1.6**	**0.9**	**1.2**	**1.3**	**2.5**	**1.5**
MIN	0.8	0.8	0.5	0.5	0.8	0.8	0.5	0.6	1.0	0.7

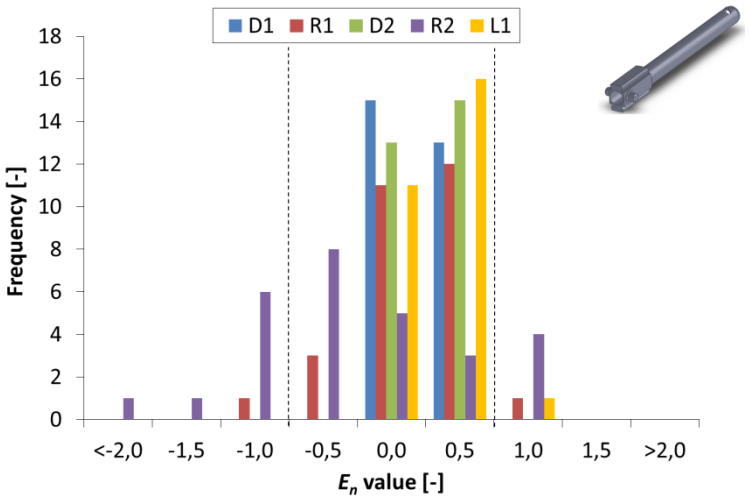

Figure 2.45. Threaded tube – Histogram of E_n values for all measurands. December 2012 vs. August 2013.

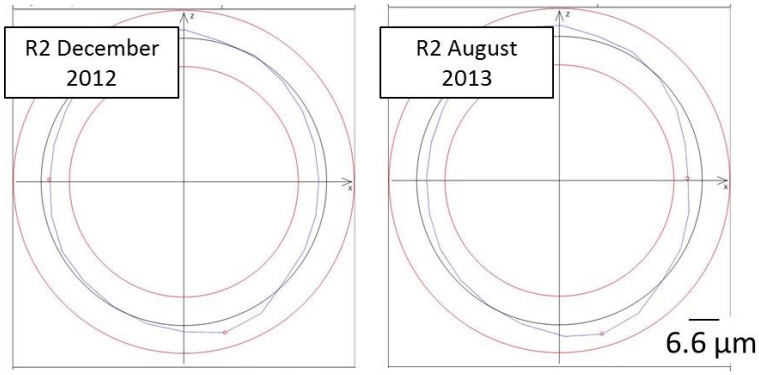

Figure 2.46. Threaded tube ID no. 19 – Form of the roundness R2.

Table 2.12. Reference expanded uncertainties (k=2) for threaded tube. Average values based on all items. Values are in µm.

	D1	R1	D2	R2	L1
MAX	2.6	6.4	3.4	3.4	5.2
AVG	**1.5**	**2.1**	**1.6**	**1.6**	**2.5**
MIN	0.8	0.6	0.8	0.8	1.0

2.6 LEGO brick from the toy industry

The plastic part from the toy industry was a 64 mm length LEGO brick featuring eight knobs, see Figure 2.47. The part is made of Acrylonitrile Butadiene Styrene (ABS) [52]. For purposes of this thesis, this component is used in an interlaboratory comparison on CT for industrial applications in the manufacturing industry. Altogether, 30 LEGO bricks (with each their ID no.) were selected by the author. Material characteristics as density and thermal expansion coefficient data are shown in Table 2.13.

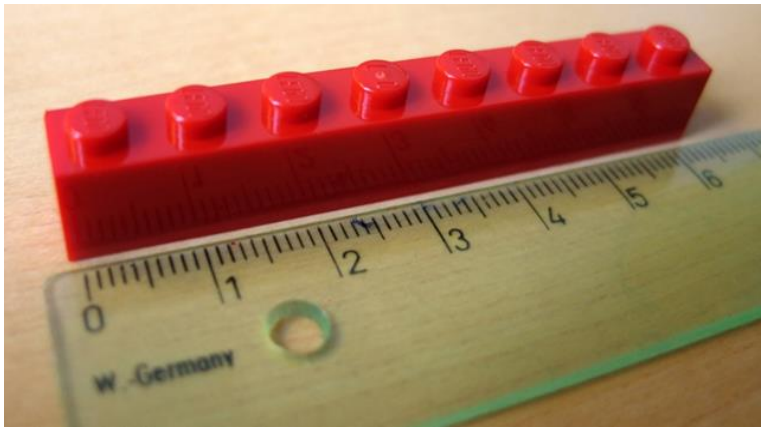

Figure 2.47. LEGO brick from the toy industry.

Table 2.13. Density and thermal expansion coefficient of LEGO brick.

Density [g/cm³]	Thermal expansion coefficient [10^{-6} K^{-1}]
1.040	95±15

2.6.1 Calibration and transfer of traceability

The coordinate measuring machine used at DTU to calibrate the LEGO brick was a mechanical CMM equipped with a static probe. The CMM is of the type Zeiss UPMC 850 CARAT (see Figure 2.48). The maximum permissible error (MPE) of the CARAT is MPE_{U3} = (0.8+*L*/600) µm (*L* in mm). A probe with a diameter of Ø1.0 mm with 32 mm long stylus was used (see Figure 2.49). The CMM is placed in a temperature controlled room where the temperature is 20.0±0.4°C. A ring gauge and a gauge block were used as diameter/roundness references and length references respectively to generate traceability. The measuring force resulting in deflection of styli and polymer work piece was estimated as a systematic compensation. The deflection experiments were performed for 0.10 and 0.15 N, and they were compensated with respect to a force of 0.05 N. The force of 0.05 N was used for creating a zero point. A graph showing the measuring force resulting in deflection of styli and LEGO brick is shown in Figure 2.50. Additionally the systematic deviation due to reference artefact was considered too. Compensation of the results for temperature changes were made automatically through the used software.

Figure 2.48. CMM of the type Zeiss UPMC 850 CARAT.

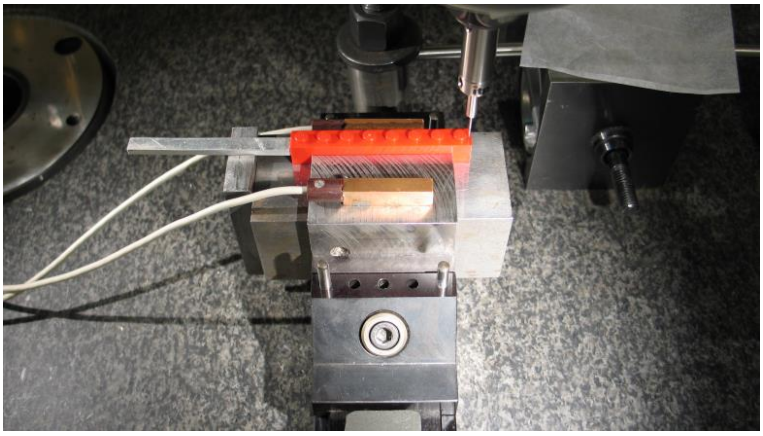

Figure 2.49. Measurement setup for calibration of LEGO brick using the CARAT.

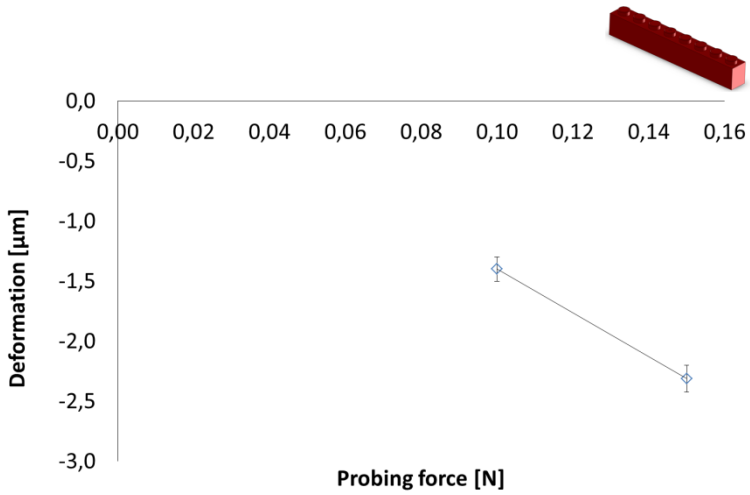

Figure 2.50. Performed probe force experiments for LEGO brick using the CARAT.

The coordinate system in Figure 2.51 is defined as follows:

- The primary/spatial alignment is created by a least square fitting of 46 points on the plane area at the bottom of the knobs.
- The secondary/plane alignment is defined as a line based on the center of two knobs on each edge of the LEGO brick, 1 mm from the plane area at the bottom of the knobs.
- The tertiary alignment to generate the zero point in the third axis is defined as the intersection point between the primary and secondary alignments positioned

at the center of the knob placed at the edge of the LEGO brick and positioned three knobs away from the inlet.

The LEGO brick features three measurands, identified as D1, R1 and L1. The measurands are illustrated in Figure 2.52.

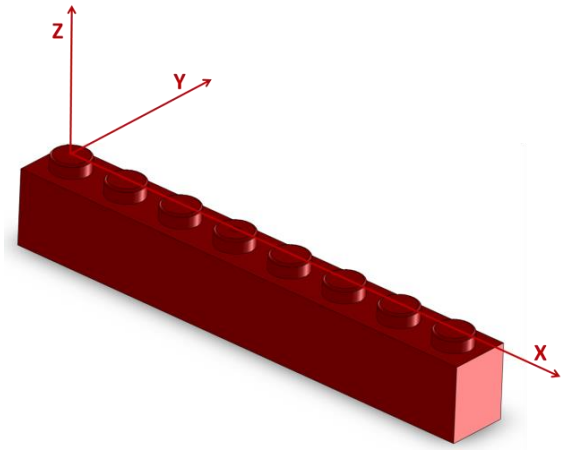

Figure 2.51. Definition of the reference system.

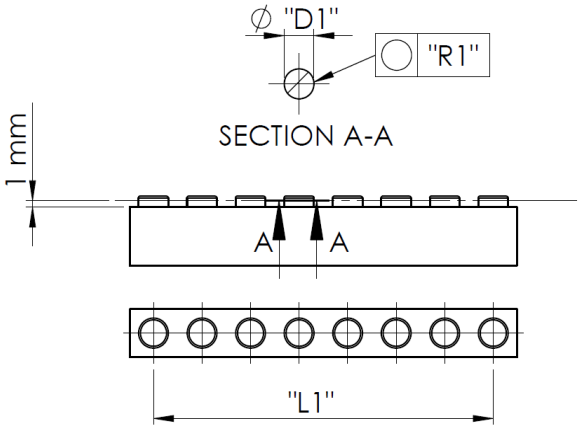

Figure 2.52. Definition of measurands.

PUMA approach [21] was used for uncertainty assessment. The uncertainty contributions estimated were similar to the ones for the threaded tube, see section 2.5.1, just adding 4.5) component from measuring force $u_{e(5)}$. The models in (2.16) and (2.17) are used for uncertainty estimation.

$$U = k \cdot u_c \qquad (k = 2) \tag{2.16}$$

In this case U is the expanded uncertainty, u_c is the combined standard uncertainty and k is the coverage factor (k=2 for a coverage probability of 95 %). The considered uncertainty contributors are given in (2.17).

$$U = k \cdot \sqrt{u_r{}^2 + u_{rep}{}^2 + u_w{}^2 + u_{e(1)}{}^2 + u_{e(2)}{}^2 + u_{e(3)}{}^2 + u_{e(4)}{}^2 + u_{e(5)}{}^2 + u_p{}^2} \quad \textbf{(2.17)}$$

An example of the distribution of uncertainty contributions is summarized in Figure 2.53 for the LEGO brick in December 2012 (ID no. 2). The graph shows that the contribution from the work piece is significant for D1. The significant contributions for R1 are repeatability on the calibration sphere and the work piece. The significant contributions for L1 are the following temperature contributions: the difference between workpiece and instrument, and the deviation from standard reference temperature for workpiece.

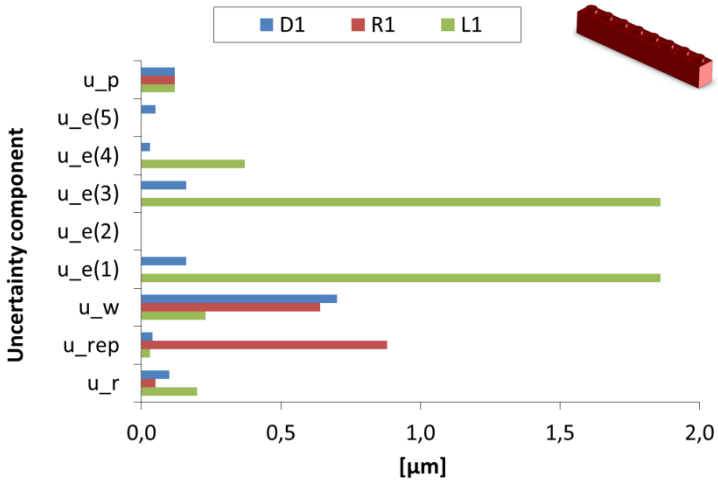

Figure 2.53. LEGO brick ID no. 2 – Comparison example of the distribution of uncertainty contributions acquired from the calibrations in December 2012.

2.6.2 Stability investigation

In order to judge the agreement between reference values, the E_n value normalised with respect to the estimated uncertainty was computed as it was done for the threaded tube in section 2.5 according to ISO 17043 guidelines [46]. The LEGO brick was measured three times (three measurement rounds in December 2012, May 2013, and August 2013, respectively). The months indicated refer to a subset of items: see [51] for the precise time periods. Some temperature problems were detected (see Figure 2.54 and Figure 2.55) during the 2nd round, in connection with measurements on the LEGO bricks. New reference measurements were thus performed at the Centre for Geometrical Metrology CGM (3rd round). A histogram of all the E_n values between 3rd and 2nd round is shown

in Figure 2.56. NPL had supported with CMM measurements for the length L1 using their Zeiss F25 micro-CMM for nine LEGO bricks (with the ID numbers 1-6 and 8-10). The data from NPL were based on the average of 5 repeated measurements with a general expanded uncertainty of 0.37 µm (k=2). Values by CGM for the length L1 are compared with values by NPL (F25) in Figure 2.57. These measurements confirmed the measurements performed by CGM. As a general conclusion, the LEGO brick has shown a good stability over the 6 months. The expanded uncertainties (k=2) from the measurement rounds are shown in Table 2.14, and are based on all the respective 30 samples. Examples of form plots of the roundness R1 are shown in Figure 2.58. It is obvious from the form plots, that they are almost identical to one another, although they have been measured in three different time sequences. Depending on item and measurand, average reference expanded measurement uncertainties (k=2) ranging from 1.6 µm to 5.5 µm were estimated, see Table 2.15. All reference values and uncertainties for each single item are reported in [51].

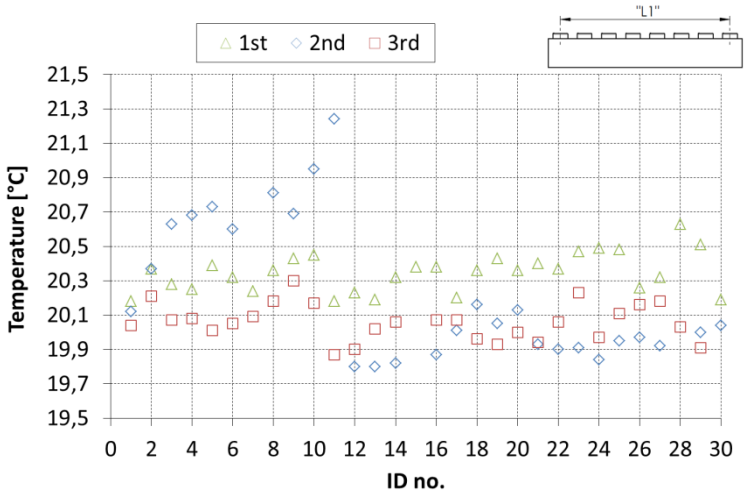

Figure 2.54. LEGO brick – Temperature for L1 in the three measurement rounds.

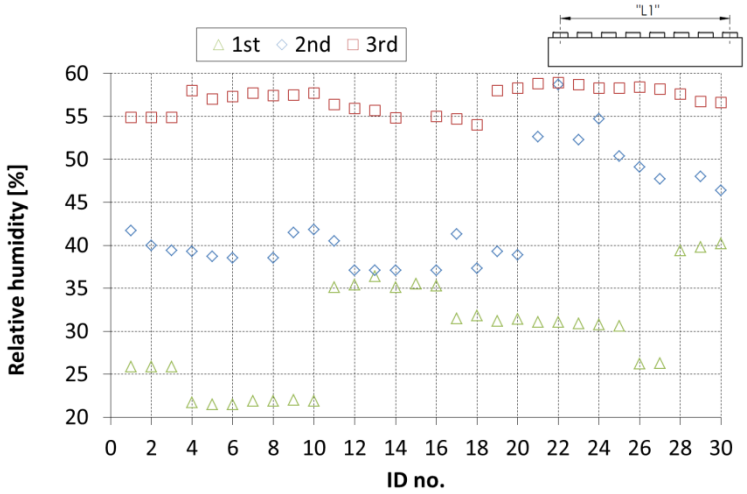

Figure 2.55. LEGO brick – Relative humidity for L1 in the three measurement rounds.

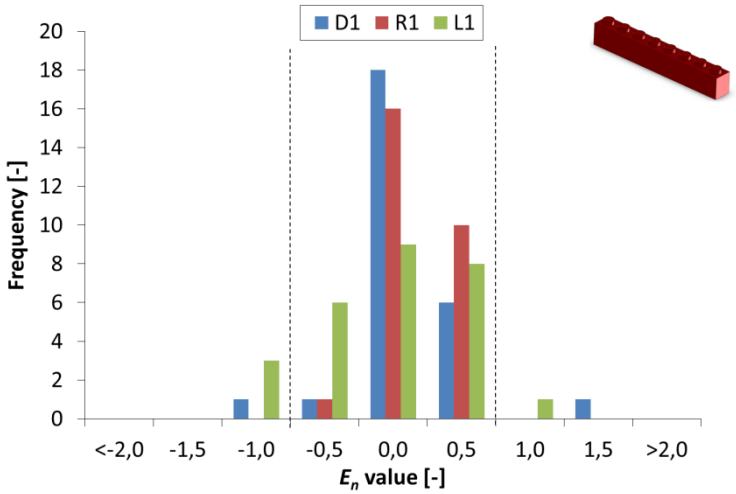

Figure 2.56. LEGO brick – Histogram of E_n values between 3rd and 2nd round for all measurands.

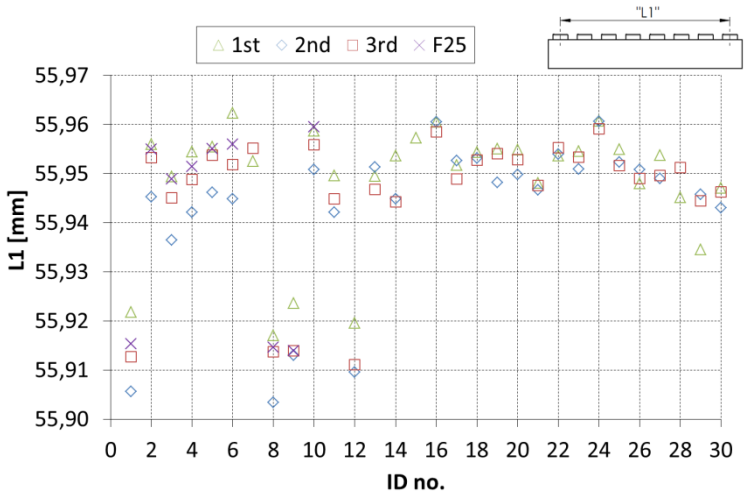

Figure 2.57. LEGO brick – Length L1 in the three measurement rounds. NPL's results are included in the case for L1 (using F25).

Table 2.14. LEGO brick – Average, minimum and maximum expanded uncertainties (k=2). Average values based on 30 samples. Values are in µm. Number of measurement round (RND) as indicated.

	D1			R1			L1		
RND	1st	2nd	3rd	1st	2nd	3rd	1st	2nd	3rd
MAX	2.3	2.2	2.3	4.6	3.9	3.7	5.4	5.6	5.4
AVG	**1.6**	**1.5**	**1.6**	**2.1**	**2.0**	**2.0**	**5.4**	**5.5**	**5.3**
MIN	0.8	0.9	1.0	1.8	1.8	1.8	5.3	5.5	5.3

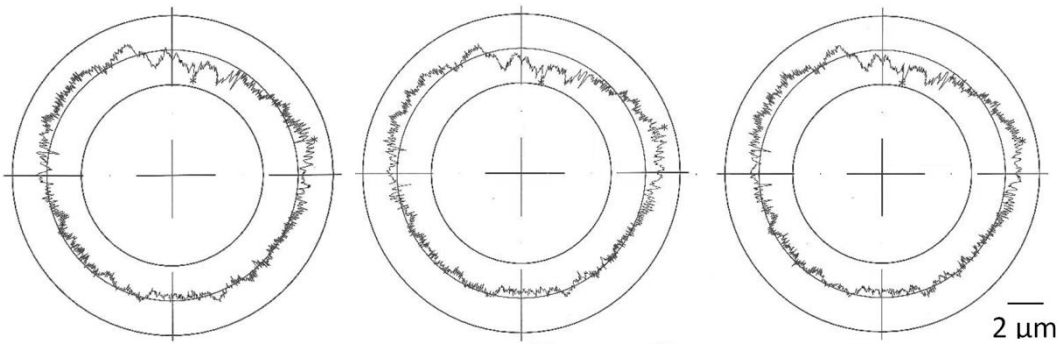

Figure 2.58. LEGO brick ID no. 2 – Profile of roundness R1, 1st round (left), 2nd round (middle), and 3rd round (right).

Table 2.15. Reference expanded uncertainties (k=2) for LEGO brick. Average values based on all items. Values are in µm.

	D1	R1	L1
MAX	2.3	4.6	5.6
AVG	**1.6**	**2.2**	**5.5**
MIN	1.1	1.8	5.3

2.7 Chapter conclusion

In this chapter, different considered standards and guidelines to generate traceability in CT in manufacturing industry are presented and different influence factors are presented. Currently many standardized procedures are still under development which means that the traceability of CT cannot be ensured. One of them is the German guideline VDI/VDE 2617-13 which is considered as a fundamental one for specification and verification of CT system used for coordinate metrology in the manufacturing industry. Various methods and reference objects have been developed in this Ph.D. project to establish metrological traceability of measurements, which can be achieved by documenting the measurements and calibrate the tested reference objects using instruments with known measurement uncertainty. In this work, three kinds of reference objects are introduced: step gauge, step cylinder and a cylindrical multi-material assembly. Moreover, two reference objects are calibrated objects from the manufacturing industry: a threaded tube from the medical industry and a LEGO brick from the toy industry. The quality assurance is carried out using CMMs. The documentation of traceability and the metrological compatibility has been based on various aspects such as form errors, stability over time, uncertainties and temperature effects. The stability has been documented for all reference objects except for the step cylinder and the cylindrical multi-material assembly. These measurements can be used to correct measurement errors in data from a CT. Additionally a brief presentation is made on error sources in CT such as scale errors, threshold offsets, beam hardening, cone beam artifacts and scattered radiation.

Chapter 3 Performance enhancement and characterization on a CT system using step gauges

This chapter presents a design of experiment (DOE) method for evaluating measuring errors in a CT system in terms of material density and orientation of scanned objects. The method for performing a DOE was inspired by another paper with the topic on the influence of image quality in CT [53]. Step gauges were selected with uni- and bidirectional lengths. The number of required scans in the DOE was reduced to save time by documenting that the used CT system was repeatable.

3.1 Analysis of variance on repeatability of the used CT system

A Two-Factor Factorial Design (DOE) was performed to investigate the relationship between repeatability and uni- and bidirectional lengths and by documenting that the used CT system was repeatable. An experiment was conducted using 3 levels of replicated CT scans and five replicated measurements of the measurands on one of the step gauges, and the aluminium step gauge was chosen for this purpose. For the four chosen measurands, two uni- and two bidirectional incremental lengths were selected (see Figure 3.1). The measurands were defined from the left side of the 6th groove to the following: left side of the 7th groove (L_{UNI-1} = 4 mm), left side of the 11th groove (L_{UNI-2} = 20 mm), right side of the 6th groove (L_{BI-1} = 2 mm), and right side of the 11th groove (L_{BI-2} = 22 mm). Regarding alignment and procedure, see section 2.2. The two factors (scan no. and measurand) were specified at 3-4 levels to investigate the repeatability and measurands of the step gauges, as presented in Table 3.1. An analysis of variance (ANOVA) on the repeatability of the CT system was performed regarding the guidelines stated in [54]. The significance level was set to be $\alpha = 0.05$. All scanning and setting parameters were optimized and were the same during all the experiments. An experimental overview of setup and scanning parameters is shown in Table 3.2 and Table 3.3. Furthermore a 1.5 mm copper pre-filter was applied for the aluminium step gauge to reduce beam hardening artifacts. The power P is calculated based on (3.1). Here, U is voltage and I is current.

$$P = U \cdot I \tag{3.1}$$

The resolution of the voxels depends on source-detector distance, source-object distance and detector pixel size. The geometrical magnification m and the voxel size s, are calculated based on (3.2) [6].

$$s = \frac{p}{m} = p \cdot \left(\frac{SOD}{SDD} \right) \tag{3.2}$$

In this case *SDD* is source-detector distance, *SOD* is source-object distance and *p* is detector pixel. An overview of *SDD*, *SOD* and *p* is shown in Figure 3.2.

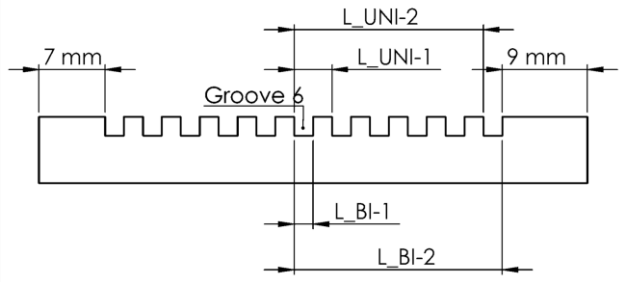

Figure 3.1. Step gauge sketch with measurands.

Table 3.1. Analysis of variance.

Factor	Level			
	1	2	3	4
Scan no.	1	2	3	
Measurand	L_{UNI-1}	L_{UNI-2}	L_{BI-1}	L_{BI-2}

Table 3.2. Experimental plan.

No.	Scan no.	Measurand
1	1	L_{UNI-1}
2	1	L_{UNI-2}
3	1	L_{BI-1}
4	1	L_{BI-2}
5	2	L_{UNI-1}
6	2	L_{UNI-2}
7	2	L_{BI-1}
8	2	L_{BI-2}
9	3	L_{UNI-1}
10	3	L_{UNI-2}
11	3	L_{BI-1}
12	3	L_{BI-2}

Table 3.3. Scanning parameters.

Parameter	Value
Voltage in kV	205
Current In µA	225
Power in W	46.1
Source-detector distance in mm	1145.66
Source-object distance in mm	228.58
Geometrical magnification	5.0
Original voxel size in µm	39.90
No. of projections	3142
Integration time in s	0.1
No. of image averaging	1
Binning	1
Scanning time in min	54

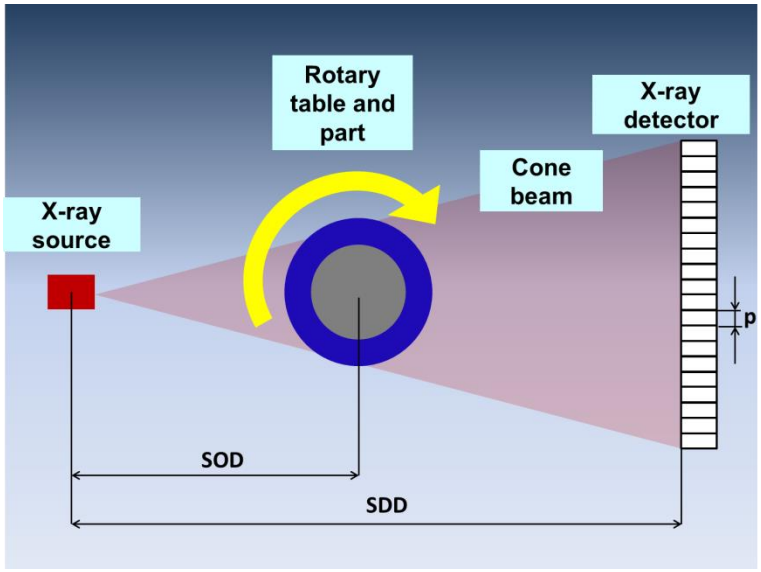

Figure 3.2. Typical geometry of CT (from the top) of the used geometries for determining the magnification and voxel size.

3.2 Design of experiment

A Three-Factor Factorial Design (DOE) was used to investigate the relationship between material density and orientation of uni- and bidirectional lengths. The experiments were performed without any replicated scans, because it was documented that the used CT was repeatable. The three material types were aluminium, PPS and PEEK. The three tested orientations in the experiments are illustrated in Figure 3.3. The three factors (material, orientation, and measurand) were specified at 3-4 levels to investigate the orientation and density effect of the step gauges as presented in Table 3.4. An ANOVA for the material density types and orientations of the step gauges was performed with three replicated measurements of the measurands following the

guidelines stated in [54]. The significance level was set to be $\alpha = 0.05$. Normally the same setting (of inclined orientation) is not proper when the object is placed horizontally, because there is a big difference on the maximum penetration length due to voltage, filter and current. But for the DOE there were too many influencing factors, and it was necessary to keep as many parameters constant as possible. Instead good settings were found for all three step gauges with all orientations, and 3 general settings were found: each setting corresponds to one type of material and could be applied when the step gauge was orientated differently. An experimental overview is shown in Table 3.5 and Table 3.6. A 1.5 mm copper pre-filter was applied for the aluminium step gauge as already mentioned. No filters were applied for the PEEK and PPS step gauges. The remaining setup and parameters were already stated in Table 3.3.

Figure 3.3. Orientations (B) at three levels. From left to right: horizontal, vertical, and inclined.

Table 3.4. A Three-Factor Factorial Design (DOE).

Factor	Level			
	1	2	3	4
Material	Aluminium	PPS	PEEK	
Orientation	Horizontal	Vertical	Inclined	
Measurand	L_{UNI-1}	L_{UNI-2}	L_{BI-1}	L_{BI-2}

Table 3.5. Experimental plan.

No.	Material	Orientation	Measurand
1	Aluminium	Horizontal	L_{UNI-1}
2	Aluminium	Horizontal	L_{UNI-2}
3	Aluminium	Horizontal	L_{BI-1}
4	Aluminium	Horizontal	L_{BI-2}
5	Aluminium	Vertical	L_{UNI-1}
6	Aluminium	Vertical	L_{UNI-2}
7	Aluminium	Vertical	L_{BI-1}
8	Aluminium	Vertical	L_{BI-2}
9	Aluminium	Inclined	L_{UNI-1}
10	Aluminium	Inclined	L_{UNI-2}
11	Aluminium	Inclined	L_{BI-1}
12	Aluminium	Inclined	L_{BI-2}
13	PPS	Horizontal	L_{UNI-1}
14	PPS	Horizontal	L_{UNI-2}
15	PPS	Horizontal	L_{BI-1}
16	PPS	Horizontal	L_{BI-2}
17	PPS	Vertical	L_{UNI-1}
18	PPS	Vertical	L_{UNI-2}
19	PPS	Vertical	L_{BI-1}
20	PPS	Vertical	L_{BI-2}
21	PPS	Inclined	L_{UNI-1}
22	PPS	Inclined	L_{UNI-2}
23	PPS	Inclined	L_{BI-1}
24	PPS	Inclined	L_{BI-2}
25	PEEK	Horizontal	L_{UNI-1}
26	PEEK	Horizontal	L_{UNI-2}
27	PEEK	Horizontal	L_{BI-1}
28	PEEK	Horizontal	L_{BI-2}
29	PEEK	Vertical	L_{UNI-1}
30	PEEK	Vertical	L_{UNI-2}
31	PEEK	Vertical	L_{BI-1}
32	PEEK	Vertical	L_{BI-2}
33	PEEK	Inclined	L_{UNI-1}
34	PEEK	Inclined	L_{UNI-2}
35	PEEK	Inclined	L_{BI-1}
36	PEEK	Inclined	L_{BI-2}

Table 3.6. Scanning parameters.

Material	Voltage in kV	Current In µA	Power in W
Aluminium	205	225	46.1
PPS	100	170	17.0
PEEK	100	155	15.5

3.3 Experimental setup

The experiment was carried out using a Nikon Metrology MCT225 scanner at KUL (Figure 3.4). The reconstruction of the 2D X-ray images was carried out using software CT Pro provided by Nikon Metrology, too. Data analysis was performed using VolumeGraphics on surface data (STL). It is important to have in mind that converting files to STL results in voxel information being lost [5]. No data filtering and scale error correction was achieved. For the ANOVA on repeatability of the used CT system, the object was scanned in an inclined orientation. This orientation reduces the occurrence of beam hardening and scattering artifacts [2; 4]. For the DOE, the objects were scanned in three different orientations (as already indicated in section 3.2). For orientations with vertical and inclined cases, the end with a material thickness of 9 mm was placed on the top. The objects were attached to a fixture material made of expanded polystyrene, see Figure 3.5. Expanded polystyrene is widely used as a fixture in CT applications due to its high penetrability. The measured temperature was around 20 °C through all the experiments.

Figure 3.4. Nikon Metrology MCT225 scanner at KUL.

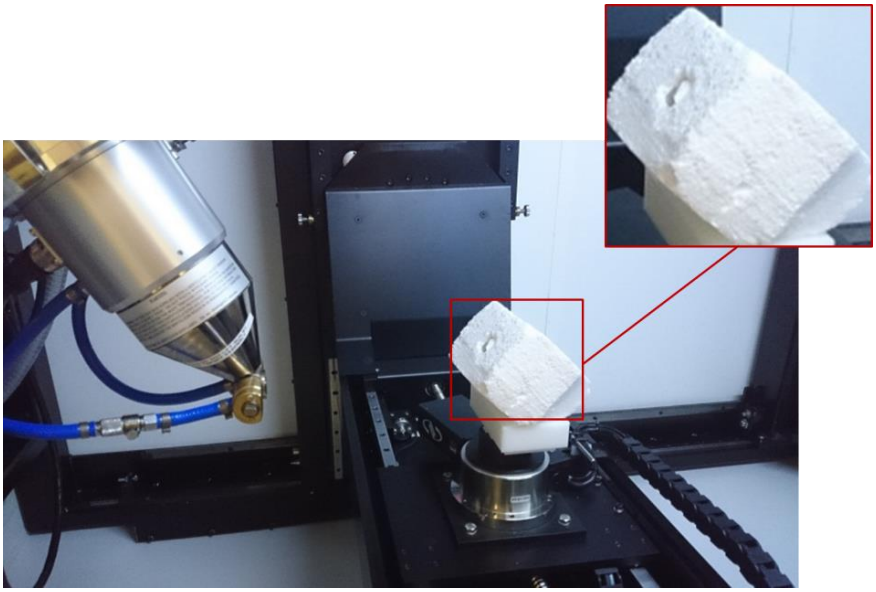

Figure 3.5. Measurement setup of the object in the CT. Expanded polystyrene was used as fixture material for the step gauges. The step gauge was placed inside the expanded polystyrene.

3.4 Data evaluation

ISO 50% (global one) was used for surface segmentation between material and air for the bidirectional lengths (threshold edge dependent), see Figure 3.6. For the evaluation of the data, the error was defined as the deviation between CT and reference measurements.

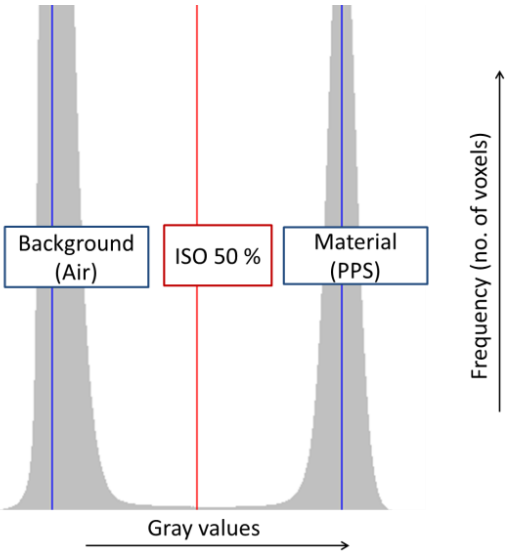

Figure 3.6. Histogram of gray value distribution of the reconstructed 3D volume of the PPS step gauge and determination of threshold value.

3.5 Results and discussion

The statistical analysis was performed using Minitab while a description of the used statistical abbreviations can be found in Nomenclature. The residuals were estimated in accordance with the repeatability. With a significance level on $\alpha = 0.05$ the P value for the residuals must not be smaller than 0.05 otherwise the residuals fail the normality test. Residuals and model adequacy checking showed that the residuals failed the normality test, because of the small P value as shown in Figure 3.7. It means that the data does not follow one of the assumptions of the regression. Some solutions to achieve a large P value are one or more of the following: 1) fit a different model, 2) evaluate the data differently or 3) exclude outliers. The author evaluated that there were too few data to delete eventual outliers. Instead it was assumed to neglect the two-factor interactions, in which these were implemented in the error for the ANOVA. This assumption gave a higher P value as shown in Figure 3.8. The main effect and interaction plots are shown in Figure 3.9. From these it was clear that the mean variation between the three scans was quite small, below 1 µm. Based on the ANOVA in Table 3.7 it was decided that the CT used was repeatable. The measured deviations from the reference values can be corrected by a combination of the following: scale error correction, correct surface segmentation for threshold edge dependent distances, and by applying linear regression. The calculations for the edge offsets *b* show two different offsets due to the bidirectional size as shown in Table 3.8. The variation width (difference between maximum and minimum) was quite small with a maximum of 0.7 µm. The difference between the two *b* values could be due to error sources such as beam hardening artifacts and scattered radiation. Instead it was assumed to use the average of the two *b* values for the corrections. The data before and after applying scale error and threshold offset correction are shown in Figure 3.10, and the maximum deviation from reference value was reduced from 12 µm to 2 µm.

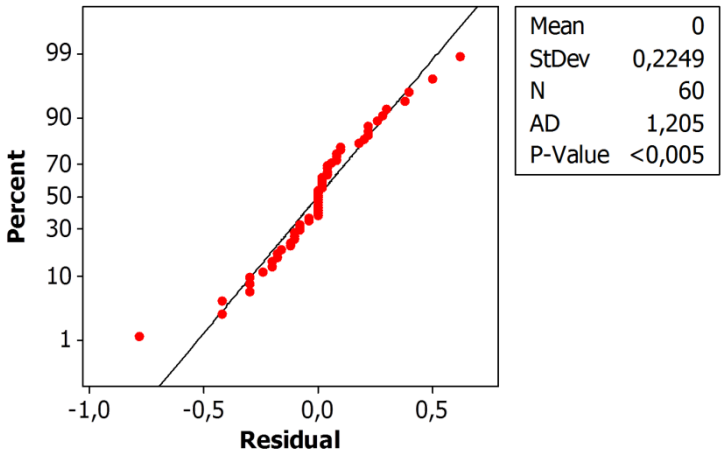

Figure 3.7. Normal probability plot of residuals (including interaction AB).

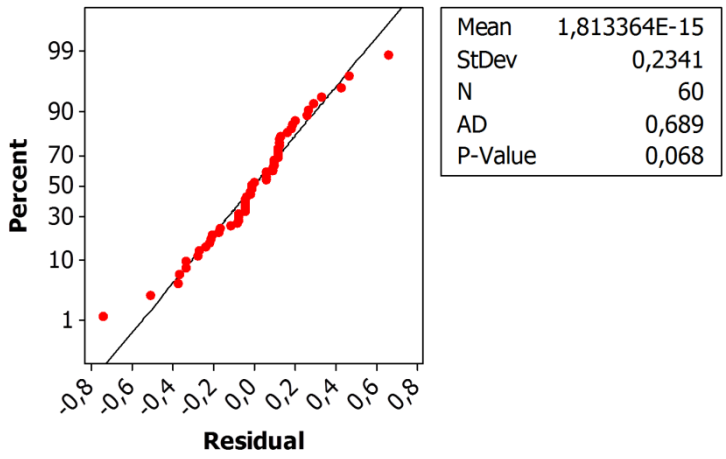

Figure 3.8. Normal probability plot of residuals (excluding interaction AB).

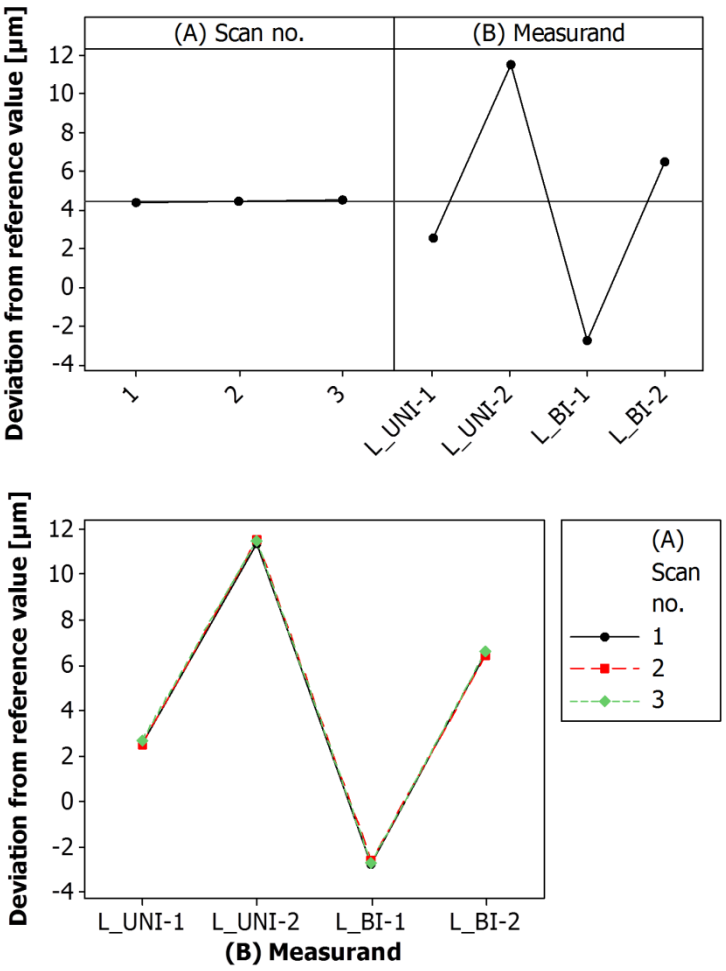

Figure 3.9. Main effect and interaction plots.

Table 3.7. Analysis of variance on repeatability of CT system using an aluminium step gauge.

Source of variation	SS	df	MS	F value	P value
Scan no. (A)	0.17	2	0.084	1.41	0.253
Measurand (B)	1624.41	3	541.471	9042.20	0.000
Error	3.23	48	0.060		
Total	1627.82	59			

Table 3.8. Calculation of the edge offsets *b*.

Measurand	Edge offset *b* [µm]	Variation width [µm]
L_{BI-1}	1.96	0.4
L_{BI-2}	3.44	0.7

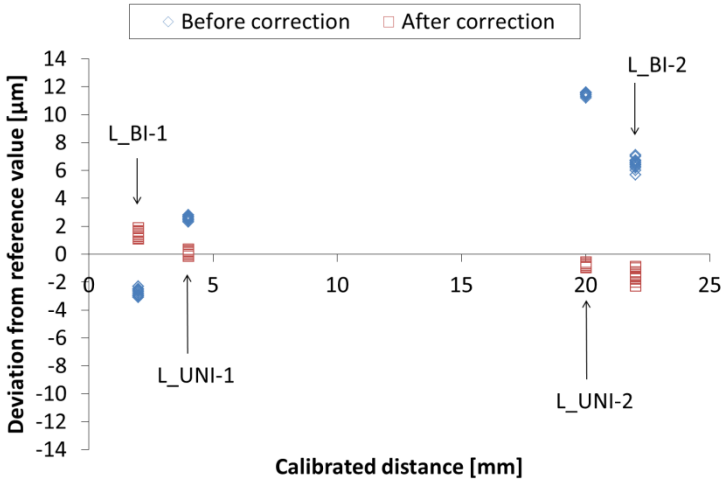

Figure 3.10. Comparison of data before and after applying scale error and threshold offset correction.

Some problems were detected for the aluminum step gauge regarding the DOE between material density and orientation. Figure 3.11 and Figure 3.12 show that the vertical orientation is more affected by the occurrence of scattering artifacts [4] compared to the inclined one.

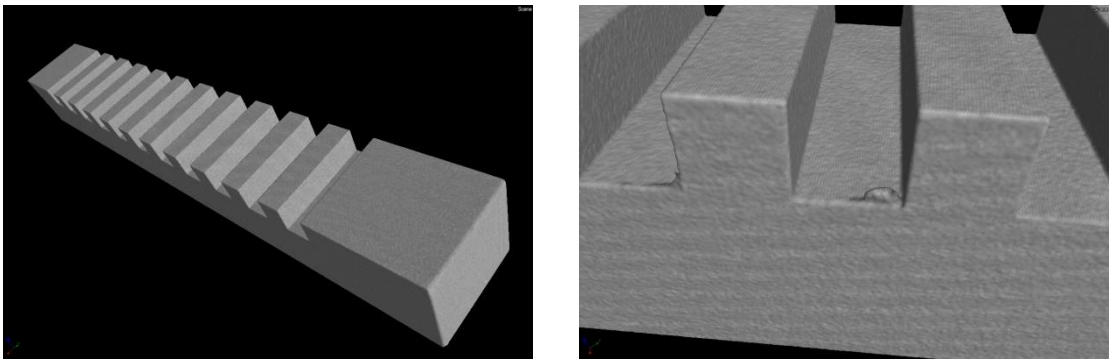

Figure 3.11. 3D volume of an aluminium step gauge mounted in the CT cabinet orientated diagonally.

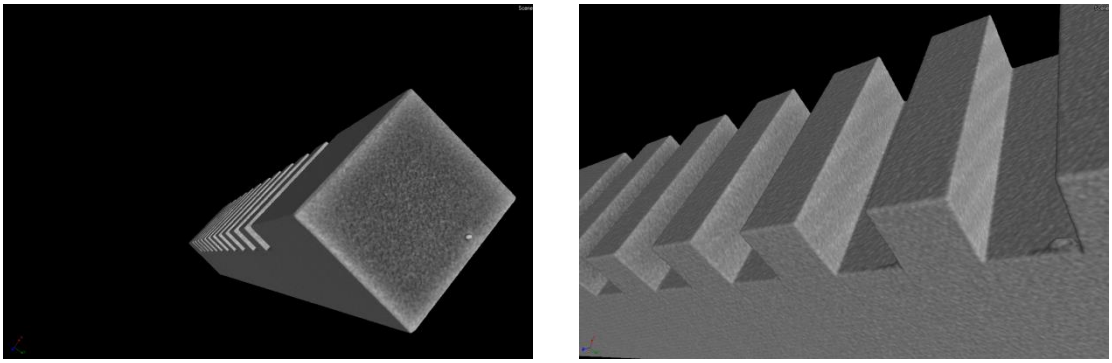

Figure 3.12. 3D volume of an aluminium step gauge mounted in the CT cabinet orientated vertically.

The residuals were estimated in accordance with the DOE. The method for evaluating the residuals was identical to the one used for the repeatability on the step gauges mentioned previously. Residuals and model adequacy checking showed that the residuals failed the normality test because of the small P value as shown in Figure 3.13. Instead it was assumed to neglect the three-factor interaction, in which this was implemented in the error for the ANOVA. This assumption gave a higher P value as shown in Figure 3.14. The main effect and interaction plots are shown in Figure 3.15. From these it can be seen that maximum deviations from reference values of approximately 20 µm is obtained. Based on the ANOVA in Table 3.9 it was evaluated that all main factors and their interactions were significant. The following conclusions can be drawn based on the main factors only:

- The material density affects the measurement results. The measured distance changes with approximately 10 µm between aluminium and PEEK. The reason can be that the measurement results can be affected by filtering in which a 1.5 mm copper filter was applied for the aluminium step gauge.
- A vertical orientation is not recommended because of error sources such as scattering artifacts. Approximately no difference was detected between horizontal and inclined orientations, and the measured distance was 10 µm smaller for the inclined one compared to the vertical one.

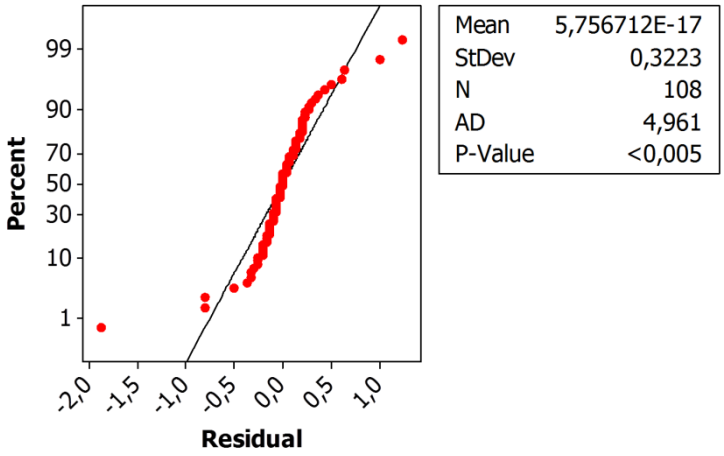

Figure 3.13. Normal probability plot of residuals (including interaction ABC).

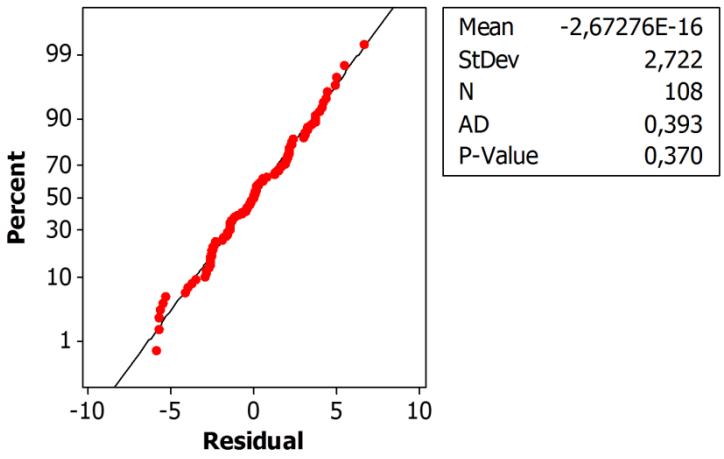

Figure 3.14. Normal probability plot of residuals (excluding interaction ABC).

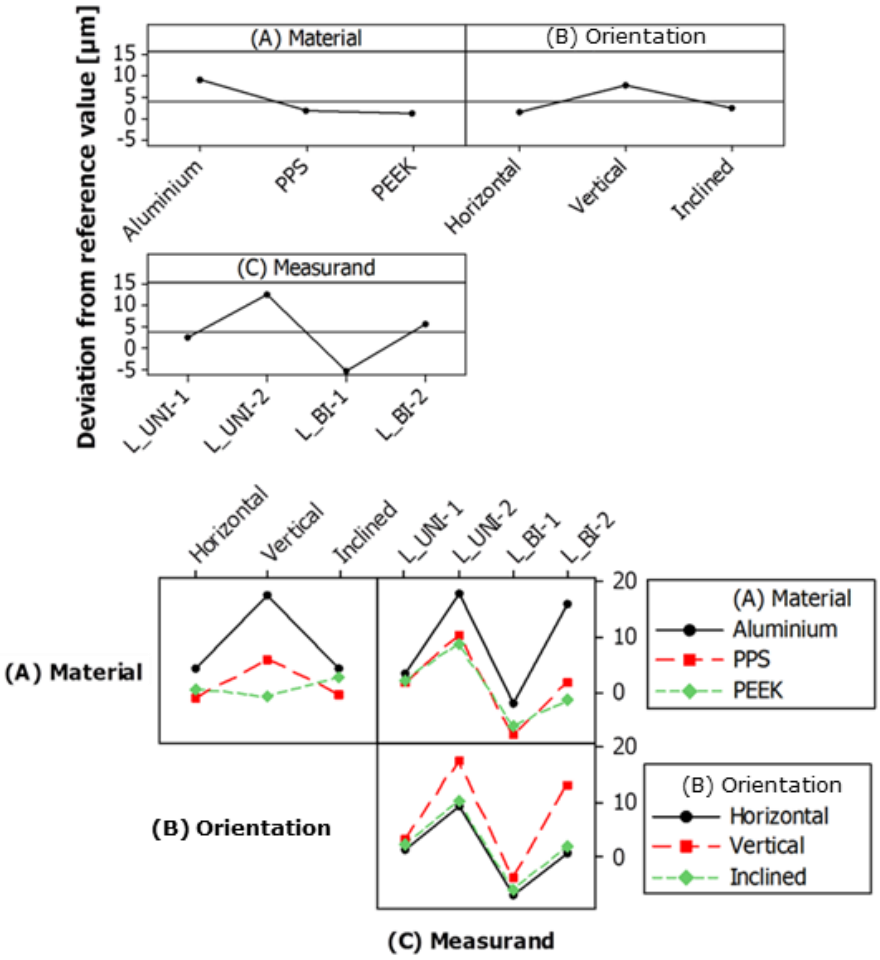

Figure 3.15. Main effect and interaction plots. Values are in µm.

Table 3.9. Analysis of variance on material density and orientation of uni- and bidirectional lengths.

Source of variation	SS	df	MS	F value	P value
Material (A) at three levels	1396.37	2	698.19	74.00	0.000
Orientation (B) at three levels	848.05	2	424.03	44.94	0.000
Measurand (C) at four levels	4350.93	3	1450.31	153.72	0.000
Interaction (AB)	1025.56	4	256.39	27.18	0.000
Interaction (AC)	741.92	6	123.65	13.11	0.000
Interaction (BC)	418.47	6	69.75	7.39	0.000
Error	792.52	84	9.43		
Total	9573.82	107			

Scale error and offset corrections were carried out on the measurement results from the DOE. It was discovered that the linear regression coefficient mainly changes depending on material and orientation (see main plot and interaction plots in Figure 3.16). It seems that the regression coefficient *a* increases with increasing material density which indicated that the voxel size increases with increasing material density. The increasing

regression coefficient, due to the vertical orientation, seems to be caused by scattering artifacts. The offset changes are dependent on material, orientation and geometrical size (see Figure 3.17), and the offset changes with changing material density probably due to the changing grey value. Furthermore the offset changes depending on the geometrical size which indicates some unknown error sources. It was assumed to use the average of the two *b* values for the corrections of each case (material vs. orientation). The main plots and interaction plots after applying scale error and threshold offset correction are shown in Figure 3.18, and the maximum deviation from reference value was reduced from 20 µm to 12 µm. It is clear that it is more complicated to correct for vertical orientations in high density materials.

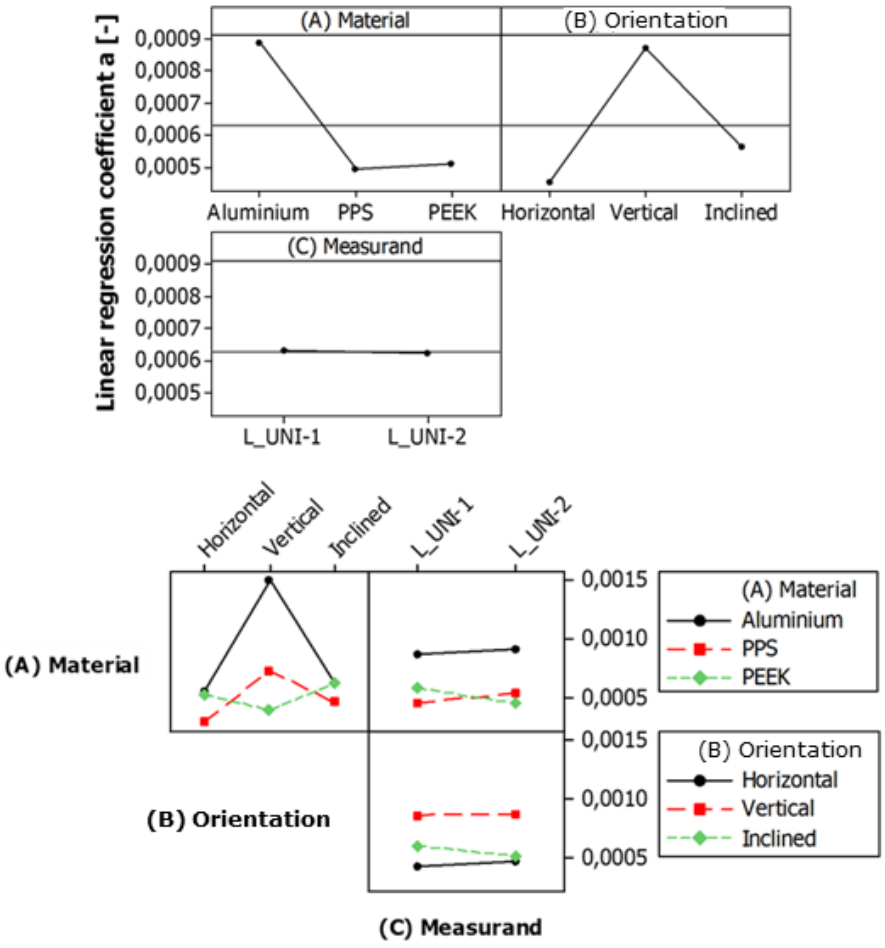

Figure 3.16. Main effect and interaction plots for the linear regression coefficient *a*.

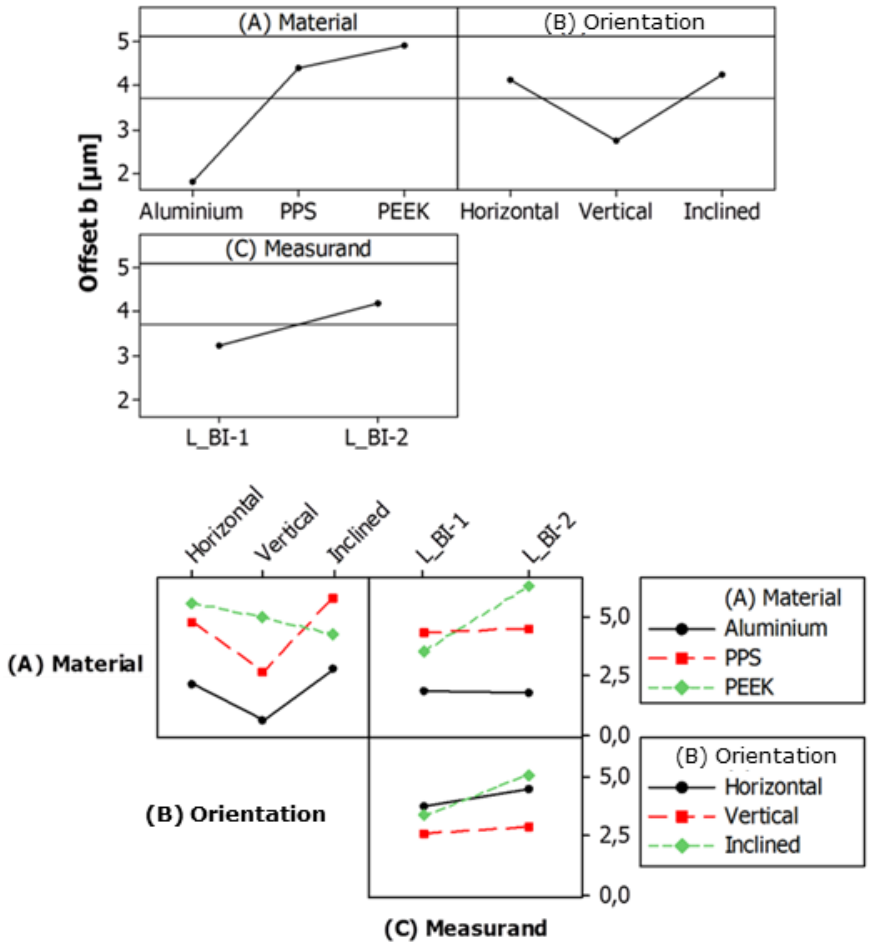

Figure 3.17. Main effect and interaction plots for the offset *b*. Values are in µm.

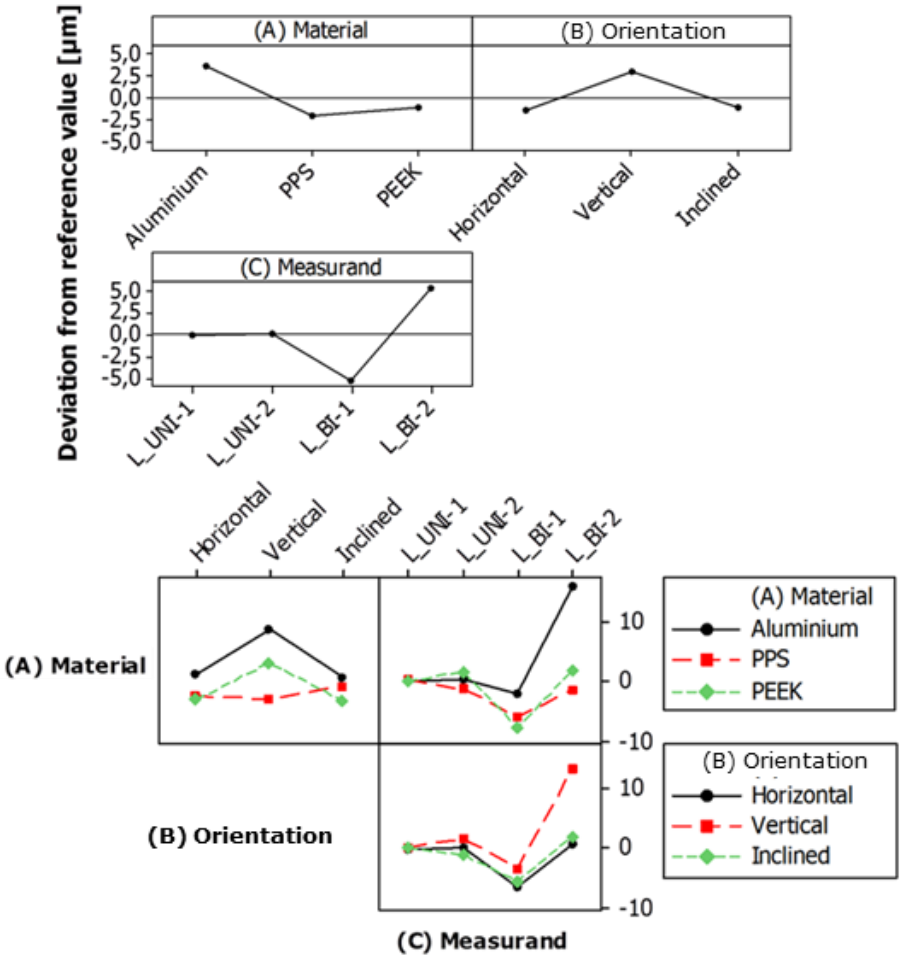

Figure 3.18. Main effect and interaction plots after correction. Values are in µm.

3.6 Chapter conclusion

This chapter presents a method for evaluating measuring errors arising in a CT system in terms of material density and the orientation of the scanned objects. Step gauges are selected with uni- and bidirectional lengths. The ANOVA shows that all main factors and their interactions are significant. The following conclusions can be drawn based on the main factors only: 1) the material density affect the measurement results, 2) a vertical orientation is not recommended because of X-ray scattering noise and relatively lower scattering noise ratio on the planes that are parallel to the X-ray beams, and 3) approximately no difference is detected between horizontal and inclined orientations. The maximum deviation from the reference value can be reduced by compensating for systematic errors such as scale error correction and threshold offsets. But it is more complicated to correct for vertical orientations in high density materials.

Chapter 4 Interlaboratory comparisons on CT scanners for industrial applications in the manufacturing industry

This chapter focuses on the application of CT for traceable measurement of dimensions and form on mechanical components in the manufacturing industry. Comparisons allow to collect information about measurement performance in state-of-the-art industrial CT. A previous international comparison has involved a number of objects typically used for CT performance testing, featuring easy X-ray penetration and well defined geometries with low form errors [55]. However, even when the performance of the measuring instrument has been validated through calibration or verification, the influence from the object properties and from the measuring procedure followed by the operator can add considerably to the total measurement uncertainty. This is important to address when dealing with a new technology such as CT. In this chapter, two comparisons: a preliminary and a main comparison are described based on the use of common industrial items that are more relevant for industrial measurements, in terms of material, dimensions and geometrical properties. The comparisons were based on earlier experience in coordinate metrology at the department [56; 57]. The use of industrial components as reference items raises a number of challenges in the form errors, temperature sensitivity, and lower material stability over time degrade the metrological compatibilities and increase the resulting measurement uncertainty. A key issue in the comparisons has been to document that the industrial items used are stable and controllable, and can be used as reference objects to evaluate dimensional measurements from CT scanning, in terms of systematic errors and estimated uncertainties.

4.1 Preliminary interlaboratory comparison

A preliminary comparison involved three items (see Figure 4.1) measured by six participants: 3D-CT A/S (DK), Carl Zeiss IMT GmbH (DE), Danish Technological Institute (DK), Zebicon A/S (DK), Novo Nordisk A/S Device R&D (DK), Novo Nordisk A/S DMS Metrology & Calibration (DK) [58].

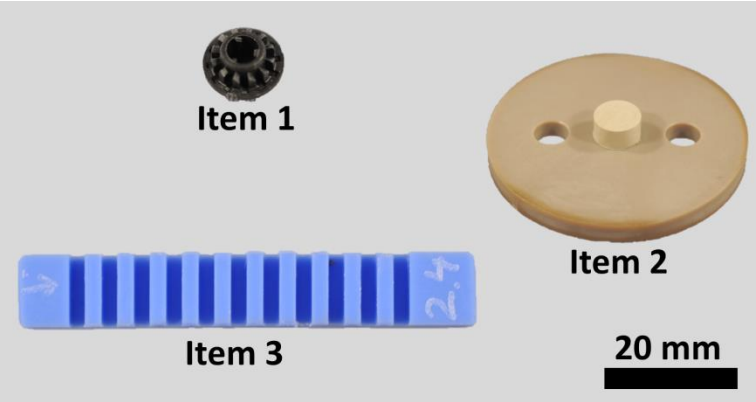

Figure 4.1. The three items in the preliminary comparison **[58]**.

The comparison was carried out from November 2010 to July 2012 and the activities encompassed planning, calibration, circulation, data analysis, reporting and dissemination. A purpose of the comparison was to test the applicability of CT, in terms of systematic errors and estimated uncertainties, to carry out measurements on small polymer objects. Aim of the measurements was to determine different measurands, encompassing diameter (D), roundness (R), and length (L). Definition of measurands, reference measurements and item stability analysis were performed using CMM and are documented in [58]. Depending on item and measurand, average expanded uncertainties in the range 1-23 µm were obtained for CMM measurements (see Table 4.1).

Table 4.1. Reference expanded uncertainties (k=2) for Items 1, 2 and 3. Average values based on calibrations at three different times. Values are in µm.

	Item 1			Item 2			Item 3			
	D1	R1	L1	D1	R1	L1	L1	L2	L3	L4
MAX	22.0	7.1	7.6	23.1	0.8	7.0	5.3	6.9	7.0	6.5
AVG	**22.0**	**7.1**	**7.6**	**23.1**	**0.7**	**7.0**	**5.2**	**6.4**	**6.2**	**5.8**
MIN	22.0	7.1	7.6	23.1	0.7	7.0	5.0	5.9	5.3	5.0

The results of CT measurements by single participants were analysed and compared with reference values obtained by the coordinator. Figure 4.2, Figure 4.3 and Figure 4.4 show typical results. Depending on item and measurand, the participants stated average expanded uncertainties for CT measurements in the range 11-17 µm, with maximum values up to 49 µm, see Table 4.2. Some challenges were detected: 1) Item 3 was exposed to deformations as previously mentioned in section 2.2 and 2) a significant form error was detected on the surface of Item 2, which influences the definition of datums and alignment [58; 59]. For this reason, it was decided to carry out a new comparison, called main comparison, described in the following section.

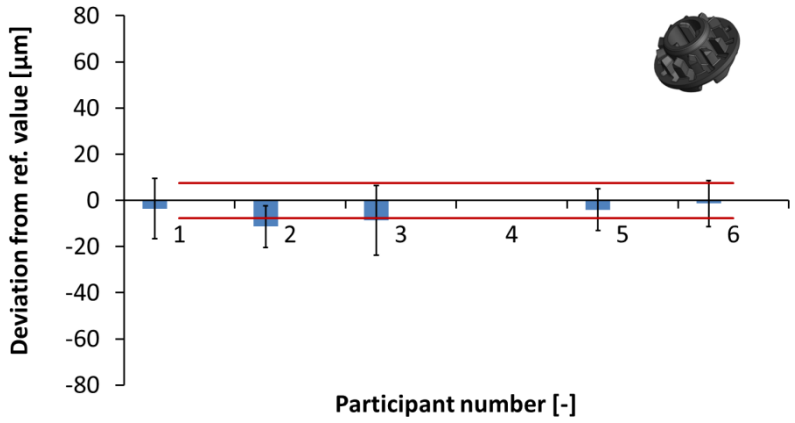

Figure 4.2. CT results for Item 1. Length L1. Error bars show expanded uncertainties. Reference uncertainty indicated by red lines.

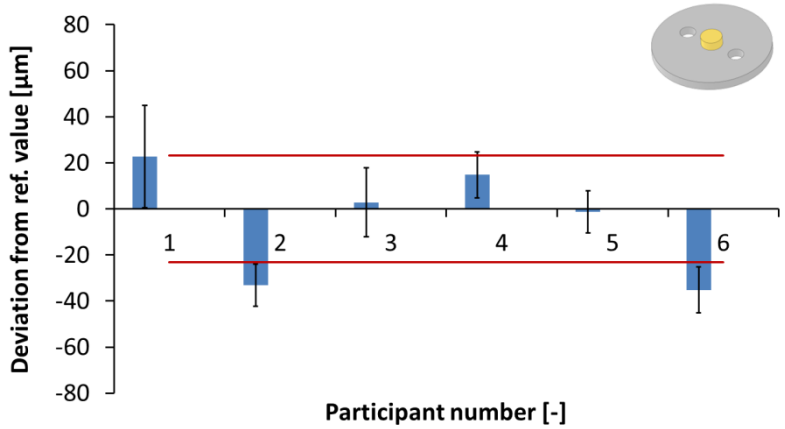

Figure 4.3. CT results for Item 2. Diameter D1. Error bars show expanded uncertainties. Reference uncertainty indicated by red lines.

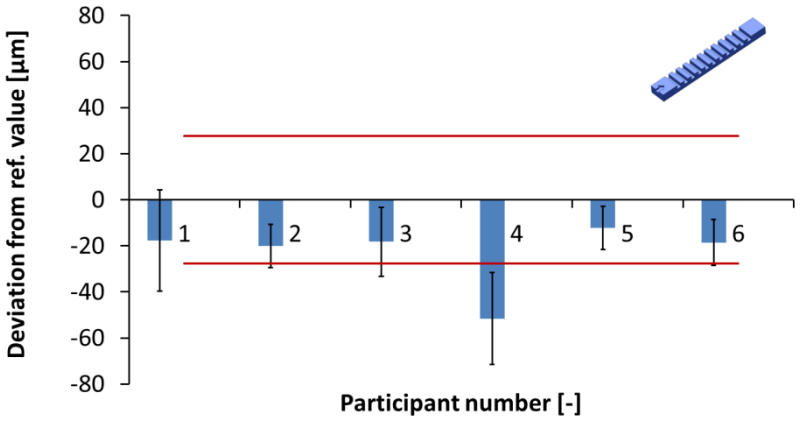

Figure 4.4. CT results for Item 3. Length L4. Error bars show expanded uncertainties. Reference uncertainty indicated by red lines.

Table 4.2. Expanded uncertainties stated by the participants (k=2). Average values based on all participants. Values are in µm.

	Item 1			Item 2			Item 3			
	D1	R1	L1	D1	R1	L1	L1	L2	L3	L4
MAX	35.4	17.7	15.0	22.2	42.2	48.6	15.0	20.5	27.8	22.0
AVG	**15.8**	**12.1**	**11.2**	**12.6**	**15.9**	**17.0**	**12.0**	**13.2**	**13.5**	**14.3**
MIN	9.2	9.0	9.0	9.2	9.0	9.1	9.2	9.3	9.0	9.4

4.2 Main interlaboratory comparison

The documented challenges and problems in the preliminary comparison were re-considered in terms of involving items in the main comparison with improved mechanical properties and geometrical features. In addition the main comparison has involved parallel circulation of a set of two items to each participant, in order to achieve a short circulation time.

4.2.1 Project management and time schedule

The phases in the project involved were: 1) plan, participants' definition, 2) item calibrations, 3) circulation, 4) analysis of results, and 5) reporting and dissemination. The timeline in Figure 4.5 gives an indication of the different phases.

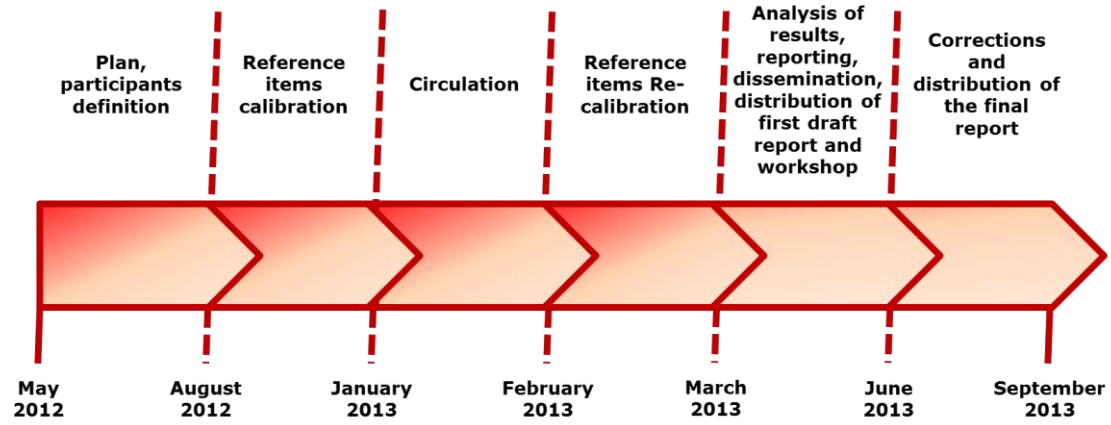

Figure 4.5. Time schedule for the CIA-CT comparison.

4.2.2 Participants and comparison items

The CIA-CT interlaboratory comparison on industrial X-ray CT was organized by CGM, DTU MEK and carried out within the project "CIA-CT - Centre for Industrial Application of CT scanning". The comparison was carried out in the period from May 2012 to October 2013, involving 27 laboratories from 8 countries (see Figure 4.6): 3D-CT A/S (DK), BAM Federal institute for materials research and testing (DE), Braun GmbH (DE), Carl Zeiss IMT GmbH (DE), Danish Technological Institute (DK), Fraunhofer Development Center for X-ray Technology (DE), Zebicon A/S (DK), GRUNDFOS A/S (DK), Hexagon Metrology Inc. (US), Huddersfield University (UK), FMT Institute of Manufacturing Metrology Friedrich-Alexander-University Erlangen-Nuremberg (DE), Katholieke Universiteit Leuven (BE), LEGO System A/S (DK), AIST National Institute of Advanced Industrial Science and Technology (JP), NPL National Physical Laboratory (UK), Nikon Metrology (UK), Novo Nordisk A/S Device R&D (DK), Novo Nordisk A/S DMS Metrology & Calibration (DK), SGS Institut Fregenius GmbH (DE), SIMTech (SGP), UNCC Center for Precision Metrology (USA), University of Padova (IT), University of Southampton (UK), Wenzel Volumetrik GmbH (DE), Werth Messtechnik GmbH (DE), IPK Fraunhofer-Institut für Produktionsanlagen und Konstruktionstechnik (DE), YXLON International GmbH (DE) [52].

Figure 4.6. The 27 participants in the CIA-CT circulation.

The general purpose of the comparison was to test applicability of CT, in terms of systematic errors and estimated uncertainties, to carry out measurements on small objects commonly manufactured in industry, which are more representative than reference objects used for calibration and verification of CT. The items circulated in the comparison, were selected among common industrial parts: a polymer part (Item 1) and a metal part (Item 2). Item 1 is a polymer brick from the Danish toys company LEGO. Item 2 is a tubular component from an insulin pen produced by the Danish medical company Novo Nordisk. Both items were presented in Chapter 2. The items were contained in a box. Pictures of the box and the items can be seen in Figure 4.7. In short, the aim of the measurement was to determine different measurands, encompassing diameter (D), roundness (R), and length (L). Item 1 features three measurands, identified as D1, R1, and L1. The measurands for Item 2 are the following: D1, R1, D2, R2, and L1. The measurands for Item 1 and 2 are illustrated in Figure 4.8. Measurement procedures were sent to each participant together with the items to be measured. The measurement procedures can be carried out on CT as well as on CMMs, and are described in detail in [52]. Setting parameters were freely chosen by each single participant, who also was free to select measurement set-up and way of fixing the items. Figure 4.9 shows examples of measurement set-up and way of fixing the items during CT scanning by one of the participants.

Figure 4.7. Internal box containing the two items (left) and external box for storage and transportation of the items (right).

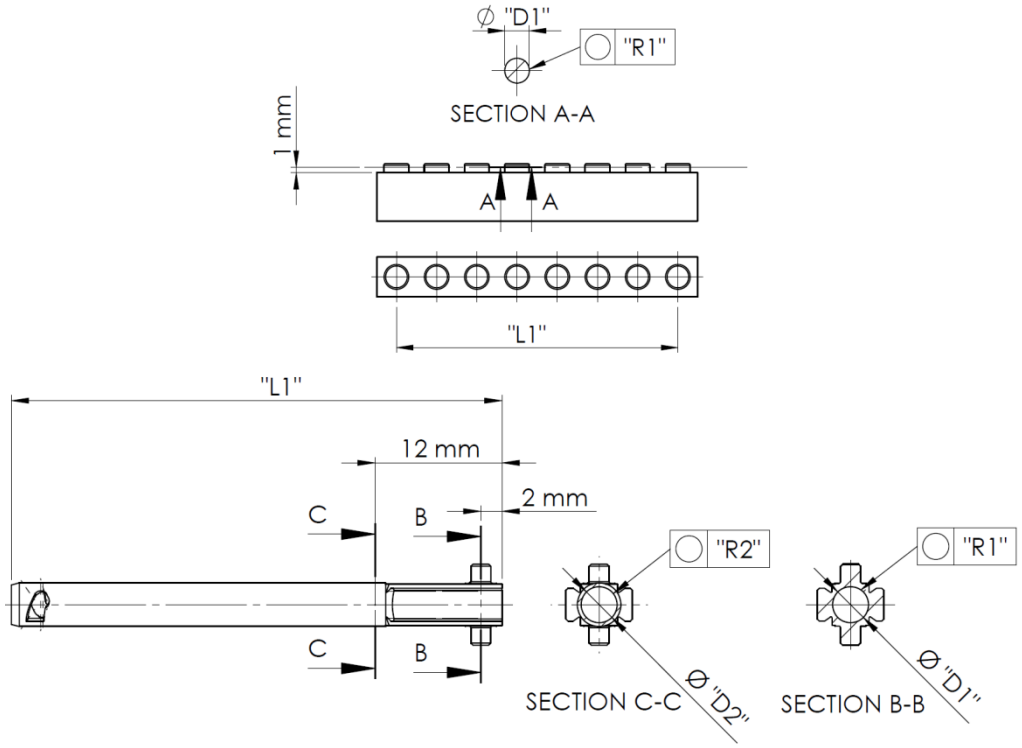

Figure 4.8. Top: Item 1 – Overview of measurands; D1, R1 and L1. Bottom: Item 2 – Overview of measurands; D1, R1, D2, R2 and L1.

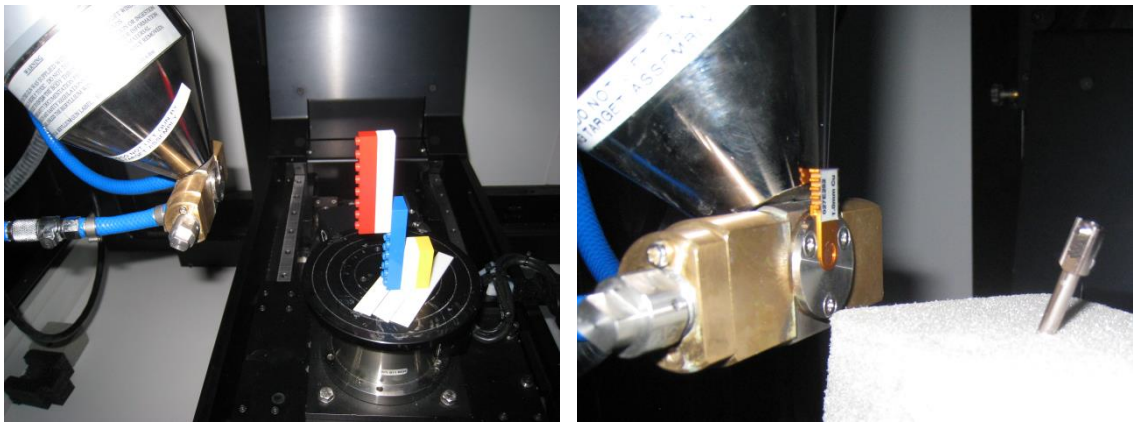

Figure 4.9. Measurement set-up and fixture for Item 1(left) and Item 2 (right) in a Nikon CT scanner. Courtesy of KUL, Belgium.

4.2.3 Analysis of participants' data

Reference measurements and item stability were presented in Chapter 2. Altogether, 27 sets of items were circulated in parallel to the participants in the period January 2013 to July 2013. Most participants accomplished their measurements within one month, as originally planned, after removing identified outliers using the interquartile rule for outliers [60], see Table 4.3. Some others concluded their measurements subsequently, and three participants were delayed until July 2013 due to scanner problems. All participants carried out measurements following without problems the measurement instructions distributed by the coordinator. Information about the CT and measurement set-ups used by the participants, as well as tables and graphs with data analysis of the single CT, were elaborated and reported in [52]. The results by each participant are kept confidential. Each participant can identify his own results using a personal identification number provided by the coordinator. Statistics of collected information concerning instrument settings and operator adjustments have shown that the participants in the comparison have followed state-of-the-art procedures for their measurements, taking steps to minimize beam hardening artifacts and blurred edges. As expected, a higher voltage was used for the metal item compared to the plastic item while the applied current is similar for both items. An applied voxel size by the participants was calculated based on detector pixel size, source-detector distance and source-object distance. The average voxel size for the plastic item was 43.3 µm, while it was 38.7 µm for the metal item. The participants applied different approaches to uncertainty assessment, among the following: ISO 14253-2 [21], GUM [20], ISO 23165 [61], ISO 15530-3 [18], repeatability and T-factors, hybrid methods, manufacturer specifications, and own developed assessments. 9 out of 27 participants did not apply reference objects for scale error correction and establishment of traceability, while some individual participants applied ball bars, dual ruby spheres, or the industrial items themselves. Depending on item and measurand, the participants stated average expanded uncertainties in the range 6-15 µm, with maximum values up to 51 µm after removing identified outliers using the interquartile rule for outliers [60], see Table 4.4. All participants' single values and uncertainties are reported in [52].

Table 4.3. Accomplishment of measurements by the participants. Average values based on all participants after outlier removal. Values are in days.

MAX	83
AVG	**33**
MIN	14

Table 4.4. Expanded uncertainties stated by the participants (k=2). Average values based on all participants after outlier removal. Values are in µm.

	Item 1			Item 2				
	D1	R1	L1	D1	R1	D2	R2	L1
MAX	11.2	14.6	22.3	23.2	50.9	16.0	32.2	30.2
AVG	**5.9**	**7.9**	**11.2**	**8.2**	**14.9**	**6.8**	**10.8**	**12.0**
MIN	0.0	1.5	1.5	1.0	2.0	1.0	2.0	1.1

The results of the single participants were analysed and compared with reference values obtained by the coordinator. Figure 4.10 and Figure 4.11 show typical results. Systematic errors were detected for some participants concerning diameters and lengths, which may be due to measurement errors as threshold determination, non-corrected scale, or uncompensated temperature. For the diameters and lengths for both items, there is a good agreement between most participants' results and the reference values, except for few participants. The roundness for both items measured by the participants is higher than the reference value, with no effect from filtering [52]. Form measurements are more problematic compared to size measurements. From Table 4.5 it is clear that R1 for Item 2 is problematic compared to the other measurands. It appears that deviation from the reference value increases in the case of roundness when the wall thickness increases (the wall corresponding to R1 is thicker compared to the region where R2 is measured), see Figure 4.11. This may be due to the influence of scatter and noise of CT data, and to the thicker wall producing higher attenuation of the X-rays. In order to judge the agreement between reference values and participant values, the $|E_n|$ value normalised with respect to the stated uncertainty was computed according to ISO 17043 guidelines [46]. Out of a total of 167 single results obtained by the participants using CT scanning, 54% of the measurements yield $|E_n|$ values less than 1, and 46% values larger than 1. Disagreement can be caused by systematic errors in the measurement or be due to an underestimation of the uncertainty.

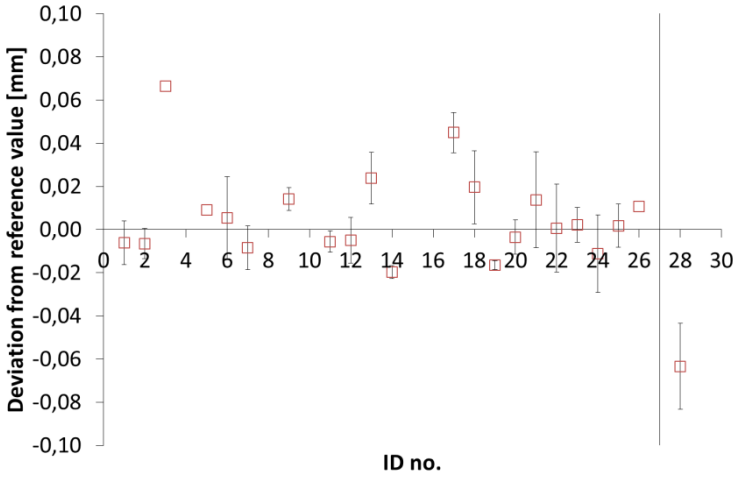

Figure 4.10. Results for Item 1. Length L1.

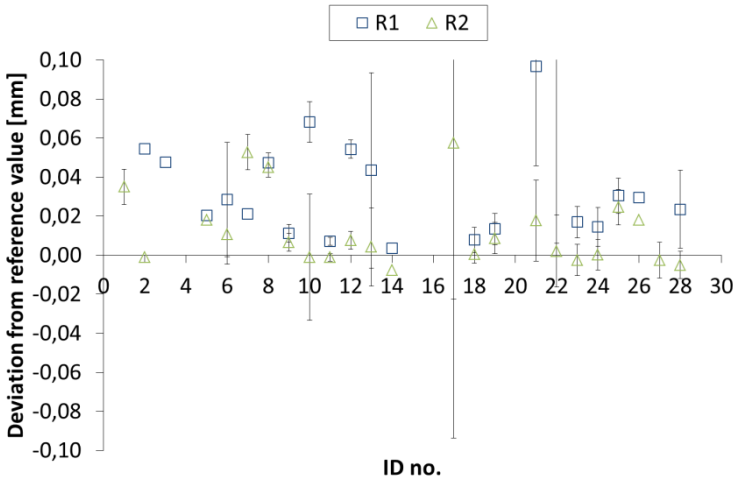

Figure 4.11. Results for Item 2. Roundness R1 and R2.

Table 4.5. Distribution of $|E_n|$ values for Item 1 and 2. Values are in %.

	Item 1			Item 2				
	D1	R1	L1	D1	R1	D2	R2	L1
$\|E_n\|<1$	74	48	57	57	17	71	63	38
$\|E_n\|\geq 1$	26	52	43	43	83	29	37	62

A recalculation of uncertainties in order to achieve $|E_n| = 0.99$ was carried out for those results that had led to $|E_n|$ values larger than 1. Some results were identified as outliers using the interquartile rule for outliers [12] and excluded from the calculations. It was concluded that likely uncertainties for the laboratories would lie in the range 14-53 µm and maximum values up to 158 µm, see Table 4.6. This approach is limited by the fact that all deviations are treated as random, including systematic errors, yet it clearly indicates that uncertainties of 6-15 µm stated by the participants are underestimated.

The comparison has shown that CT measurements on the small industrial parts that have been used can be divided into two groups, see Figure 4.12: a group with average measurement uncertainties in the range 6-15 µm, and a group with average uncertainties in the range 14-53 µm, and maximum values up to 158 µm, compared to average uncertainties below 5.5 µm using CMMs. Generally speaking, the comparison has shown that CT measurements on the industrial parts used lie in the range 6-53 µm, with maximum values up to 158 µm.

Table 4.6. Recalculated expanded uncertainties to achieve $|E_n| = 0.99$ (k=2). Average values based on all measurements originally giving $|E_n| \geq 1$ after outlier removal. Values are in µm.

	Item 1			Item 2				
	D1	R1	L1	D1	R1	D2	R2	L1
MAX	69.4	25.0	126.6	41.9	157.6	49.3	53.2	70.7
AVG	**19.7**	**13.6**	**49.4**	**22.3**	**52.9**	**29.9**	**25.9**	**34.7**
MIN	0.6	6.0	13.2	4.7	6.9	18.7	6.6	6.5

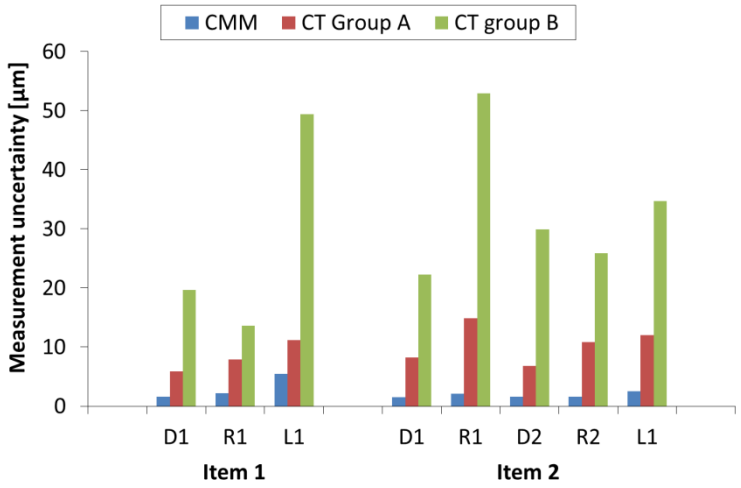

Figure 4.12. Expanded uncertainty (k=2) of measurements on the two industrial items. Group A refers to results in agreement with reference values; Group B indicates those measurements for which a plausible uncertainty was recalculated.

4.2.4 Correction of participants' data using scale error and offset corrections

The acquired data from the participants can be compensated for scale errors and offsets. The methods for finding *a* for and *b* are applied using the equations in section 2.1.5. Figure 4.13 shows *a* for and *b* for all participants. Some outliers were detected and the interquartile rule for outliers was applied for values *a* and *b* in Table 4.7 [60]. Graphs are shown after scale error and offset corrections for all the geometrical measurands except the roundness in Figure 4.14-Figure 4.18. It is possible to correct the lengths and diameters for scale error and offset except for D1 for Item 2. This might be due to beam

hardening artifacts and the thicker wall thickness. This statement was also documented for the roundness R1 for Item 2 which is located in the same place as D1.

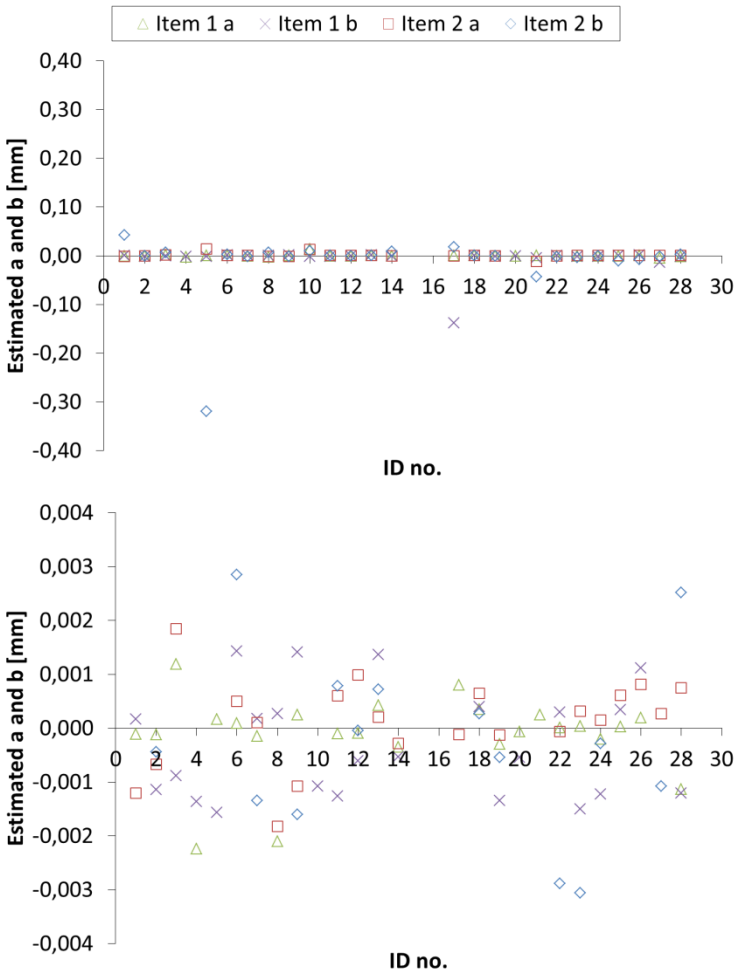

Figure 4.13. Estimated regression coefficient *a* and offset *b*. Top: deviation range ± 0.4 mm. Bottom: deviation range ± 0.004 mm.

Table 4.7. Regression coefficient *a* and offset *b*. Based on all participants after outlier removal.

	Item 1		Item 2	
	Regression coefficient *a* [-]	Offset *b* [mm]	Regression coefficient *a* [-]	Offset *b* [mm]
MAX	0.0008	0.0014	0.0018	0.0096
AVG	0.0001	-0.0003	0.0002	0.0011
MIN	-0.0004	-0.0016	-0.0012	-0.0078

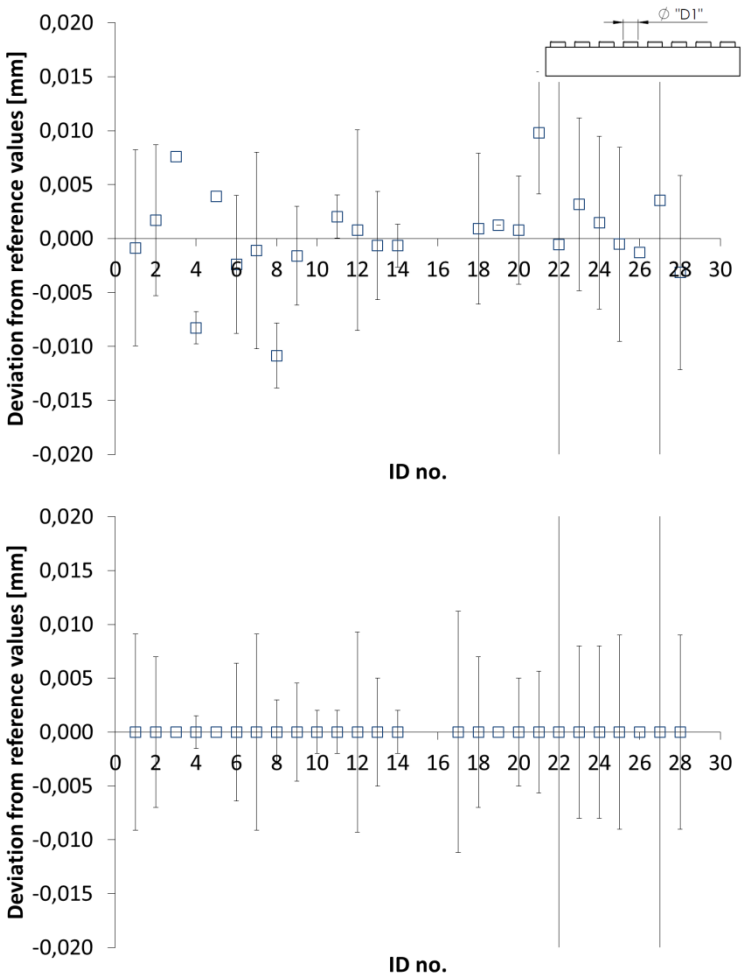

Figure 4.14. Item 1 D1. Top: before correction. Bottom: after correction.

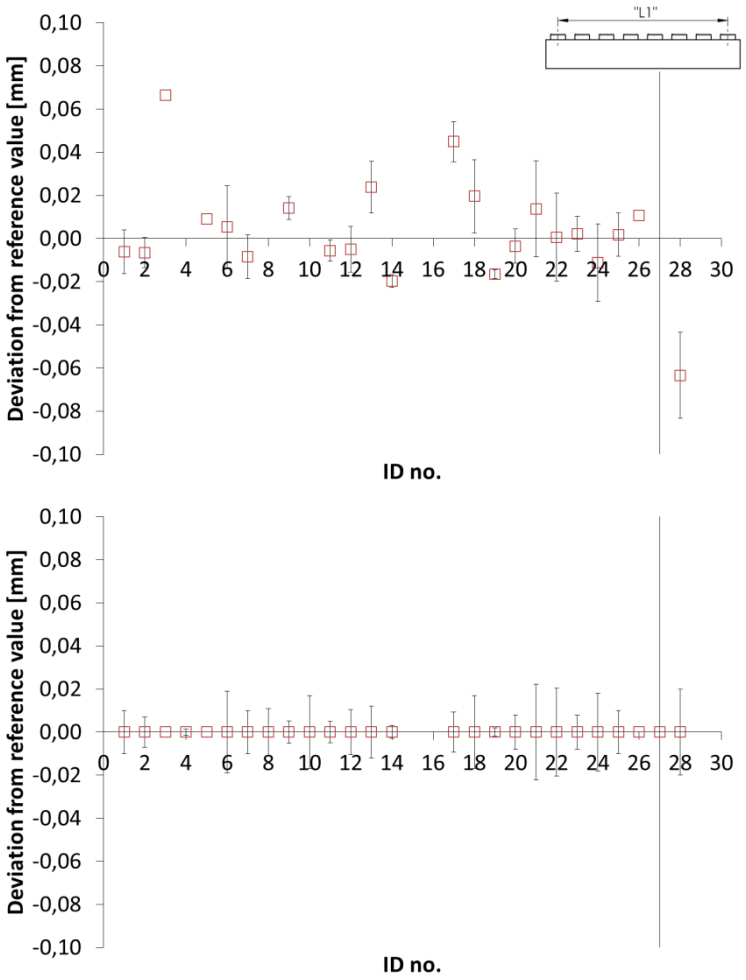

Figure 4.15. Item 1 L1. Top: before correction. Bottom: after correction.

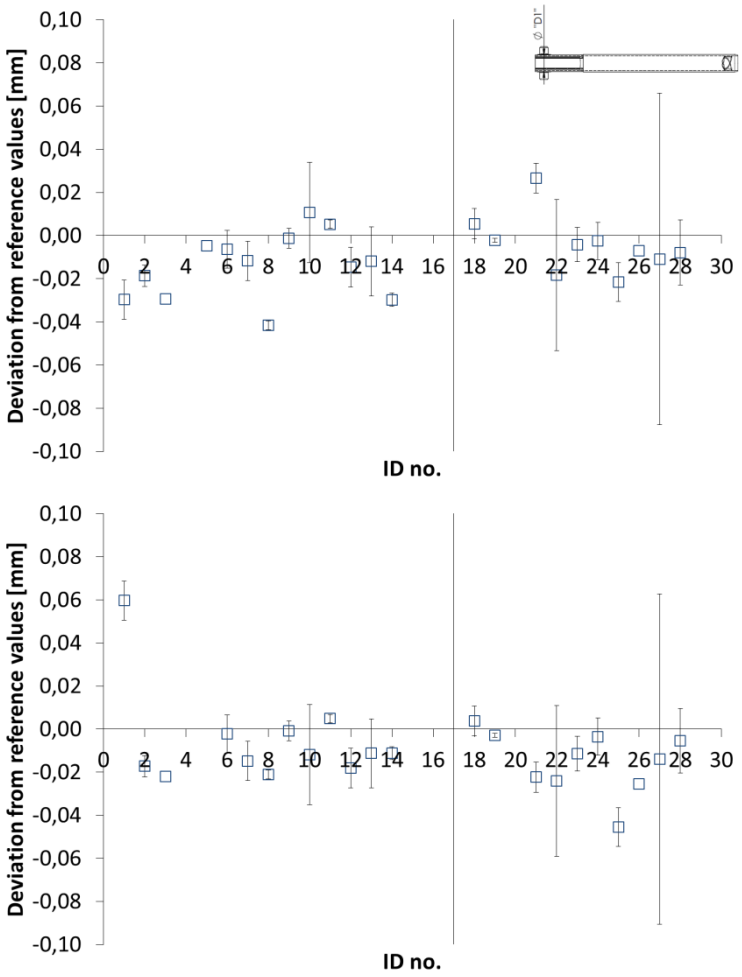

Figure 4.16. Item 2 D1. Top: before correction. Bottom: after correction.

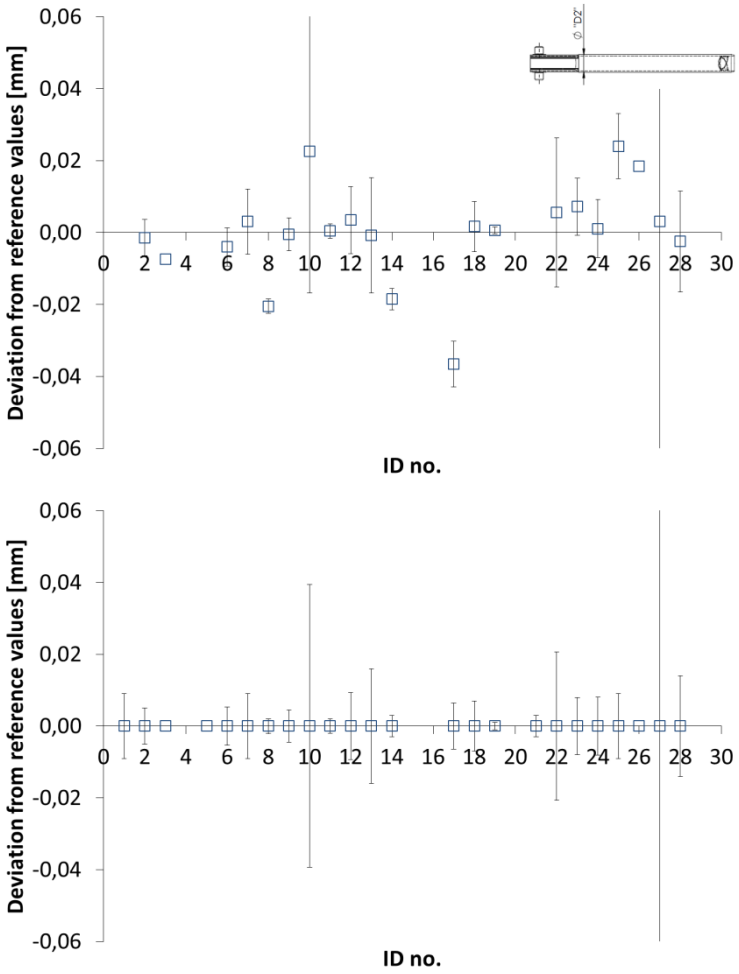

Figure 4.17. Item 2 D2. Top: before correction. Bottom: after correction.

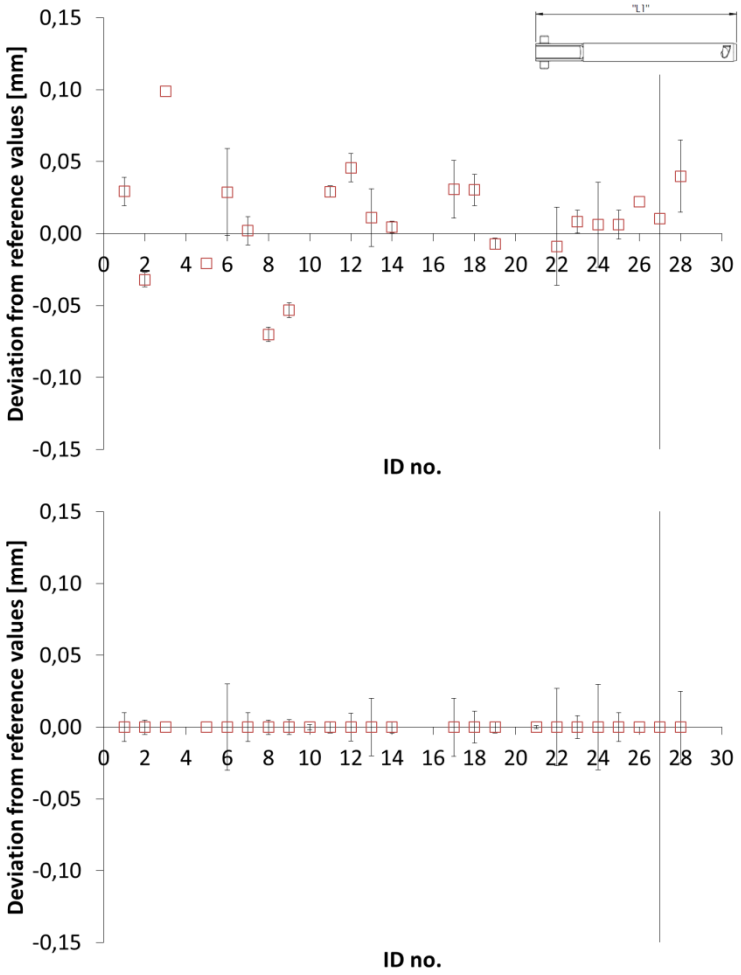

Figure 4.18. Item 2 L1. Top: before correction. Bottom: after correction.

4.3 Chapter conclusion

The main conclusions which were drawn from the main comparison are outlined in the following.

- The CIA-CT comparison on Computed Tomography involved real industrial items. 27 participants from 8 countries participated.
- Altogether, 30 plastic parts and 29 metal components were selected from industrial production and used as items.
- Parallel circulation of 27 sets started in January 2013 and could be carried out in one month, apart from some participants who completed their measurements in July 2013.
- Different measurands were considered, encompassing diameter, roundness, and length.
- Reference values for all items were provided by CGM using CMMs, with average expanded measurement uncertainties in the range 1.5-5.5 µm.
- All items have shown a good stability, within the measurement uncertainty, over the 6 months of circulation.
- Results by the single participants were compared with the reference values provided by CGM.
- Systematic errors were detected for some participants on the diameters and lengths, which can be due to measurement errors as threshold determination or uncorrected scale or temperature. It is possible to correct the lengths and diameters for scale error and offset except for D1 for Item 2, which may be due to beam hardening artifacts and the surrounding wall thickness.
- The roundness for both items measured by the participants is higher than the reference value, with no effect from filtering. It is clear from the comparison that form measurements are more problematic compared to size measurements because form measurements are more affected by scatter and noise on CT data.
- A clear influence from the surrounding wall thickness on the measurement of roundness was documented for the metal item.
- Out of a total of 167 results obtained by the participants using CT scanning, 54% of the measurements yield $|E_n|$ values less than 1 and 46% larger than 1.
- As a general conclusion, the comparison has shown that CT measurements on the industrial parts used lie in the range 6-53 µm, with maximum values up to 158 µm, compared to average uncertainties below 5.5 µm using CMMs.
- The comparison has shown that the two industrial items are suitable artefacts for CT measurements of this kind.

Chapter 5 Using grating based X-ray contrast modalities for metrology

Traditionally, segmentation between multi-materials in CT scanning is done by using different edge detection techniques and threshold algorithms, but these are only available for multi-materials where the densities are not close to each other [25]. A novel method called Grating-interferometer Based Imaging (GBI) overcomes this problem [62]. In this chapter, GBI is evaluated with respect to its metrological compatibility by comparing it to traceable measurements acquired from a tactile CMM. GBI is selected, because the technique demonstrates that it is possible to distinguish fine details in soft materials, which are indistinguishable in standard CT [63]. GBI consists of three gratings; a source grating (G_0), a phase grating (G_1) and an analyzer absorption grating (G_2) [64]. G_0 makes it possible to use conventional X-ray tube sources with square millimetre sized focal spots. G_1 works as a periodic phase mask, transforming the periodic phase modulation into a periodic intensity modulation through the Talbot effect before the X-rays hit G_2. In Figure 5.1 there are three figures, where (a) shows an illustration of the set-up of a grating interferometer (it is not to scale), (b) illustrates the Talbot effect, which occurs between G_1 and G_2, and (c) shows the intensity modulation detected in a detector pixel. Figure 5.2 shows scanning electron micrographs of G_0, G_1 and G_2 gratings to get an idea of the shape and size of the gratings. The output images from GBI are dark field, phase contrast and transmission images. The dark field technique can detect the reflection and diffractions effect using the gratings. The gratings allow the reflected and diffracted X-rays to be registered by the detector, when the non-reflected and non-diffracted X-rays are not implemented on the dark field image. It means that the reflection and diffraction effects, which lead to dark field images, are dependent on the structure and not the density and thickness as it is known from conventional X-ray transmission images. The technique of dark field is known from conventional light microscopes, where the sample is lighted inclined from the sides and the reflected areas in the sample appear as white areas on a black background [65]. From the literature, a comparison example between a conventional X-ray transmission image, a differential phase-contrast image and a dark-field image is shown in Figure 5.3 [62]. Furthermore the intensity oscillations extracted from a series of eight images of different slice values is shown in Figure 5.3 too.

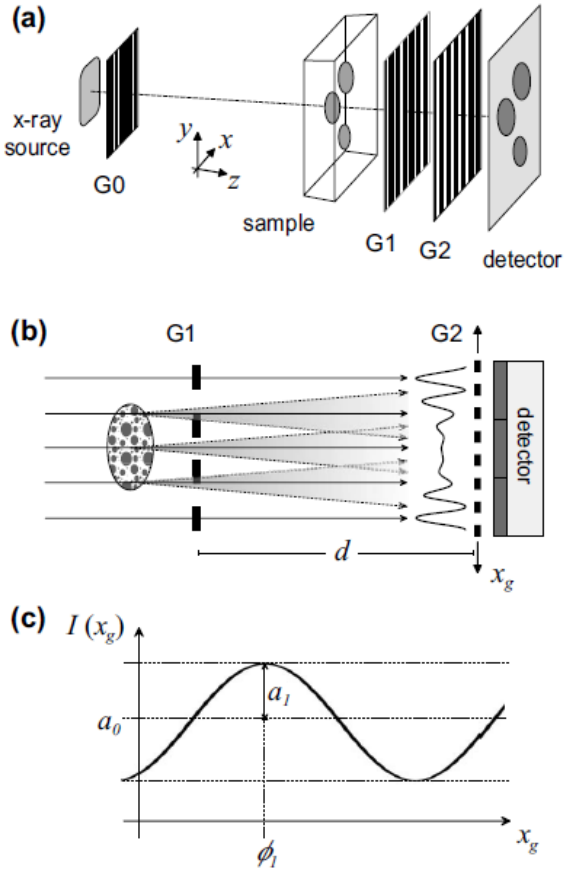

Figure 5.1. Illustration of the set-up of a grating interferometer **[62]**.

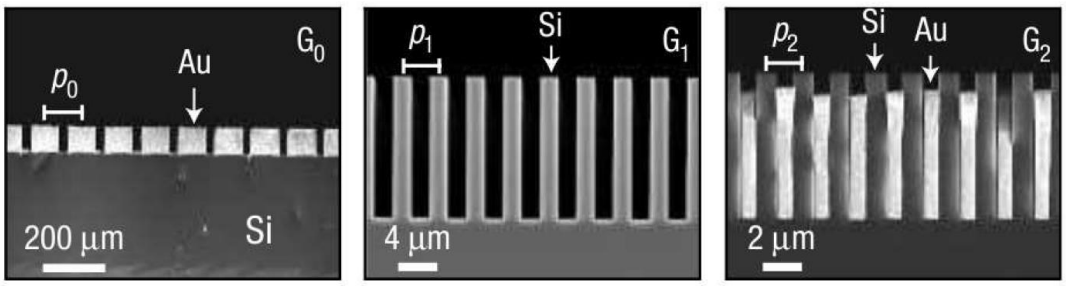

Figure 5.2. Scanning electron micrographs of G_0, G_1 and G_2 gratings **[66]**.

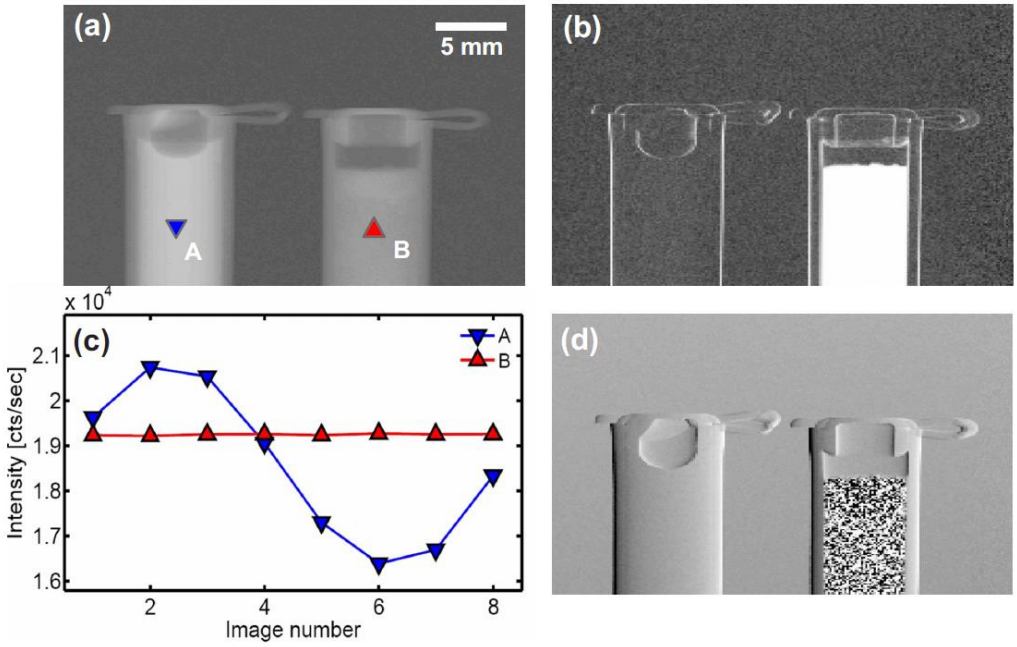

Figure 5.3. A comparison example between (a) a conventional X-ray transmission image, (d) a differential phase-contrast image and (b) a dark-field image. Note that (c) shows the intensity oscillations extracted from a series of eight images of different slice values **[62]**.

5.1 Preparation of experiments

The parts used in the experiments were a 10 mm high cylindrical multi-material assembly consisting of male and female parts in three different combinations, including a combination with approximately the same densities (see description of object in section 2.4). Furthermore, a 15 mm high step cylinder (see description of object in section 2.3) was selected to investigate error sources such as beam hardening artifacts in internal dimensions in GBI [2]. The selected geometrical features were inner (ID) and outer (OD) diameters (Figure 5.4), and both were measured from circles and compared to traceable CMM measurements. The step cylinder was measured from top to bottom at equidistance slices, where the first position (ID1 and OD1) refers to the top.

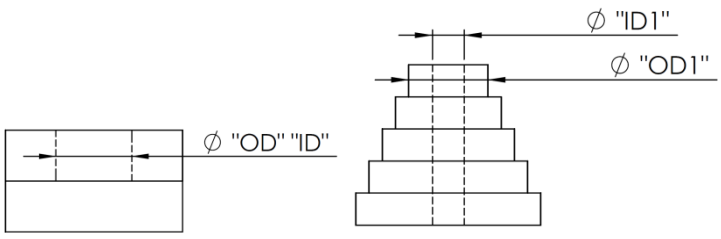

Figure 5.4. Assembly sketch with measurands (left). Step cylinder sketch with measurands (right).

Experiments were carried out to investigate the relationship between image types and deviation from calibrated diameters, and were performed without any replicated scans. The three treated image types were dark field, phase contrast and transmission images.

5.2 Experimental setup

The used GBI is a prototype from NBI. A GBI consists of three gratings (G_0, G_1 and G_2), see Figure 5.5.

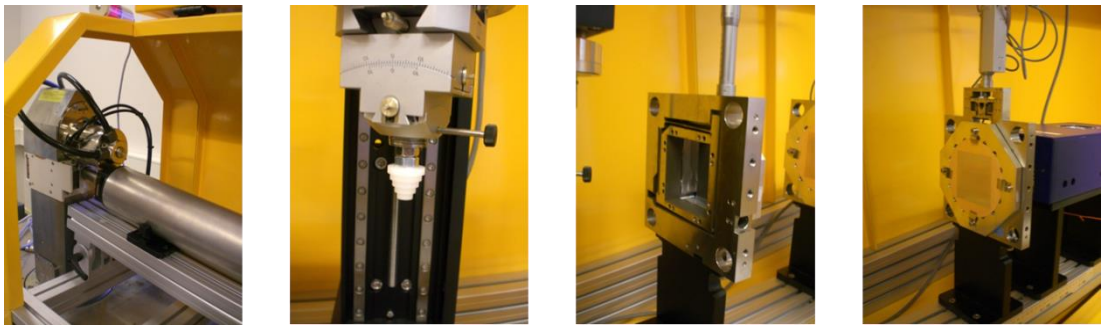

Figure 5.5. Experimental set-up at NBI. From left to right: X-ray source and source grating (G0), rotary table and step cylinder, phase grating (G1), and analyzer absorption grating (G2) followed by a detector.

The used scanning parameters are shown in Table 5.1 in which a X-ray energy of 28 keV was selected because of a phase shift. Some of the parameters were found through the calculations presented in (5.1) and (5.2). In (5.1) the m^{th} fractional Talbot can be calculated [67].

$$d = a\frac{L}{L-a} \tag{5.1}$$

Hence d is the mth fractional Talbot, L is the distance between G_0 and G_1, when a can be found through (5.2).

$$a = m\frac{{G_1}^2}{8\lambda} \tag{5.2}$$

G_1 is the period for G_1, m is the selected Talbot number and λ is the wavelength. In the given experiment the change regarding the 5th Talbot (m=5) can be calculated as 204.76 mm. The used scanner at NBI uses 8 phase steps for each projection, thus making the scanning time eight times longer than conventional industrial CT.

Table 5.1. Some selected scanning parameters.

Parameter	Value
Temperature	20
Number of projections on one rotation in °C	241
Period for G_0 in µm	14
Period for G_1 in µm	3.5
Period for G_2 in µm	2
X-ray energy *E* in keV	28
Wavelength λ in Å	0.4286
Distance (*L*) between G_0 and G_1 in mm	140
Number of phase steps for each projection	8
Distance (*d*) between G_1 and G_2 in mm	204.76

5.3 Data evaluation

ISO 50% (global one) was used for surface segmentation between material and air (as performed in Chapter 3). The reconstruction of the 2D X-ray images and data analysis of the tomograms were carried out using VolumeGraphics software. For the evaluation of the data, the error was defined as the deviation between CT and reference measurements.

5.4 Results and discussion

The images of single projections show that it is possible to distinguish between assemblies with approximately same densities using the dark field image (see Figure 5.6). Challenges related to stability made it impossible to generate tomograms for the assemblies. The tomograms for all three image types are shown in Figure 5.7 for the step cylinder, and a lot of noise was detected on the dark field tomogram compared to phase contrast and transmission tomograms and made it impossible to measure it.

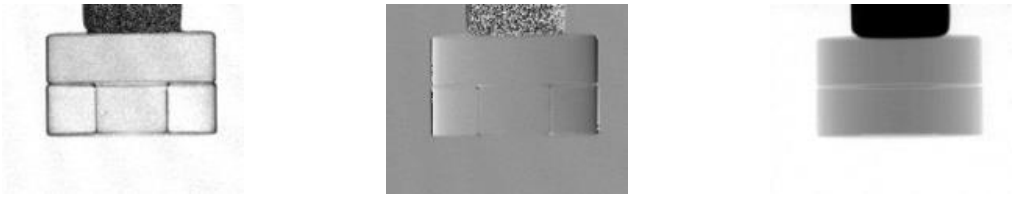

Figure 5.6. Example of single projections for assembly with the combination PP-PE. From left to right: dark field, phase contrast, and transmission images.

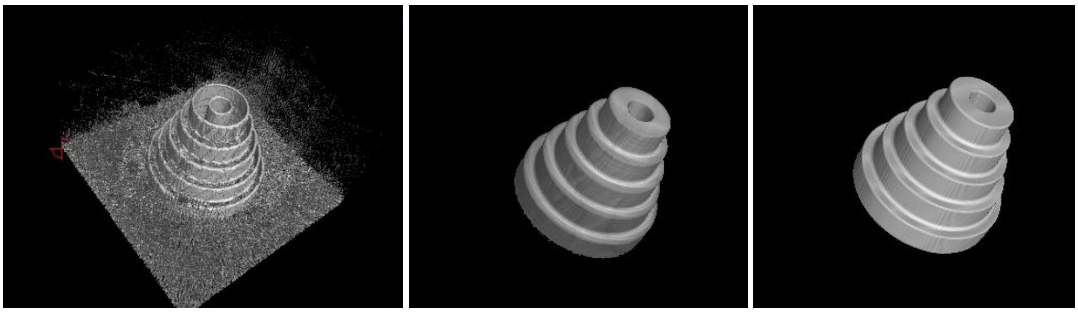

Figure 5.7. Tomograms of step cylinder – From left to right: dark field, phase contrast and transmission.

The acquired deviations from the reference values for the step cylinder can be used in calculating the edge correction terms for internal and external features. Scale error and threshold offset corrections are performed by applying linear regression on the tomograms (see Figure 5.8 and Figure 5.9), in which the graphs are valid after removal of outliers using the interquartile rule for outliers [60], because the variation width for the calculated regression coefficient *a* and offset *b* are large. Table 5.2 shows the variation width before removal of outliers and after. Table 5.2 shows that *a* and *b* values differs between internal and external features which could be due to scattering artifacts, beam hardening artifacts and/or other error sources [2]. It was also detected that the regression coefficient *a* and offset *b* are different for transmission and phase contrast tomograms. Before correction the deviation from CMM values was up to 800 µm and the deviation was reduced to 80 µm after correction.

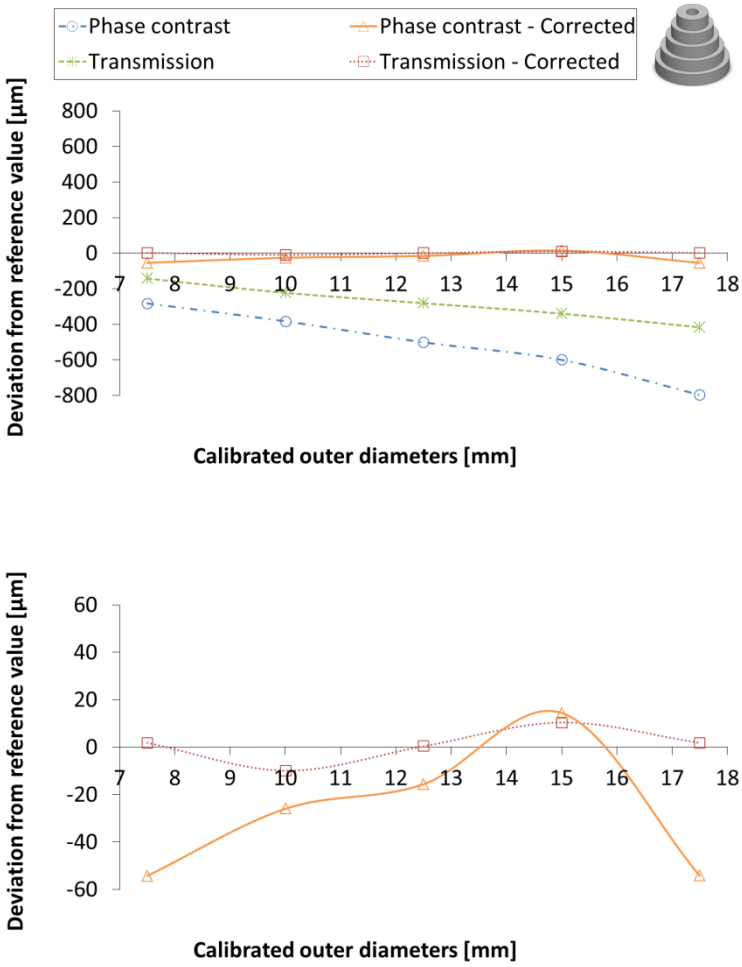

Figure 5.8. Step cylinder – Dimensional errors on outer diameters. Top: deviation range ± 800 µm. Bottom: deviation range ± 60 µm.

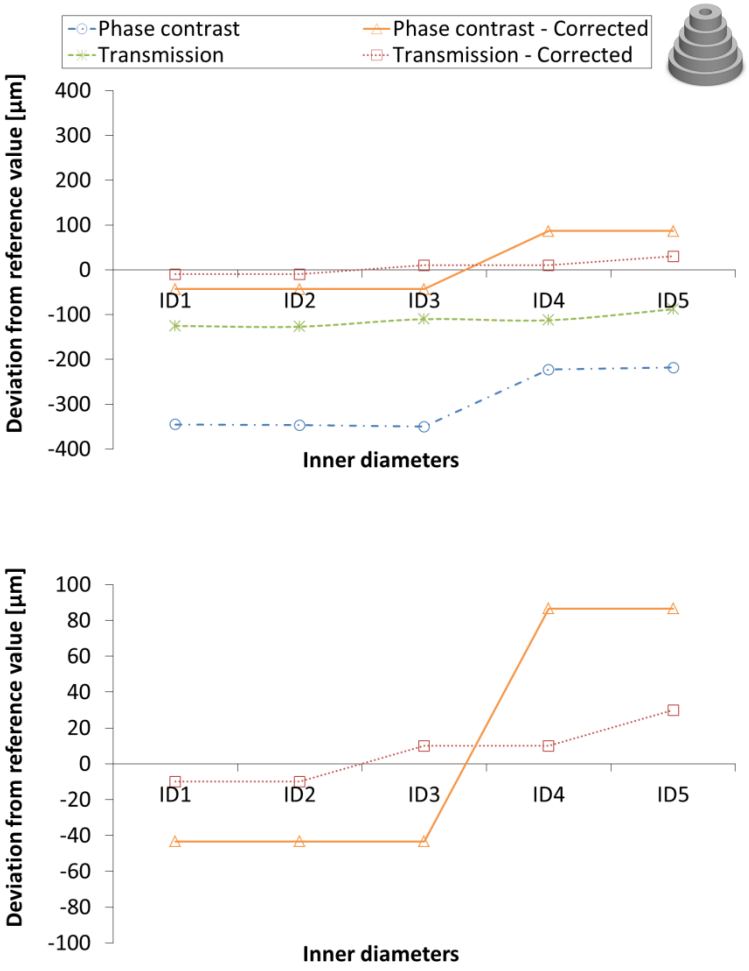

Figure 5.9. Step cylinder – Dimensional errors on inner diameters measured from top to bottom. Top: deviation range ± 400 µm. Bottom: deviation range ± 100 µm.

Table 5.2. Regression coefficient *a* and offset *b*.

Feature	Description	Transmission		Phase contrast	
		Regression coefficient *a* [-]	Offset *b* [mm]	Regression coefficient *a* [-]	Offset *b* [mm]
Inner	Variation width	40.1603	60.4535	52.0000	78.3276
	Variation width after outlier removal	0.0000	0.0100	0.0000	0.0650
	Corrected value after outlier removal	-1.0000	-1.4450	-1.0000	-1.3517
Outer	Variation width	0.0088	0.0567	0.0395	0.2963
	Variation width after outlier removal	0.0088	0.0567	0.0395	0.2963
	Corrected value after outlier removal	-0.0275	-0.0308	-0.0515	-0.0790

5.5 Chapter conclusion

In this chapter, a test is performed to check if X-ray contrast modalities can be applied for metrological purposes. Traditionally, segmentation between multi-materials in CT scanning is done by using different edge detection techniques and threshold algorithms, but these are only available for multi-materials where the densities are not close to each other. X-ray contrast modalities overcome this problem by constructing dark field, phase contrast and transmission images. For this purpose a step cylinder and cylindrical multi-material assemblies are used in the experiments. The images show that it is possible to distinguish between multi-materials with densities close to each other using the dark field technology. Measurement results show that further development related to stability issues on the used CT is needed to create a metrological tool using X-ray contrast modalities.

Chapter 6 Reference objects for applications in the meat processing industry

This chapter presents a brief state-of-the-art about reference objects, standards and guidelines relevant for CT used for volume measurements in the meat processing industry. Two reference objects are calibrated objects from DMRI (*Phantom 1* and *Phantom 2*). The used phantoms pose a number of challenges. Some of these challenges taken into consideration are temperature sensitivity and lower material stability over time which degrade the volumetric properties and increase the measurement uncertainty. A key issue has been to document that the phantoms mentioned above are stable and controllable, and useful as reference objects for evaluating volume measurements from CT scanning, in terms of detecting systematic errors and estimated uncertainties.

6.1 Traceability of CT measurements

There are no guideline for specification and verification of CT systems used for volume measurements. In general, evaluation of the measurement uncertainty with assessment of all influential contributors constitutes a challenge with respect to the establishment of traceability and quality assurance. For this purpose reference objects can be applied in which the measurement traceability can be implemented in CT by the use of other instruments and methods with known uncertainty. Traceable volume measurements can be achieved by using the gravimetric method (also called water displacement method) as a suitable and traceable method to calibrate a reference object using ISO 17025 [68; 69]. But the estimation of volumes can be more accurate based on dimensional measurements using CMM [70]. Literature studies show that the volume of small micro cavities (see Figure 6.1) and a phantom for voxel correction (see Figure 6.2) have been evaluated in CT and compared to reference volumes acquired by using CMM [71; 72]. Examples of some other reference objects used for performance evaluation and calibration of clinical CT on the hospitals are shown in Figure 6.3 and consist generally of different reference materials such as polymers which represent tissue materials in humans.

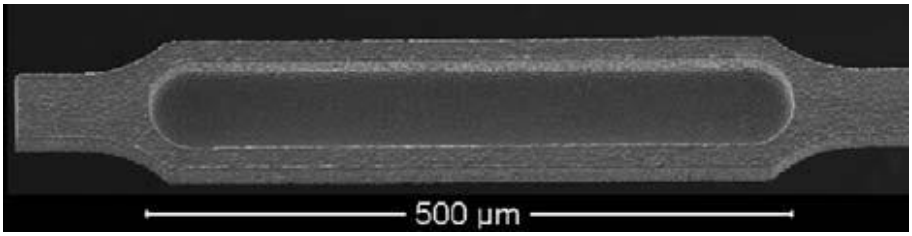

Figure 6.1. Scanning electron microscope image of micro cavity for volume applications in CT **[71]**.

Figure 6.2. Phantom for volume applications in CT **[72]**.

Figure 6.3. From left to right: CT head and body dose phantom, performance phantom, and abdomen/lumbar spine phantom **[73]**.

The considered influence factors and error sources in clinical CT are more or less similar to the ones mentioned for the CT used in the manufacturing field in section 2.1.2.

6.2 Phantoms

DMRI has developed 450 mm length synthetic phantoms represented real pig carcasses, see Figure 6.4. The parts were made of several polymer components such as poly methyl methacrylate (PMMA), polyethylene (PE) and polyvinyl chloride (PVC) [74]. The polymer materials PMMA, PE and PVC represented tissue types as respectively: lean meat, fat, and bone, and can be identified through their colour codes, see Figure 6.5. The colours were as follows: transparent (PMMA), white (PE) and black (PVC). The two phantoms presented representing a skinny (Phantom 1) and a fat (Phantom 2) pig carcass respectively (see approximated fat distribution in Figure 6.6). For purposes of this Ph.D. project, these phantoms are used in connection with an interlaboratory comparison on CT for industrial applications in the meat processing industry. Material characteristics such as density and thermal expansion coefficient data are shown in Table 6.1. Compared to the other stated reference objects in section 2.2-2.6, the meat industry had no interest in geometrical measurands, in which their interest belonged to volume estimates of the different material contents in the two phantoms.

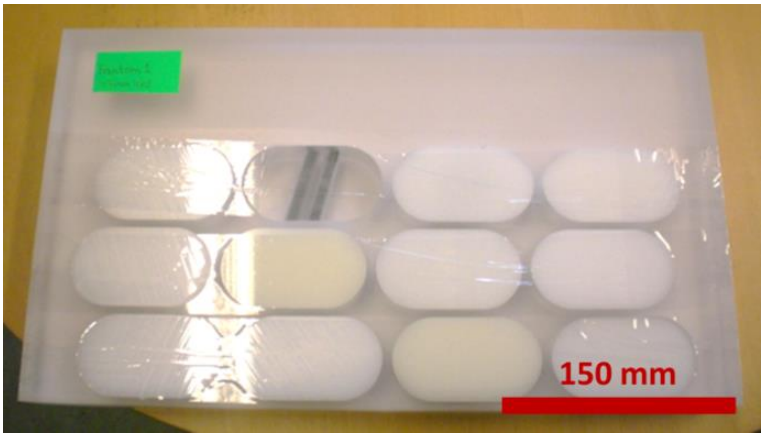

Figure 6.4. Phantom from DMRI.

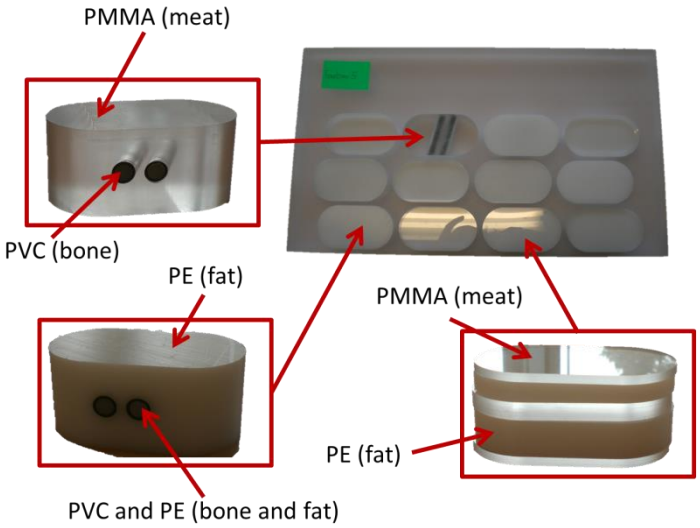

Figure 6.5. Identification of polymer materials through their colour codes. The colours are as follows: transparency (PMMA), white (PE) and black (PVC).

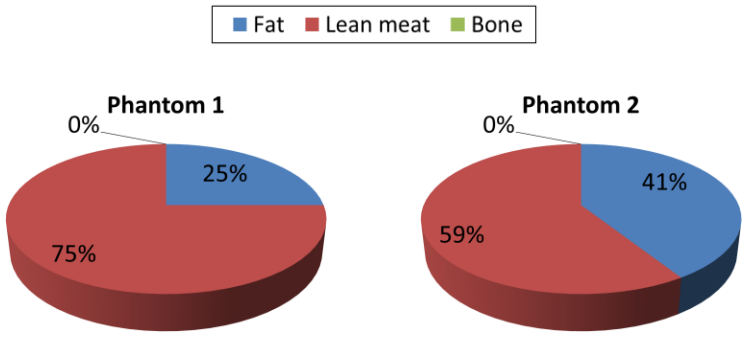

Figure 6.6. Approximated fat distribution in a skinny (Phantom 1) and a fat (Phantom 2) pig carcass.

Table 6.1. Density and thermal expansion coefficient of polymer components in a phantom.

Material	Supplier	Grade	Density [g/cm³]	Thermal expansion coefficient [10^{-6} K^{-1}]
PMMA	RIAS A/S	RIACRYL XT1030/PlexiglasXT	1.190	70.0
PE	RIAS A/S	RIALEN HD 500	0.950	200.0
PVC	RIAS A/S	RIANYL PVC-U	1.380	75.0

6.2.1 Calibration and transfer of traceability

The phantoms were calibrated using the gravimetric method (also called water displacement method) [68]. This method was chosen rather than CMM because of low tolerance demands in the meat processing industry. The method is based on finding the absolute density [75]. A pycnometer (Figure 6.7) was used for determination of specific gravity weight per unit volume of the used liquid such as distilled water. A technical weight (Figure 6.8) was used for weighing of the measured objects. A thermometer and a barometer were used for compensation of the results for the interaction of temperature and atmospheric pressure changes respectively. Weights with certificate were used as weight references to generate traceability. The influence of surface tension from the distilled water was neglected. Each phantom consisted of three measurands, identified as the volumes of PMMA, PE and PVC.

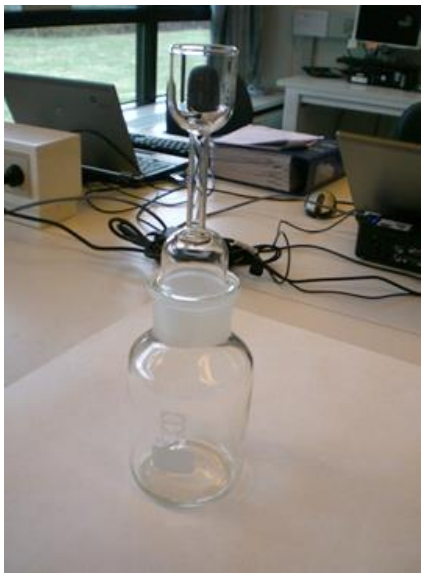

Figure 6.7. Pycnometer of the type SCHOTT DURAN 1000 mL.

Figure 6.8. Technical weight of the type Satorius BP 3100 S.

The PUMA approach [21] was used for the uncertainty assessment. The uncertainty contributions estimated were the following: 1) measuring weights u_r, 2) water absorption for object u_a, 3) technical weight u_w, 4) temperature effects u_t, and 5) reproducibility due to the measurement process u_p. The contribution from the temperature was divided into three sub categories: 4.1) difference for instrument u_{t1}, 4.2) difference for object u_{t2}, and 4.3) deviation from the standard reference temperature u_{t3}. The models in (6.1) and (6.2) are used for uncertainty estimation.

$$U = k \cdot u_c \qquad (k = 2) \tag{6.1}$$

In this case U is the expanded uncertainty, u_c is the combined standard uncertainty and k is the coverage factor ($k=2$ for a coverage probability of 95 %). The considered uncertainty contributors are given in (6.2).

$$U = k \cdot \sqrt{u_r{}^2 + u_w{}^2 + u_{t1}{}^2 + u_{t2}{}^2 + u_{t3}{}^2 + u_p{}^2 + u_a{}^2} \tag{6.2}$$

An example of the distribution of uncertainty contributions is summarized in Figure 6.9 for Phantom 1 and Figure 6.10 for Phantom 2. It is clear that the uncertainty component is larger for water absorption in the case of PMMA compared to PE and PVC. It might be due to the fact that PMMA absorbs humidity (and water), whereas PE and PVC are resistant to humidity and water [39].

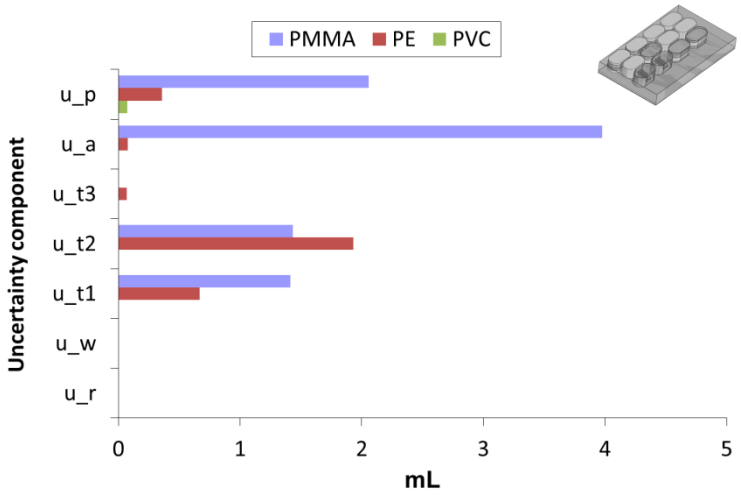

Figure 6.9. Phantom 1 – Comparison example of the distribution of uncertainty contributions acquired from the calibrations. All values are in mL.

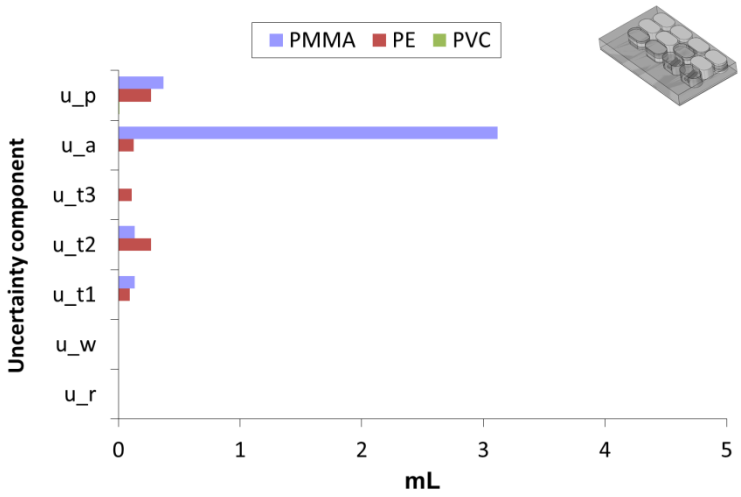

Figure 6.10. Phantom 2 – Comparison example of the distribution of uncertainty contributions acquired from the calibrations. All values are in mL.

6.2.2 Stability investigation

The stability of the phantoms was carried out in an assembled way, and a Two-Factor Factorial Design (DOE) was performed to investigate the relationship between material type and period of time. The experiments were carried out with nine repeated measurements. The two factors (material and period of time) were specified at 3 levels to investigate the time and material effects on the phantoms, as presented in Table 6.2. The three material types were PMMA, PE and PVC. The three tested periods of time were November 2011, December 2011 and February 2012. An ANOVA for the material types and period of times on the phantoms was performed regarding the guidelines

stated in [54]. The significance level was set to be $\alpha = 0.05$. An experimental overview is shown in Table 6.3. All the scans were carried out on a clinical CT under the same conditions at DMRI (Figure 6.11) [74]. The scanning parameters used are shown in Table 6.4. For computing volumes contents of PMMA, PE and PVC in the phantoms, commercial software called PigClassWeb was used [16]. Compensation of the results for temperature changes were made manually. The residuals were estimated in accordance with the stability of both phantoms. The residuals were evaluated and the method was done in the same way as for the repeatability on the step gauge (see section 3.5). Residuals and model adequacy checking showed that the residuals failed the normality test for Phantom 1, because of the small P value as shown in Figure 6.12. It was assumed to neglect the two-factor interactions, in which these were implemented in the error for the ANOVA. This assumption gave a higher P value as shown in Figure 6.13. The main effect and interaction plots are shown in Figure 6.14. Similar results were obtained for Phantom 2, see Figure 6.15, Figure 6.16 and Figure 6.17. From these it was clear that the mean variation between the three time periods were quite small, below 30 mL. Based on the ANOVAs in Table 6.5 and Table 6.6 it was evaluated that the used materials were stable. Depending on phantom and material, reference expanded measurement uncertainties (k=2) ranging from approx. 0 mL up to approx. 10 mL were estimated based on the calibrations, see Table 6.7. All reference values and uncertainties are reported in [74].

Table 6.2. A Two-Factor Factorial Design (DOE).

Factor	Level		
	1	2	3
Material	PMMA	PE	PVC
Period of time	November 2011	December 2011	February 2012

Table 6.3. Experimental plan.

No.	Material	Period of time
1	PMMA	November 2011
2	PMMA	December 2011
3	PMMA	February 2012
4	PE	November 2011
5	PE	December 2011
6	PE	February 2012
7	PVC	November 2011
8	PVC	December 2011
9	PVC	February 2012

Table 6.4. Scanning parameters.

Parameter	Value
Voltage in kVp	140
Current In mA	80
Slice width in mm	10
Time per 360° rotation in s	1
Number of revolutions (360° rotation)	54
Source-detector distance in mm	1099.3
Source-object distance in mm	630
Target material	Tungsten

Figure 6.11. DMRI's mobile CT scanner Scannerborg **[76]**.

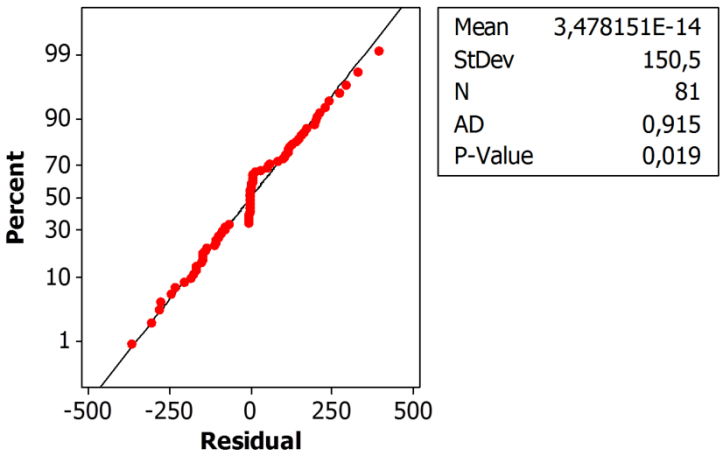

Figure 6.12. Phantom 1 – Normal probability plot of residuals (including interaction AB).

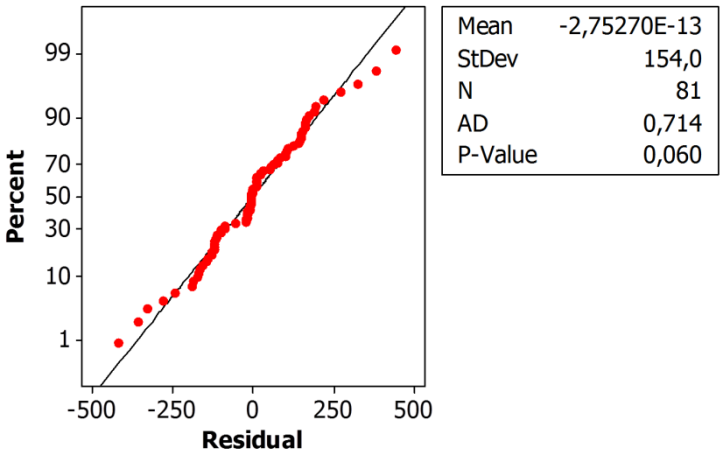

Figure 6.13. Phantom 1 – Normal probability plot of residuals (excluding interaction AB).

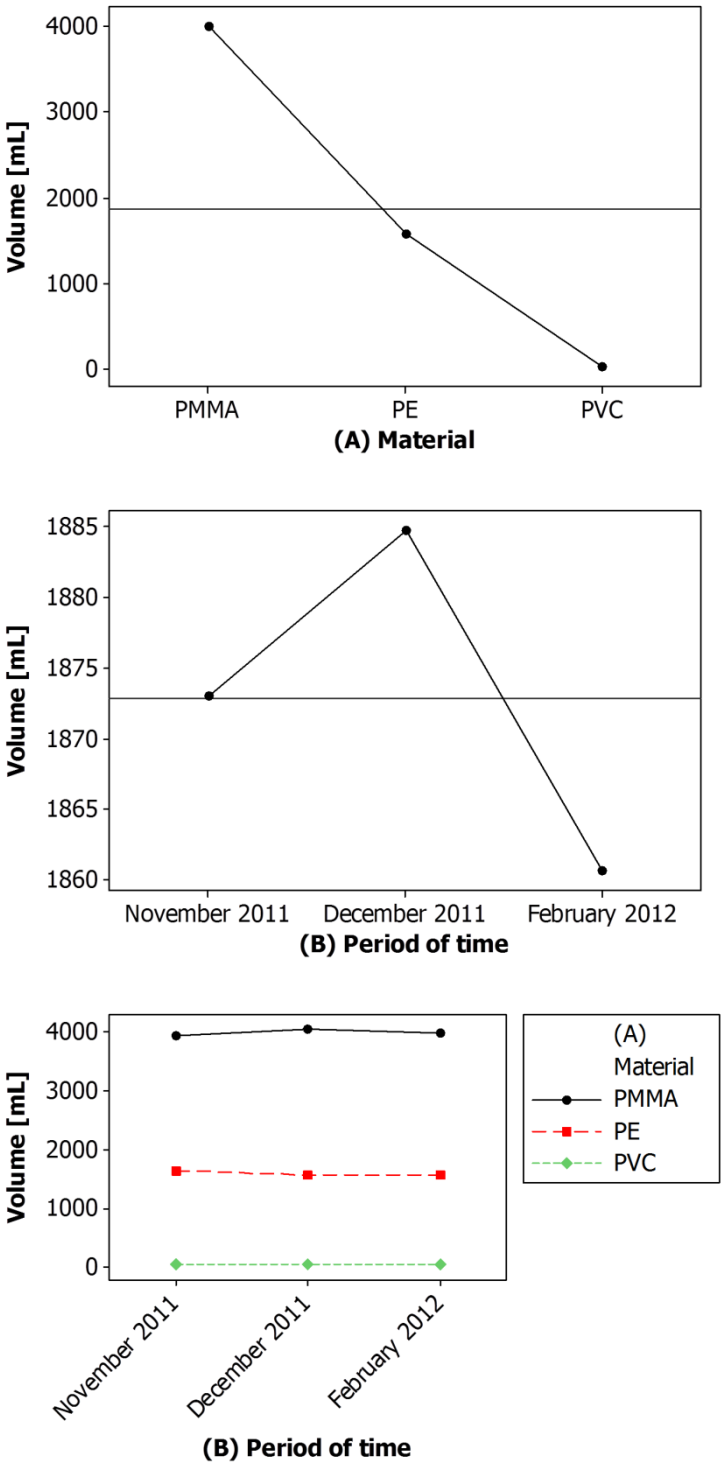

Figure 6.14. Phantom 1 – Main effect and interaction plots.

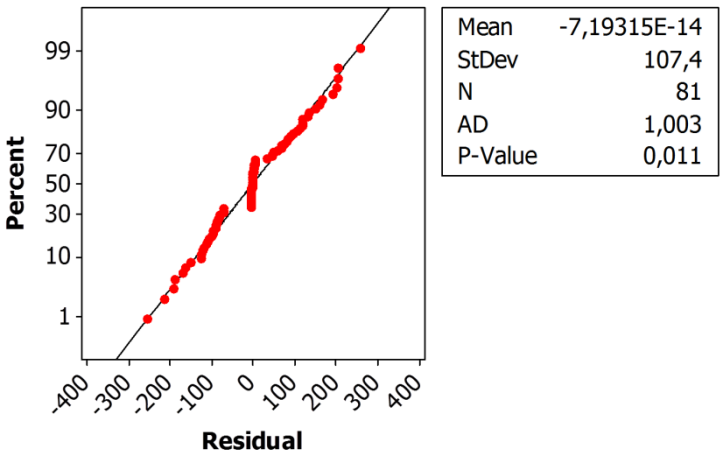

Figure 6.15. Phantom 2 – Normal probability plot of residuals (including interaction AB).

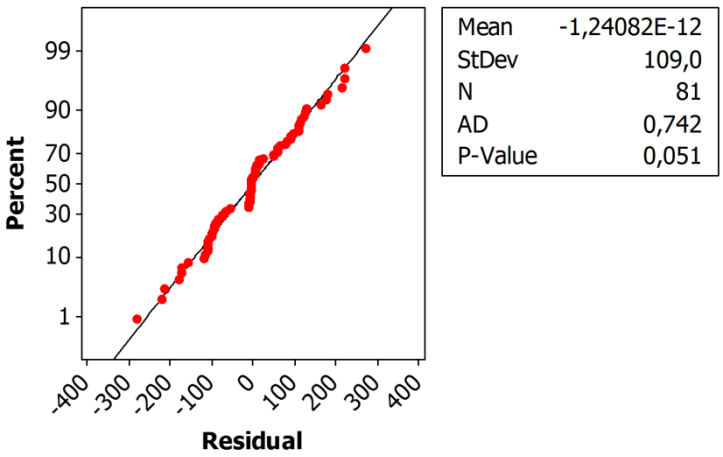

Figure 6.16. Phantom 2 – Normal probability plot of residuals (excluding interaction AB).

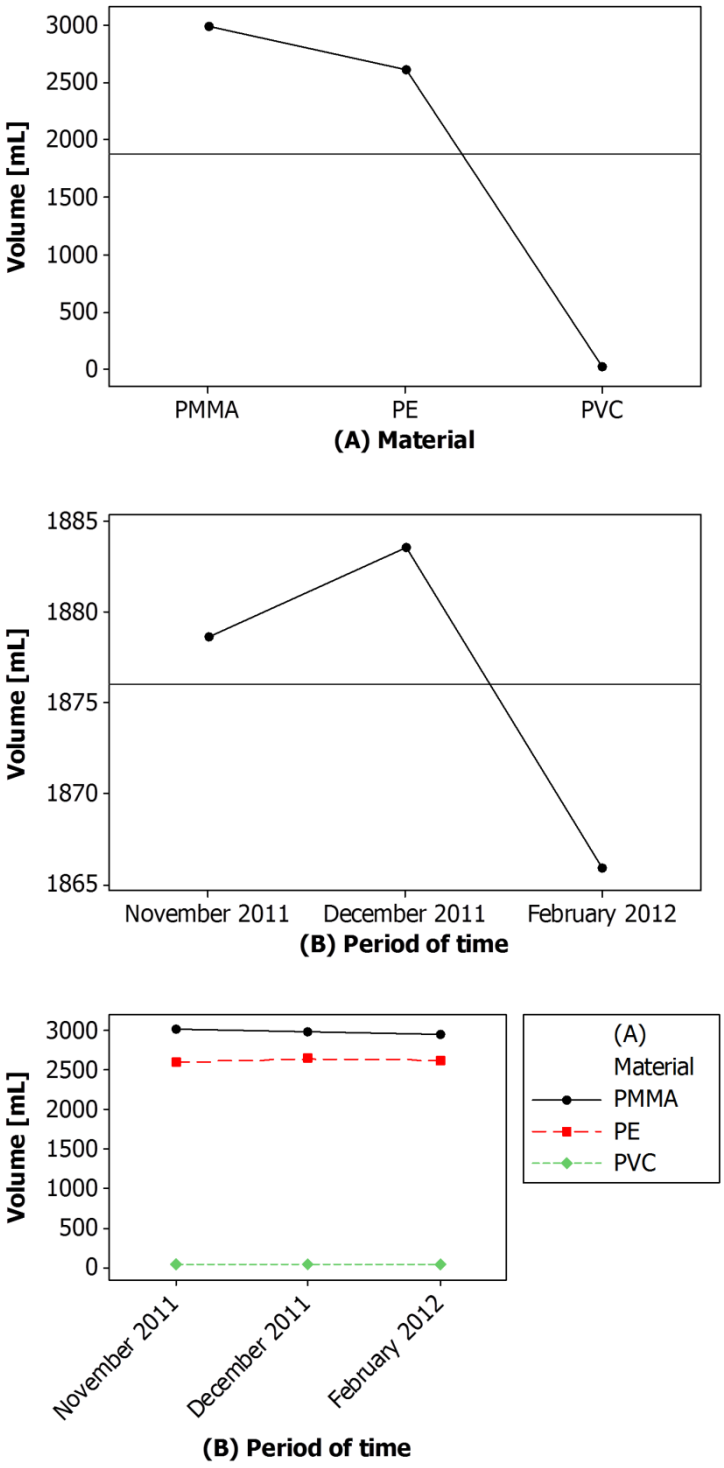

Figure 6.17. Phantom 2 – Main effect and interaction plots.

Table 6.5. Phantom 1 – Analysis of variance on volume of materials.

Source of variation	SS	df	MS	F value	P value
Material (A) at three levels (PMMA. PE and PVC)	215496285	2	107748142	4317.27	0.000
Period of time (B) at three levels (November 2011, December 2011 and February 2012)	7813	2	3906	0.16	0.855
Error	1896766	76	24957		
Total	217400863	80			

Table 6.6. Phantom 2 – Analysis of variance on volume of materials.

Source of variation	SS	df	MS	F value	P value
Material (A) at three levels (PMMA. PE and PVC)	140103757	2	70051879	5598.20	0.00
Period of time (B) at three levels (November 2011, December 2011 and February 2012)	4497	2	2248	0.18	0.836
Error	951010	76	12513		
Total	141059264	80			

Table 6.7. Phantoms – Reference expanded uncertainties (k=2). Values are in mL.

	PMMA	PE	PVC
Phantom 1	9.8	4.1	0.1
Phantom 2	6.3	0.9	0.0

6.3 Chapter conclusion

In this chapter, DMRI has developed two synthetic reference phantoms which represent real pig carcasses and are made of several polymer components, which stand for tissue types such as lean meat, fat, and bone. Currently there are no guideline for specification and verification of CT systems used for volume measurements, and the evaluation of the measurement uncertainty with assessment of all influential contributors constitutes a challenge with respect to the establishment of traceability and quality assurance. For this purpose, the developed reference phantoms can be applied by documenting the reference measurements using instruments with known measurement uncertainty. Traceable volume measurements for the phantoms are achieved by using the gravimetric method (also called water displacement method), and the stability has been documented for the two phantoms.

Chapter 7 Interlaboratory comparison on CT scanners for industrial applications in the meat processing industry

This chapter focuses on the application of clinical CT for traceable measurement of volumes on polymer phantoms in the meat processing industry. No one else has done similar before on this issue. The uncertainty considerations and challenges were very similar to the one from the comparison on industrial CT for industrial applications in manufacturing industry in Chapter 4. The main differences between this comparison and the comparison in Chapter 4 were the following: 1) clinical CT were applied, 2) volumes were investigated, and 3) multi-materials were applied.

7.1 Project management and time schedule

The phases in the project involved were: 1) plan, participants' definition, 2) phantoms calibrations, 3) circulation, 4) analysis of results, and 5) reporting and dissemination. The timeline in Figure 7.1 gives an indication of the different phases.

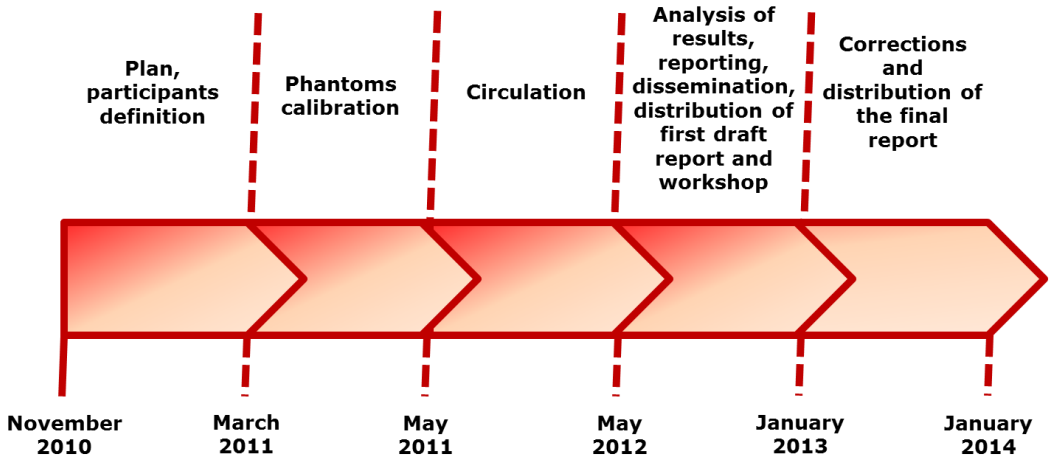

Figure 7.1. Time schedule for the CIA-CT comparison.

7.2 Participants and comparison phantoms

The CIA-CT interlaboratory comparison on X-ray CT for industrial applications in the slaughterhouses was organized by CGM, DTU MEK and carried out within the project "CIA-CT - Centre for Industrial Application of CT scanning". The comparison was

carried out in the period from November 2010 to January 2014, involving 4 laboratories from 4 countries (see Figure 7.2): DMRI Danish Meat Research Institute (DK), IFIP-Institut du Porc (FR), MRI - Department of Safety and Quality of Meat (DE), and SIC Egészségügyi Centruma (HU). A total number of 6 clinical CT took part in the comparison, because Hungary contributed with 3 scanners. Additionally, DMRI contributed with two identification numbers (in which two different software were used for volume estimation). It resulted in a total of seven identification numbers [74].

Figure 7.2. The 4 participants in the CIA-CT circulation.

The general purpose of the comparison was to test applicability of clinical CT, in terms of systematic errors and estimated uncertainties, to carry out measurements on polymer phantoms commonly representing tissue materials in pig carcasses from the meat processing industry, which are more representative than reference objects used for calibration and verification of CT. The phantoms circulated in the comparison, were a skinny pig carcass (Phantom 1) and a fat pig carcass (Phantom 2), and both phantoms were presented in Chapter 6. Regarding the circulation it was important to avoid damages and limit contamination of the phantoms, so they were sealed and wrapped in flamingo boxes. The phantoms were kept in trunks (see Figure 7.3). In short, the aim of the measurement was to determine different volume measurands, encompassing volumes of polymer materials as PMMA, PE and PVC. Measurement procedures were sent to each participant together with the phantoms to be measured. The measurement procedures are described in detail in [74]. Setting parameters were freely chosen by each single participant, who also was free to select measurement set-up and way of fixing the phantoms. Figure 7.4 shows an example of measurement set-up and way of fixing the phantoms during CT scanning by one of the participants.

Figure 7.3. Internal flamingo box containing a phantom and a trunk for storage and transportation.

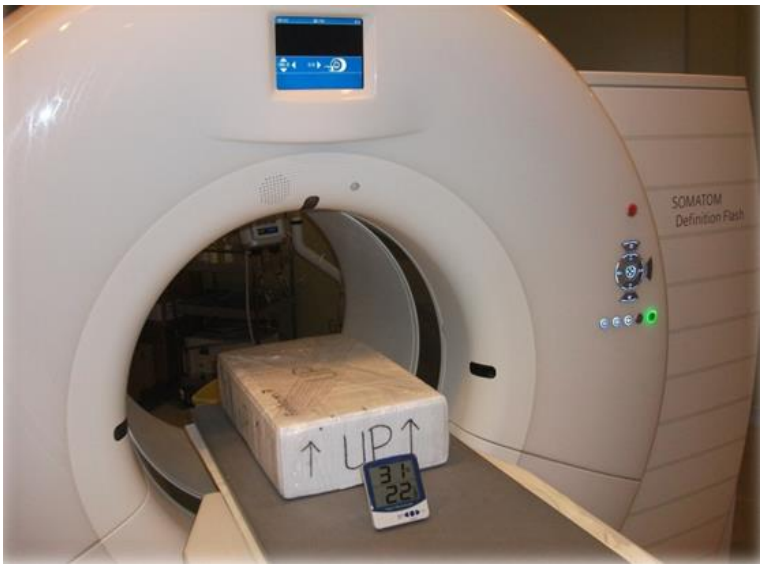

Figure 7.4. Measurement set-up and fixture for one of the phantoms in a Siemens clinical CT scanner.

7.3 Analysis of participants' data

Reference measurements and phantoms stability were presented in Chapter 6. Altogether, 2 phantoms were circulated to the participants in the period May 2011 to May 2012. All participants carried out measurements following without problems the measurement instructions distributed by the coordinator. Information about the clinical CT and measurement set-ups used by the participants, as well as tables and graphs with data analysis of the single CT, were elaborated and reported in [74]. The results by each

participant are kept confidential. Each participant can identify his own results using a personal identification number provided by the coordinator. Statistics of collected information concerning instrument settings and operator adjustments have shown that the participants in the comparison have followed state-of-the-art procedures for their measurements, taking steps to minimize beam hardening artifacts and blurred edges. 3 out of 6 clinical CT did not apply scale error correction. The most participants did not have any experience of how to outline uncertainty budgets. Only one participant had stated the uncertainties in the range 0-18 mL. All single values and uncertainties are reported in [74].

Table 7.1. Expanded uncertainties stated by the participants (k=2). Values are in mL.

	Phantom 1			Phantom 2		
	PMMA	PE	PVC	PMMA	PE	PVC
MAX	6.0	6.8	0.1	11.4	17.5	0.1
AVG	**6.0**	**6.8**	**0.1**	**11.4**	**17.5**	**0.1**
MIN	6.0	6.8	0.1	11.4	17.5	0.1

The results of the single participants were analysed and compared with reference values obtained by the coordinator. Figure 7.5 shows typical results. Systematic errors were detected for some participants concerning the polymer materials, which may be due to measurement errors as threshold determination, non-corrected scale, or uncompensated temperature. A way to identify if a participant has segmentation problems or miss to correct for scale errors, the total volume of the phantom can be used. In Figure 7.6, the total volume deviation from the reference value is shown. It is clear that scale error and/or threshold correction particularly should be considered for ID no. 1 and 7 compared to the other IDs [74]. In order to judge the agreement between reference values and participant values, the $|E_n|$ value normalised with respect to the stated uncertainty was computed according to ISO 17043 guidelines [46]. All 6 results obtained by the participants using CT scanning yield $|E_n|$ values larger than 1. Disagreement can be caused by systematic errors in the measurement or be due to an underestimation of the uncertainty.

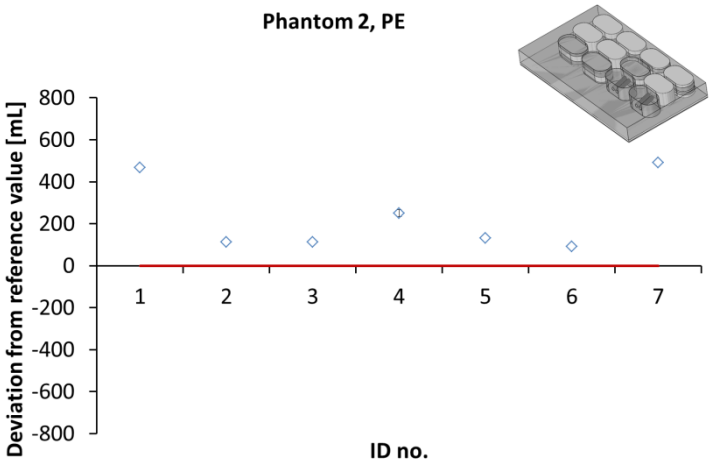

Figure 7.5. Results for Phantom 2. PE.

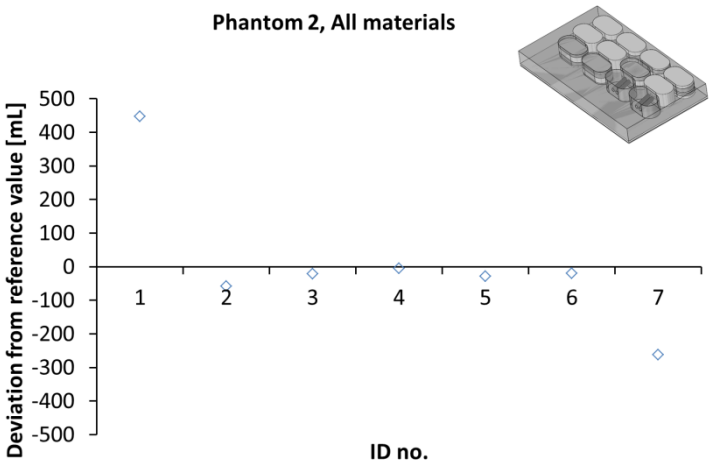

Figure 7.6. Results for Phantom 2. All materials. Indication on scale errors.

Table 7.2. Distribution of $|E_n|$ values for Phantom 1 and 2. Values are in %.

	Phantom 1			Phantom 2		
	PMMA	PE	PVC	PMMA	PE	PVC
$\|E_n\|<1$	0	0	0	0	0	0
$\|E_n\|\geq 1$	1	1	1	1	1	1

A recalculation of uncertainties in order to achieve $|E_n| = 0.99$ was carried out for those results that had led to $|E_n|$ values larger than 1. Some results were identified as outliers using the interquartile rule for outliers [12] and excluded from the calculations. It was concluded that likely uncertainties for the laboratories would lie in the range 1-1090 mL

and maximum values up to 1348 mL, see Table 7.3. This approach is limited by the fact that all deviations are treated as random, including systematic errors, yet it clearly indicates that uncertainties of 0-18 mL stated by the participants are underestimated. The comparison shows that CT scanning on phantoms, generally speaking, is connected with uncertainties in the range 1-1090 mL, as compared to an uncertainty range of 0-10 mL using the principle of water displacement. The phantoms are suitable artefacts for CT measurements of this kind.

Table 7.3. Recalculated expanded uncertainties to achieve $|E_n| = 0.99$ (k=2). Average values based on all measurements originally giving $|E_n| \geq 1$ after outlier removal. Values are in mL.

	Phantom 1			Phantom 2		
	PMMA	PE	PVC	PMMA	PE	PVC
MAX	142.0	362.8	3.2	1110.4	1348.2	3.2
AVG	69.6	124.4	1.1	997.5	1090.0	1.5
MIN	7.7	4.1	0.4	890.7	942.6	0.5

7.4 Chapter conclusion

The main conclusions which were drawn from the comparison are outlined in the following.

- The CIA-CT comparison on clinical CT involved two polymer phantoms. Circulation started in May 2011, and was completed in May 2012. 4 participants from 4 countries participated.
- Two synthetic phantoms representing real pig carcasses were circulated.
- Different volume measurands were considered, encompassing PMMA, PE, and PVC.
- Reference values for both phantoms were provided by DMRI and CGM using the principle of water displacement, with expanded measurement uncertainties in the range 0-10 mL.
- Each participant can use the comparison results to investigate the presence of systematic errors and/or any underestimation of uncertainties.
- It was found that scale error and/or threshold correction particularly should be considered for some of the participants.
- The measured values by the participants differ compared to the reference values. The reason to these trends could be due to the specified tolerances defined by the participants for threshold determination of the polymer materials.
- Statistics of collected information concerning instrument settings and operator adjustments have shown that the participants in the comparison have followed state-of-the-art procedures for their measurements.

- The most participants did not have any experience of how to outline uncertainty budgets. The expanded uncertainties stated by the participants are in the range 0-18 mL for both phantoms and all materials.
- All 6 results obtained by the participants using CT scanning yield $|E_n|$ values larger than 1.
- A recalculation of uncertainties in order to achieve $|E_n| = 0.99$ was carried out for those results that had led to $|E_n|$ values larger than 1. Some results were identified as outliers using the interquartile rule for outliers and excluded from the calculations. It was concluded that likely uncertainties for the laboratories would lie in the range 1-1090 mL and maximum values up to 1348 mL.
- The phantoms are suitable artefacts for CT measurements of this kind.

Chapter 8 Performance verification of algorithms for pig body dissection

DMRI and DTU Compute have previously developed advanced image analysis software (PigClassWeb) which performs virtual dissections in pig carcasses in connection with their collaboration in the Virtual Slaughterhouse project. A part of the Virtual Slaughterhouse was carried out dealing with different aspects of mathematical modeling, image analysis, shape modeling etc. applied to pig carcasses [15; 77; 78]. The dissections in PigClassWeb are automatically adjusted to the whole population of pigs that are scanned, in such a way that the virtual dissections are anatomically identical for each carcass, irrespective of size, weight and proportions [16]. Experiments were prepared and accomplished to document the performance of PigClassWeb through volume comparisons to real dissections of pig carcasses. The experiments were divided into three main tasks: 1) evaluation of manual dissection of pig carcass volumes using registration based software called VolumeGraphics, 2) optimization of virtual dissection facilities using PigClassWeb, and 3) performance of virtual dissection parameters by volume comparisons to manual dissection results.

8.1 Procedure for scanning approach

The volumes of the tissue materials were divided into three classes: bone, lean meat, and fat. All scans were acquired using the mobile CT scanner “Scannerborg” at DMRI (was presented in section 6.2), and all scanning and setting parameters were the same through all experiments and similar to the one in section 6.2. A dataset containing CT scanned left middle pieces (before dissection) and corresponding products (after dissection) were used to evaluate the quality and performance of both manual and virtual dissection (see Figure 8.1). The products consisted of loin ribs, spare ribs, back, and belly. The spinal column had been removed from the products compared to the left middle piece. An example of the scan setup of a pig carcass is shown in Figure 8.2. In the experiments, a population of 48 pigs were included and divided into six subgroups depending on size and weight, see Table 8.2 [79]. It was assumed that the 8 pigs in each of the 6 groups could be considered as replicates.

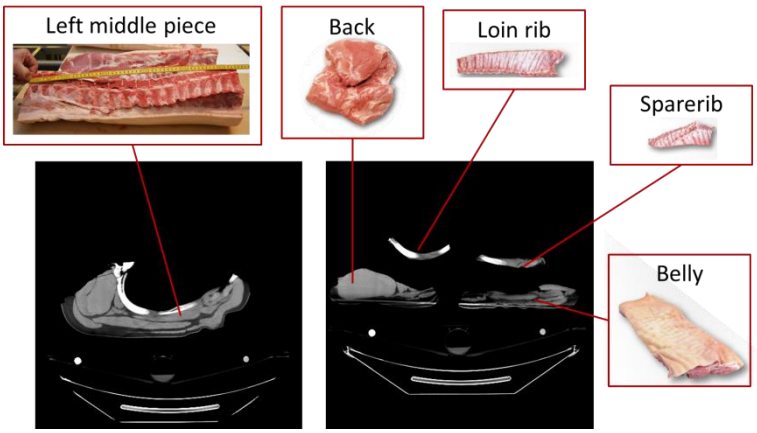

Figure 8.1. Scanned images of left middle piece (left) and products (right) from ImageJ software. Images of products are acquired from Danish Crown product catalogue **[80]**.

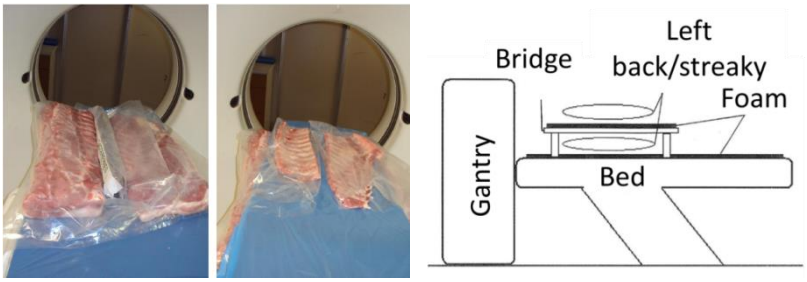

Figure 8.2. Lower layer (left) and upper layer (middle) for a pig carcass after manual dissection. Draft of the setting up for scanning of pig carcass (right) **[79]**.

Table 8.1. Batch of pigs in the experiments **[79]**.

Group no.	1	2	3	4	5	6
Settlement weight [kg]	70-75	70-75	78-83	78-83	88-94.9	88-94.9
Length [cm]	≤ 168	≥ 170	≤ 171	≥ 175	≤ 176	≥ 180
Number of pigs	8	8	8	8	8	8

8.2 Evaluation of manual dissection using registration based software

8.2.1 Design of experiment

A Two-Factor Factorial Design (DOE) was carried out to investigate the relationship between group and material. The two factors (group and material) were specified at 3-6 levels to investigate the group and material effect on material waste, as presented in Table 8.2. An ANOVA was performed with eight replicated measurements following the guidelines stated in [54]. The significance level was set to be $\alpha = 0.05$.

Table 8.2. A Three-Factor Factorial Design (DOE).

Factor	Level					
	1	2	3	4	5	6
Group	1	2	3	4	5	6
Material	Bone	Lean meat	Fat			

8.2.2 Data evaluation

The volume estimation of left middle pieces and products were made manually using commercial software called VolumeGraphics. The estimations were performed depending on the frequency of grey values for bone, lean meat, fat and their related tolerances. The grey values are estimated based on a literature investigation [14; 81; 82], in which the selected Hounsfield units (grey values) and Hounsfield ranges appear from Table 8.3 for common substances and tissue types. These values can be identified visually by the operator using the histograms for the grey values, see Figure 8.3. The procedure and the operator were identical for all pigs to avoid procedure and operator errors. The temperature was not registered during the scanning experiments, so it was not possible to compensate for thermal volumetric expansion.

Table 8.3. Hounsfield units and Hounsfield ranges for common substances and tissue types.

Substance	Hounsfield unit	Hounsfield range
Air	-1000	
Fat	-60	-300 to 0
Water	0	
Lean meat	60	1 to 150
Bone	>150	151 to 3000

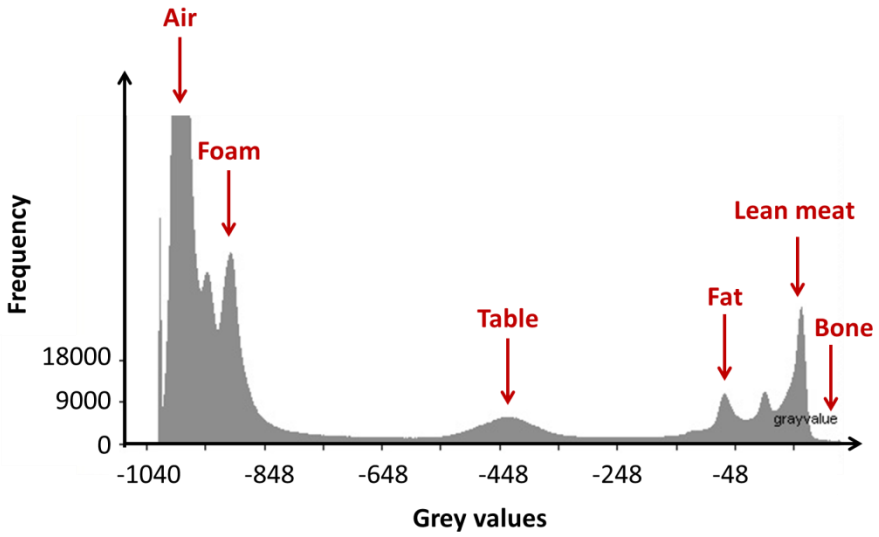

Figure 8.3. Estimated grey values from VolumeGraphics through the scanning of a pig carcass.

8.2.3 Results and discussion

The residuals were evaluated and the method was done in the same way as for the repeatability on the step gauge (see section 3.5). Residuals and model adequacy checking showed that the residuals failed the normality test, because of a small P value as shown in Figure 8.4. Instead it was assumed to neglect two-factor interactions, in which these were implemented in the error for the ANOVA. This assumption gave a higher P value as shown in Figure 8.5. Based on the ANOVA in Table 8.4 it was documented that only the tissue materials were significant for the material waste. The main effect and interaction plots are shown in Figure 8.6, and the following evaluations can be drawn based on the main factors only:

- It was expected that the volume of products should be reduced compared to left middle pieces because of waste. Surprisingly the volume of bone for the products had been added up to 250 cm^3 compared to the left middle piece. A proposal could be due to segmentation challenges for multi-materials.
- The average waste for each pig carcass increased with increasing group number due to the size of the pigs (ranging from 500 to 750 cm^3). The values are shown in percent comparing pig carcasses before and after dissection in Figure 8.7. The waste for meat and fat was in the range 15-20 %, and bone was added up to 40 %.
- The temperature stability during the scanning process was within the range of ±1°C. Approximated thermal volumetric expansion coefficients for tissue materials are shown in Table 8.5 based on literature studies [83; 84; 85]. It gave thermal volumetric expansion variations in the range 0.1-1.8 cm^3. This influence was quite small, and the thermal expansion can be neglected.
- Furthermore potential biases should be considered, because no validation was performed for the volume estimations in VolumeGraphics.

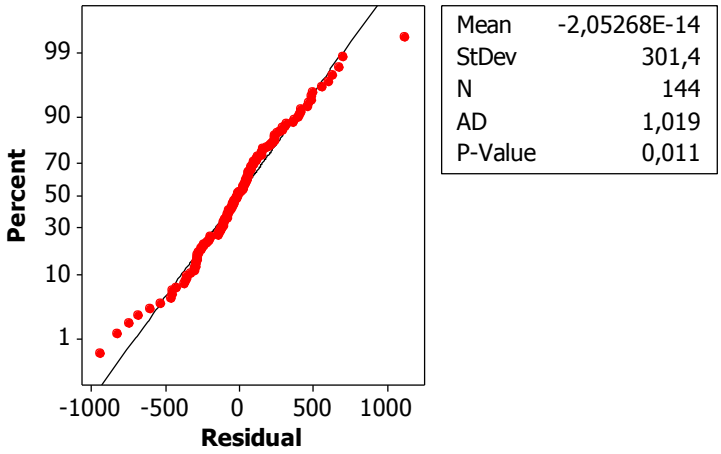

Figure 8.4. Normal probability plot of residuals (including interaction AB).

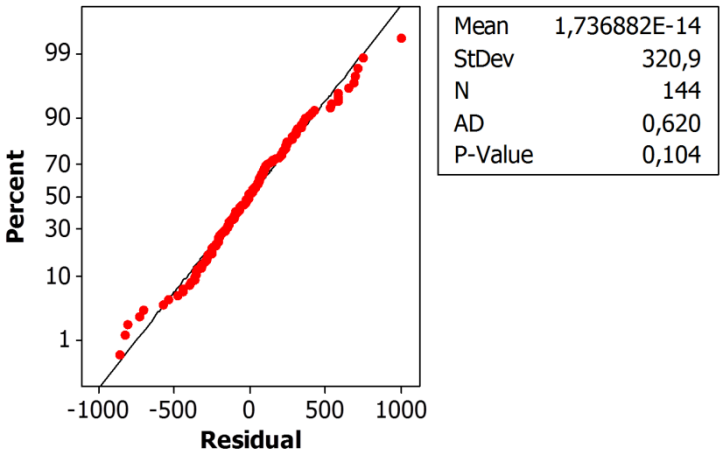

Figure 8.5. Normal probability plot of residuals (excluding interaction AB).

Table 8.4. ANOVA on material waste through manual dissection facility.

Source of variation	SS	df	MS	F value	P value
Group (A)	672024	5	134405	1.24	0.293
Material (B)	43403260	2	21701630	200.49	0.000
Error	14721156	136	108244		
Total	58796440	143			

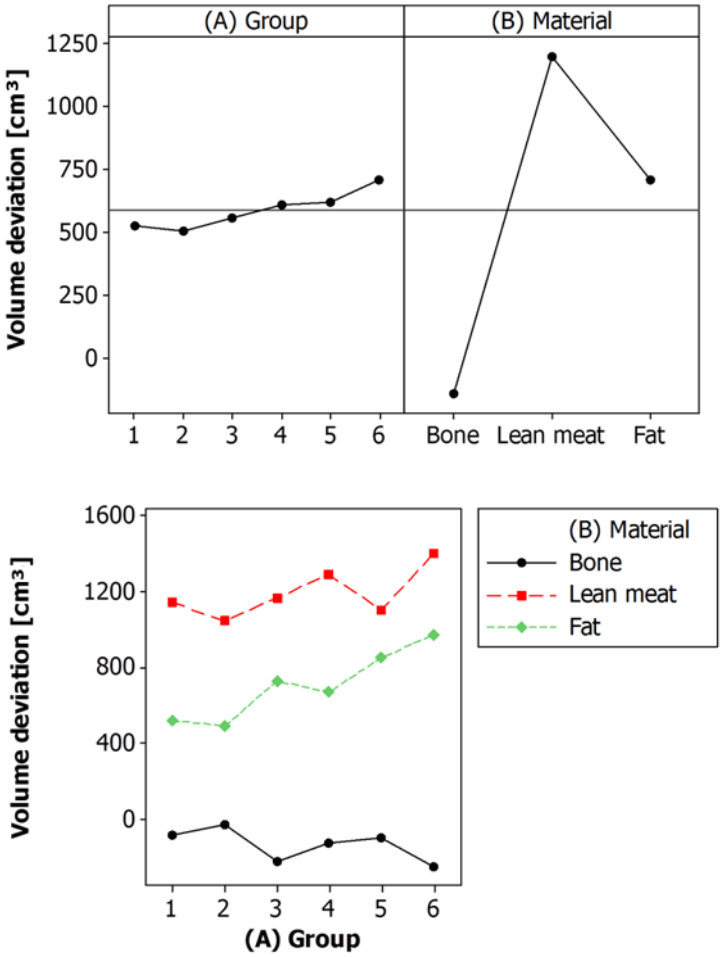

Figure 8.6. Main effect and interaction plots.

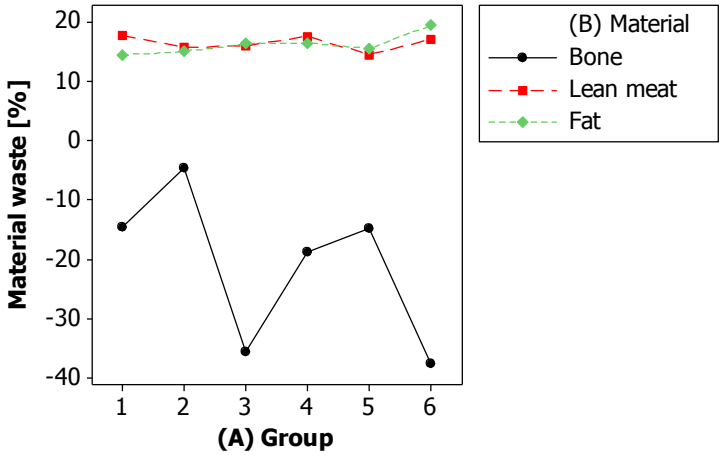

Figure 8.7. Interaction plot of material waste compared with pig carcasses before dissection in percent.

Table 8.5. Approximated thermal volumetric expansion coefficients for tissue materials **[83; 84; 85]**.

Tissue material	(x 10^{-6} K^{-1})
Bone	197
Lean meat	700
Fat	375

8.3 Optimization of virtual dissection facilities

8.3.1 Virtual dissection using simulation software

After importing the real scanned left middle piece areas in PigClassWeb, the treatment due to offset and width were possible, followed by a tri-dissection with selected offsets, as shown in Figure 8.8. For the offset, in the case of negative values refer to moving carving dissection (red and/or yellow lines in Figure 8.8) towards the posterior (inferior), while the positive values are oppositely directed and therefore in the direction of the head (superior). After the tri-dissection was performed, a four-dissection should be made with selected widths (the width of the curvature of the splitting line), without removing the fat (a fat thickness of 40 mm was assumed), so the virtual products resemble to the real products. The data outputs from PigClassWeb were in mass units (kg) and were converted to volume units (cm^3) through information of the density for bone, lean meat, and fat in the literature [14].

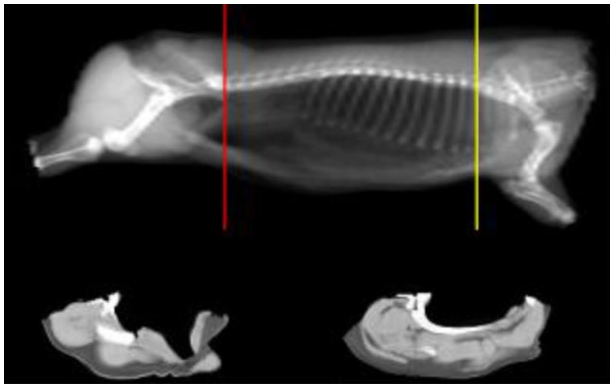

Figure 8.8. Tri-dissection example of adjusting the selected offsets in PigClassWeb. The dissection lines are shown in red (left) and yellow (right) **[16]**.

8.3.2 Design of experiment

An expected Four-Factor Factorial Design (DOE) was simplified to a Three-Factor Factorial Design. The design was simplified, because it was documented that one of the factors (offset) had no effect on the material waste in pig carcasses. The experiment was

performed to investigate the relationship between group, material and width. These three factors were specified at 3-6 levels to investigate the group, material and width effect on material waste, as presented in Table 8.6. An ANOVA was performed with eight replicated measurements following the guidelines stated in [54], and the significance level was set to be $\alpha = 0.05$.

Table 8.6. A Three-Factor Factorial Design (DOE).

Factor	Level					
	1	2	3	4	5	6
Group	1	2	3	4	5	6
Material	Bone	Lean meat	Fat			
Width	150 mm	160 mm	170 mm	180 mm	190 mm	200 mm

8.3.3 Results and discussion

The residuals were evaluated and the method was done in the same way as for the repeatability on the step gauge (see section 3.5). Residuals and model adequacy checking showed that the residuals failed the normality test, because of the small P value as shown in Figure 8.9. Assuming neglecting of two-factor and higher interactions did not modify the P value as shown in Figure 8.10. This means that the experiment was rejected, because the distribution was not normal. The reason can be that the simulation data had special problems and opportunities which were difficult to handle by current regression software. The main effect and interaction plots are shown in Figure 8.11. The following conclusions can be drawn based on the main factors only:

- The material waste increased with increasing width but the increasing value was quite small. An optimal width to reduce the amount of waste using virtual dissection was a width of 150 mm.
- The average waste for each pig carcass increased with increasing group number due to the size of the pigs (ranging from 190 to 240 cm^3). The values are shown in percent comparing pig carcasses before and after dissection in Figure 8.12. The waste for meat and fat was in the range 0-5 %, and the waste for bone was around 50 %.
- Generally it was obvious that the average waste for each pig carcass was lower for virtual dissections compared to manual ones.

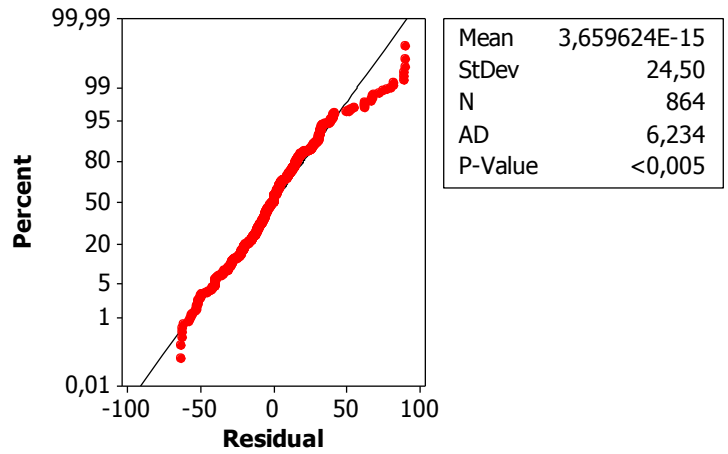

Figure 8.9. Normal probability plot of residuals (including interactions of second and higher order).

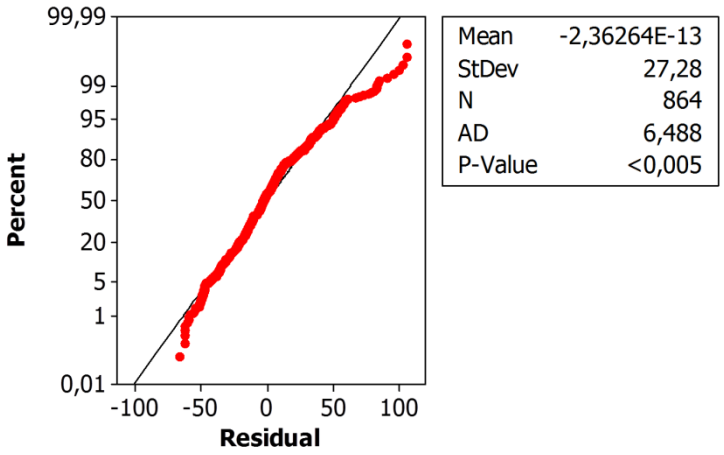

Figure 8.10. Normal probability plot of residuals (excluding interactions of second and higher order).

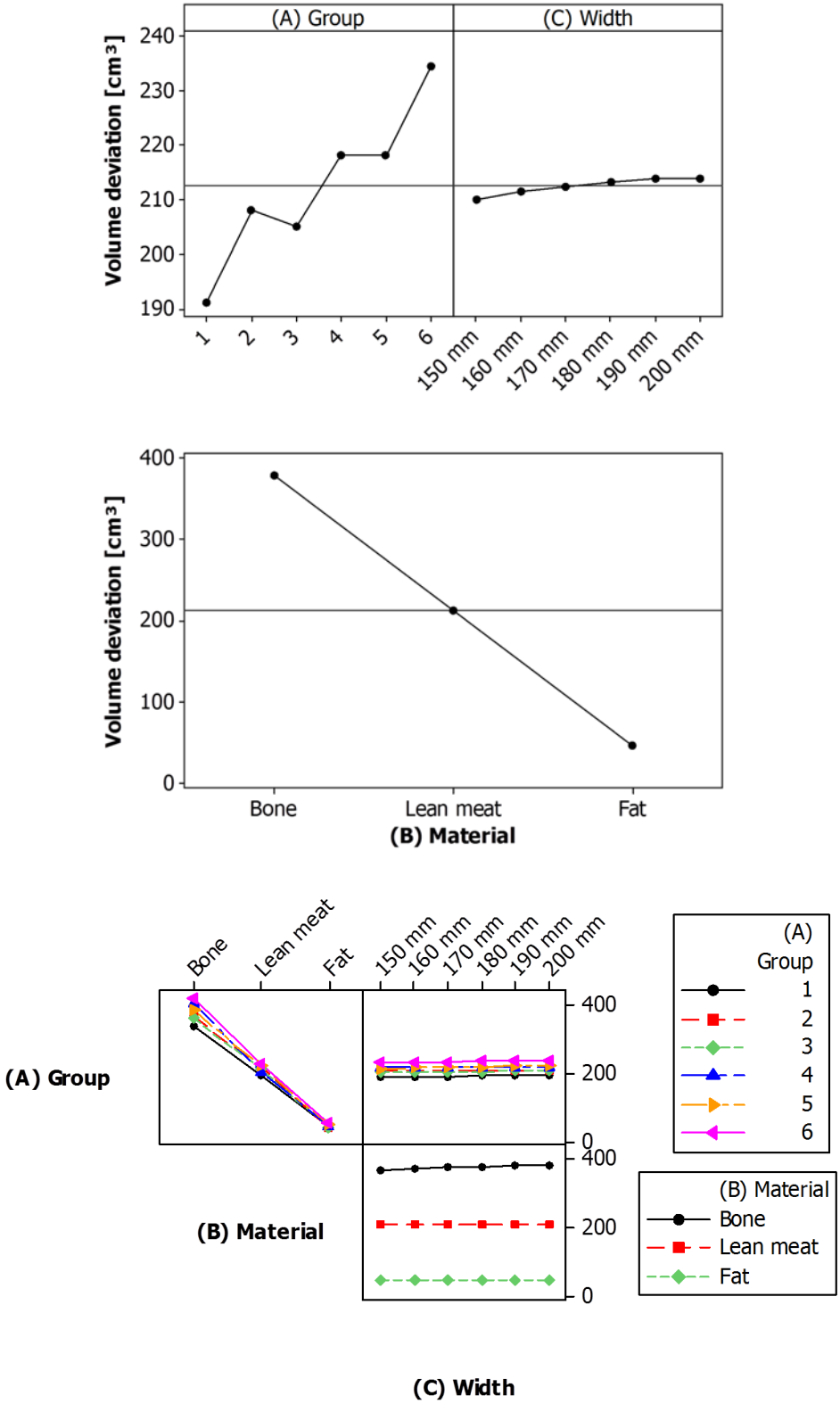

Figure 8.11. Main effect and interaction plots. Values are in cm^3.

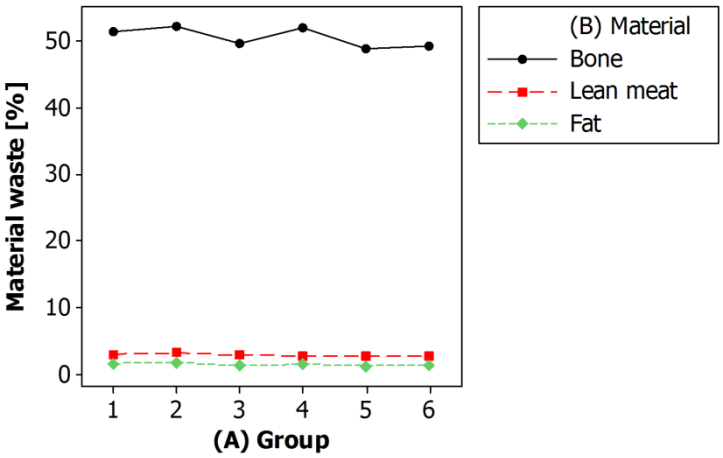

Figure 8.12. Interaction plot of material waste compared with pig carcasses before dissection in percent.

8.4 Performance of virtual dissection parameters by volume comparisons to manual dissection results

Evaluations were accomplished separately for 1) left middle pieces, 2) products, and 3) material waste. The material waste was defined as the deviation between left middle pieces and products. All evaluations were performed on volume comparisons between virtual dissection results and manual dissection results, and based on the acquired R-squared values.

8.4.1 Left middle piece

In Figure 8.13, the R-squared values are shown for bone (R^2 = 0.20), lean meat (R^2 = 0.85) and fat (R^2 = 0.87) between manual and virtual facilities of each pig carcass. In Figure 8.14, the R-squared value is (R^2 = 0.94) between manual and virtual facilities of the total volumes of each pig carcass. The following conclusions can be drawn based on the acquired R-squared values:

- From the total volumes for manual and virtual facilities it was clear that there was a linear regression for the deviation between manual and virtual facilities. The deviation could be due to scale error correction in one of the used software or both. The total volume was around 4-5 % larger for the manual one compared to the virtual one.
- Big differences were detected for tissue types between manual and virtual estimations compared to total volumes (see Figure 8.13 and Figure 8.14). These differences could be due to segmentation challenges, scale error or both.

- Some suggestions that these extreme differences for tissue types occur could be due to operator errors, software errors in PigClassWeb and/or Volume Graphics or a combination.

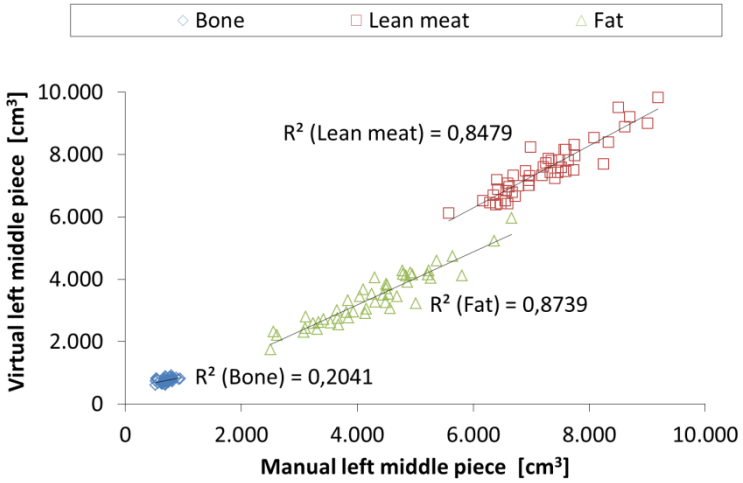

Figure 8.13. Virtual left middle piece vs. manual left middle piece. Tissue materials.

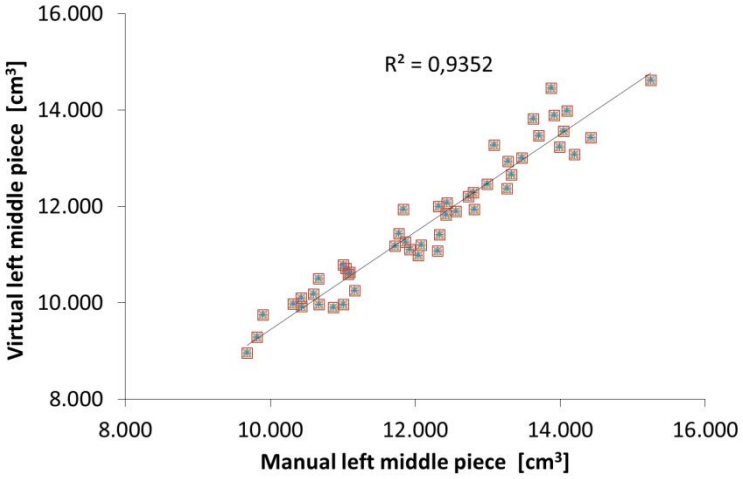

Figure 8.14. Virtual left middle piece vs. manual left middle piece. Total volumes.

8.4.2 Products

In Figure 8.15, the R-squared values are shown for bone (R^2 = 0.18), lean meat (R^2 = 0.78) and fat (R^2 = 0.82) between manual and virtual facilities of each pig carcass. In Figure 8.16, the R-squared value is (R^2 = 0.92) between manual and virtual facilities of the total volumes of each pig carcass. The following conclusions can be drawn based on the acquired R-squared values:

- The total volume was around 7-8 % smaller for the manual compared to the virtual. The main reason for this difference was that a smaller amount of waste from the virtual dissection compared to the manual (see section 8.3.3).
- The lower R-squared values compared to the one for the left middle piece (see section 8.4.1) could be due to the fact that the dissection complexity increases for algorithm and operator.
- Big differences were detected between manual and virtual estimations for tissue types compared to their total volumes of these (see Figure 8.15 and Figure 8.16).
- Other possible errors were similar to the left middle pieces (section 8.4.1).

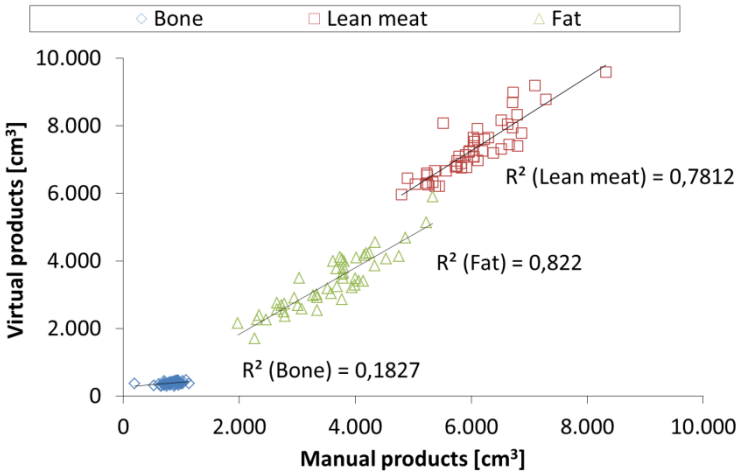

Figure 8.15. Virtual products vs. manual products. Tissue materials.

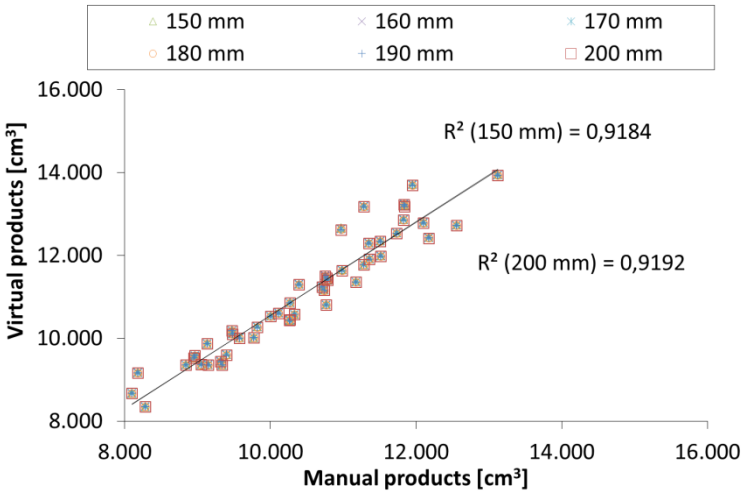

Figure 8.16. Virtual products vs. manual products. Total volumes.

8.4.3 Material waste

In Figure 8.15, the R-squared values are shown for the waste of bone (R^2 = 0.00), lean meat (R^2 = 0.06) and fat (R^2 = 0.04) between manual and virtual facilities of each pig carcass. In Figure 8.16, the R-squared value is (R^2 = 0.35-0.42) between manual and virtual facilities of the total waste of each pig carcass. The following evaluations can be drawn based on the acquired R-squared values:

- The conclusions are similar to the ones detected in section 8.4.1 and 8.4.2.
- From an optimization view, the best R-squared value for the total volumes of each pig carcass is if R^2 is close to zero. This will minimize the amount of waste during the virtual dissection process.

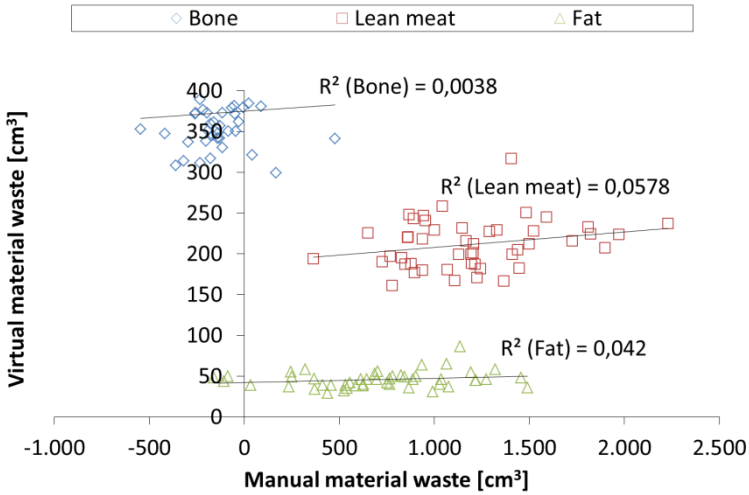

Figure 8.17. Virtual material waste vs. manual material waste. Tissue materials.

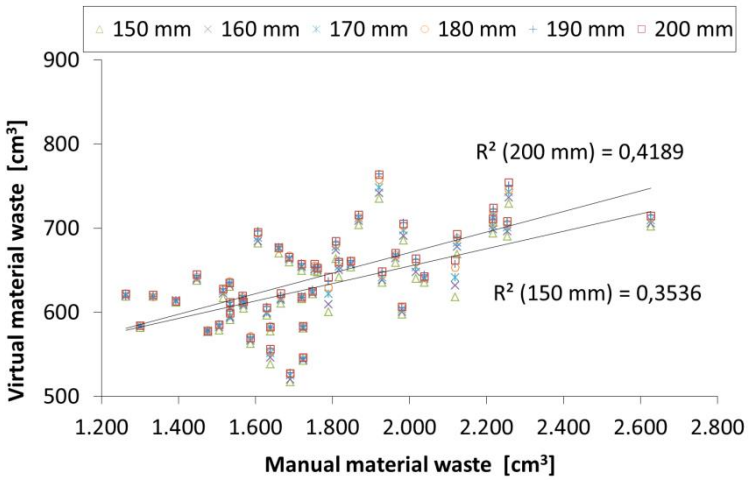

Figure 8.18. Virtual material waste vs. manual material waste. Total volumes. R^2 in the range 0.35 to 0.42 for all widths. The R^2 value increases with increasing width.

8.5 Chapter conclusion

In this chapter, DMRI and DTU Compute have previously developed advanced image analysis software (PigClassWeb) which carries out virtual dissections in pig carcasses. In this Ph.D. thesis a DOE was carried out to document the performance of PigClassWeb through volume comparisons to real dissections of pig carcasses. For the real dissections, volumes of tissue types such as bone, lean meat and fat, are estimated using commercial VolumeGraphics software. It is detected that the ANOVA and the residuals from the virtual dissection fail the normality test. The reason can be that the simulation data has special problems and challenges which are difficult to overcome by using current regression software. Some suggestions as to why these extreme differences for tissue types occur could be due to operator errors, software errors in PigClassWeb and/or Volume Graphics or a combination of the two.

Chapter 9 Conclusion

9.1 Summary

This Ph.D. thesis deals with the development of procedures for quality assurance of X-ray computed tomography for industrial measurements both in the manufacturing and in the meat processing industries. Various methods and reference objects have been developed in this project to establish metrological traceability of measurements. Moreover investigations as well as international comparisons in the field of application on the two different areas have been carried out. In the following the main conclusions of this work are drawn.

- Different considered standards and guidelines to generate traceability in CT in manufacturing industry are presented and different influence factors are presented. Currently many standardized procedures are still under development which means that the traceability of CT cannot be ensured. One of them is the German guideline VDI/VDE 2617-13 which is considered as a fundamental one for specification and verification of CT system used for coordinate metrology in the manufacturing industry. Various methods and reference objects have been developed in this Ph.D. project to establish metrological traceability of measurements, which can be achieved by documenting the reference measurements using instruments with known measurement uncertainty. In this work, three kinds of reference objects are introduced: step gauge, step cylinder and a cylindrical multi-material assembly. Moreover, two reference objects are calibrated objects from the manufacturing industry: a threaded tube from the medical industry and a LEGO brick from the toy industry. The quality assurance is carried out using coordinate measuring machines (CMMs). The documentation of traceability and the metrological compatibility has been based on various aspects such as form errors, stability over time, uncertainties and temperature effects. The stability has been documented for all reference objects except for the step cylinder and the cylindrical multi-material assembly. These measurements can be used to correct measurement errors in data from a CT. Additionally a brief presentation is made on error sources in CT such as scale errors, threshold offsets, beam hardening, cone beam artifacts and scattered radiation.

- A method is presented for evaluating measuring errors arising in a CT system from the manufacturing industry in terms of material density and the orientation of the scanned objects. Step gauges are selected with uni- and bidirectional

lengths. The analysis of variance (ANOVA) shows that all main factors and their interactions are significant. The following conclusions can be drawn based on the main factors only: 1) the material density affect the measurement results, 2) a vertical orientation is not recommended because of X-ray scattering noise and relatively lower scattering noise ratio on the planes that are parallel to the X-ray beams, and 3) approximately no difference is detected between horizontal and inclined orientations. The maximum deviation from the reference value can be reduced by compensating for systematic errors sources, such as scale errors and threshold offsets. But it is more complicated to correct for vertical orientations in high density materials.

- In an interlaboratory comparison involving 27 laboratories from 8 countries, measurements were carried out using CT on two common objects from the manufacturing industry, a threaded tube and a LEGO brick. The comparison has shown that CT measurements on the industrial parts used lie in the range 6-53 µm, with maximum values up to 158 µm, compared to average uncertainties below 5.5 µm using CMMs.

- A test is performed to check if X-ray contrast modalities can be applied for metrological purposes. Traditionally, segmentation between multi-materials in CT scanning is done by using different edge detection techniques and threshold algorithms, but these are only available for multi-materials where the densities are not close to each other. X-ray contrast modalities overcome this problem by constructing dark field, phase contrast and transmission images. Measurement results show that further development related to stability issues on the used CT is needed to create a metrological tool using X-ray contrast modalities.

- Danish Meat Research Institute (DMRI) has developed two synthetic reference phantoms which represent real pig carcasses and are made of several polymer components, which stand for tissue types such as lean meat, fat, and bone. Currently there are no guideline for specification and verification of CT systems used for volume measurements, and the evaluation of the measurement uncertainty with assessment of all influential contributors constitutes a challenge with respect to the establishment of traceability and quality assurance. For this purpose the developed reference phantoms can be applied to establish traceable volume measurements by using instruments with known measurement uncertainty. Traceable volume measurements for the phantoms are achieved by using the gravimetric method (also called water displacement method), and the stability has been documented for the two phantoms.

- For the meat processing industry concerned, a similar interlaboratory comparison using two reference phantoms from the meat processing industry

was carried out using CT, and involved four laboratories from 4 countries. The comparison has shown that CT measurements on the phantoms used lie in the range 1-1090 mL, with maximum values up to 1348 mL, compared to average uncertainties below 10 mL using the gravimetric method.

- DMRI and DTU Compute have previously developed advanced image analysis software (PigClassWeb) which carries out virtual dissections in pig carcasses. In this Ph.D. thesis a DOE was carried out to document the performance of PigClassWeb through volume comparisons to real dissections of pig carcasses. For the real dissections, volumes of tissue types such as bone, lean meat and fat, are estimated using commercial VolumeGraphics software. It is detected that the ANOVA and the residuals from the virtual dissection fail the normality test. The reason can be that the simulation data has special problems and challenges which are difficult to overcome by using current regression software. Some suggestions as to why these extreme differences for tissue types occur could be due to operator errors, software errors in PigClassWeb and/or Volume Graphics or a combination of the two.

9.2 Outlook

During the work new considerable knowledge and a number of challenges were discovered. These latter should be investigated in further scientific researches. Some further works are suggested in the following:

- For the step cylinder and the cylindrical multi-material assembly, the documentation of traceability and the metrological compatibility can be improved based on various aspects such as form errors, surface roughness, temperature effects and stability over time.

- Develop methods and/or models which can compensate for all error sources in CT measurement results such as beam hardening, cone beam artifacts and scattered radiation.

- In coordinate metrology CT, cone beam artifacts can be avoided by take up cone beam limits or use a helical trajectory.

- A method or model is needed which can define threshold tolerances on assembly materials such as an assembly of two LEGO bricks.

- For further interlaboratory comparisons in the manufacturing industry, it is recommended to ask the participants for their selected threshold values to get an overview of the segmentation challenges and optimization. It is also recommended to ask the participants for eventual scale error corrections and threshold offsets.

- Investigations are needed in CT for applications in the manufacturing industry regarding improvement of measurement of form errors such as roundness and flatness.

- Stability issues and challenges on X-ray contrast modalities must be improved before it can be achieved as a metrological tool.

- Simple phantoms consisting of single materials can be developed and tested in a clinical CT to evaluate the volume variations and performance in connection with scale error corrections and threshold offsets. This simple experiment can also be implemented in further interlaboratory comparisons in the meat processing industry.

- A suggestion as to how one can validate and minimize software errors in PigClassWeb software is to ensure the metrological compatibility and traceability. In this case, following aspects can be involved 1) dimensional stability and weight changes of tissue materials, and 2) the changes on the shape of tissue materials such as fibers, when dissections are initiated.

- A method or model is needed which can define threshold tolerances on tissue materials in pig carcasses.

References

[1] Kalender, W. A. Computed Tomography: Fundamentals, System Technology, Image Quality, Applications. John Wiley & Sons, 2011.

[2] Kruth, J. P., Bartscher, M., Carmignato, S., Schmitt, R., De Chiffre, L., Weckenmann, A. Computed tomography for dimensional metrology. Annals of the CIRP 60/2, 2011. pp. 821-842.

[3] Bergmann, R. B., Bessler, F. T., Bauer, W. Computer tomography for nondestructive testing in the automotive industry. Proc. SPIE 5535/1, 2003. pp. 464-472. doi:10.1117/12.555578.

[4] Franz, M., Funk, Ch., Hiller, J., Kasperl, S., Krumm, M., Schröpfer, S., Ezrt, F. Reliability of Dimensional Measurements by Computed Tomography for Industrial Application. Berlin, Germany : 4th European-American Workshop on Reliability of NDE, 2009.

[5] Reinhart, C. Industrial computer tomorgraphy – a universal inspection tool. Shanghai, China : 17th World Conference on Nondestructive Testing, 2008.

[6] Müller, P. Coordinate Metrology by Traceable Computed Tomography. DTU, 2012. P.hD. thesis.

[7] Hirakimoto, A. Microfocus X-ray Computed Tomography and Its Industrial Applications. Kyoto, Japan : Analytical Science 17, 2001. pp. 123-125.

[8] Pfeiffer, F., Kastner, J., Freytag, R. Method for three-dimensional evaluation and visualization of the distribution of fibres in glass-fibre reinforced injection molded parts by micro-X-ray computed tomography. Shanghai, China. : 17th World Conference on Nondestructive Testing, 2008.

[9] Luebbehuesen, J. Advanced Non-Destructive Testing by High Resolution Computed Tomography for 3D analysis of Automotive Components. GE S&IT phoenix|x-ray – Advanced NDT with high-res CT. pp. 1-15.

[10] Hofmann, J., Flisch, A., Obrist, A. Adaptive CT scanning - mesh based optimisation methods for industrial X-ray computed tomography applications. NDT&E International 37, 2004. pp. 271–278.

[11] Zebicon. http://www.zebicon.com/topstykke.html. (Online accessed 21-10-2013).

[12] Brunke, O., Hansen, F., Stuke, I., Butz, F. F. A new Concept for High-Speed atline and inlineCT for up to 100% Mass Production Process Control. Durban, South Africa : 18th World Conference on Nondestructive Testing, 2012.

[13] Godske, B. Slagterirobot skal skære lige til benet. Ingeniøren no. 23, Produktion, Automation, 6th June 2008. pp. 8-9.

[14] Vester-Christensen, M., Erbou, S. G. H., Hansen, M. F., Olsen, E.V., Christensen, L.B., Hviid, M., Ersbøll, B. K., Larsen, R. Virtual dissection of pig carcasses. Meat Science, Vol. 81, No. 4, 2009. pp. 699-704.

[15] Vester-Christensen, M. Image Registration and Optimization in the Virtual Slaughterhouse. DTU Informatics, Technical University of Denmark, Lyngby, Denmark, 2009. Ph.D. thesis.

[16] Christensen, L. B., Erbou, S. G. H., Vester-Christensen, M., Hansen, M. F., Darré, M., Hviid, M., Olsen, E. V. Optimized workflow and validation of carcass CT-scanning. Korea : 56th ICoMST, 2010.

[17] VDI/VDE-2617-13. Accuracy of coordinate measuring machines - Characteristics and their testing - Guideline for the application of DIN EN ISO 10360 for coordinate measuring machines with CT-sensors, VDI/VDE 2630-1.3. Duesseldorf, 2011.

[18] ISO/TS-15530-3. Geometrical Product Specifications (GPS), Coordinate measuring machines (CMM): Technique for determining the uncertainty of measurement, Part 3: Use of calibrated workpieces or standards. 2011.

[19] VDI/VDE-2630-1.2. Computed tomography in dimensional measurement – Influencing variables on measurement results and recommendations for computed tomography dimensional measurements. Duesseldorf : VDI/VDE Society for Metrology and Automation Engineering (GMA), 2010.

[20] ISO/IEC-Guide-98-3. Uncertainty of measurement - Part 3: Guide to the expression of uncertainty in measurement (GUM:1995). 2008.

[21] ISO-14253-2. Geometrical product specifications (GPS) - Inspection by measurement of workpieces and measuring equipment - Part 2: Guidance for the estimation of uncertainty in GPS measurement, in calibration of measuring equipment and in product verification. 2011.

[22] ISO-14253-1. Geometrical product specifications (GPS) -- Inspection by measurement of workpieces and measuring equipment -- Part 1: Decision rules for proving conformity or nonconformity with specifications. 2013.

[23] Krumm, M., Kasperl, S., Franz, M. Reducing non-linear artifacts of multi-material objects in industrial 3D computed tomography. NDT&E International 41, 2008. pp. 242-251.

[24] Blessing, N., Effenberger, I. 3D computed tomography – technology, applications and process intergration. 2004.

[25] Welkenhuyzen, F., Kiekens, K., Pierlet, M., Dewulf, W., Bleys, P., Kruth, J. P., Voet, A. Industrial Computer Tomography for Dimensional Metrology: Overview of Influence Factors and Improvement Strategies. OPTIMESS, 2009.

[26] Kiekens, K., Welkenhuyzen, F., Tan, Y., Bleys, P., Voet, A., Kruth, J. P., Dewulf, W. A test object with parallel grooves for calibration and accuracy assessment of industrial computed tomography (CT) metrology. Meas. Sci. Technol. 22, 115502, 2011. pp. 7.

[27] ISO-10360-2. Geometrical product specifications (GPS) -- Acceptance and reverification tests for coordinate measuring machines (CMM) -- Part 2: CMMs used for measuring linear dimensions. 2009.

[28] Tan, Y., Kiekens, K., Welkenhuyzen, F., Angel, J., De Chiffre, L., Kruth, J. P., Dewulf, W. Simulation-aided investigation of beam hardening induced errors in CT dimensional metrology. Aachen, Germany : The 11th International Symposium of Measurement Technology and Intelligent Instruments, 2013. pp. 1-7.

[29] Simon, M., Tiseanu, I., Sauerwein, C., Yoo, S. M., Cho, I. S. Development of multi sensor and multi source computed tomography systems. Lyon, France : International Symposium on Digital industrial Radiology and Computed Tomography, 2007.

[30] Carmignato, S. Traceability of dimensional measurements in computed tomography. Proceedings of 8th A.I.Te.M. Conference, 2007.

[31] Kasperl, S., Hiller, J., Krumm, M. Computed Tomography Metrology in Industrial Research & Development. Fürth, Germany : International Symposium on NDT in Aerospace, 2008. pp. 8.

[32] Schörner, K. Development of Methods for Scatter Artifact Correction in Industrial X-ray Cone-beam Computed Tomography. Physik Department, Technische Universität München, 2012.

[33] Baer, M., Hammer, M., Knaup, M., Schmidt, I., Christoph, R., Kachelrieß, M. Scatter Correction Methods in Dimensional CT. NDT, 2012. pp. 271-278.

[34] De Chiffre, L., Carmignato, A., Cantatore, A., Jensen, J. D. Replica calibration artefacts for optical 3D scanning of micro parts. San Sebastian : Proceedings of the Euspen International Conference, 2009. pp. 352-355.

[35] Cantatore, A., De Chiffre, L., Carmignato, S. Investigation on a replica step gauge for optical 3D scanning of micro parts. Delft : Proceedings of the Euspen International Conference, 2010. pp. 200-203.

[36] Cantatore, A., Andreasen, J. L., Carmignato, S., Müller, P., De Chiffre, L. Verification of a CT scanner using a miniature step gauge. Como Lake : Proceedings of the Euspen International Conference, 2011. pp. 46-49.

[37] ISO/IEC-Guide-99. International vocabulary of metrology -- Basic and general concepts and associated terms (VIM). 2007.

[38] Cantatore, A., Angel, J., De Chiffre, L. Material investigation for manufacturing of reference step gauges for CT scanning verification. Stockholm : Proceedings of the Euspen International Conference, 2012. pp. 129-132.

[39] Jensen, B., Johansen, J., Karbæk, K., Kjærsgård, P., Rasmussen, A. B., Rasmussen, T. B. Plast Teknologi. Erhvervsskolernes Forlag, 2005. ISBN: 87-7881-550-9.

[40] UL-IDES-Materials-Database. http://www.ides.com. (Online accessed 21-10-2013).

[41] CALCE-Center-for-Advanced-Life-Cycle-Engineering. http://www.calce.umd.edu/TSFA/Hardness_ad_.htm. (Online accessed 21-10-2013).

[42] ISO-4287. Geometrical Product Specifications (GPS) -- Surface texture: Profile method -- Terms, definitions and surface texture parameters. 1997.

[43] Davim, J. P., Silva, L. R., Festas, A., Abrão, A.M. Machinability study on precision turning of PA66 polyamide with and without glass fiber reinforcing. Materials & Design, Volume 30, Issue 2, 2009. pp. 228-234.

[44] Tosello, G., Hansen, H.N., Gasparin, S. Applications of dimensional micro metrology to the product and process quality control in manufacturing of precision polymer micro components. CIRP Annals - Manufacturing Technology, Volume 58, Issue 1, 2009. pp. 467-472.

[45] Michaeli, W., Heßner, S., Klaiber, F., Forster, J. Geometrical Accuracy and Optical Performance of Injection Moulded and Injection-compression Moulded Plastic Parts. CIRP Annals - Manufacturing Technology, Volume 56, Issue 1, 2007. pp. 545-548.

[46] ISO/IEC-17043. Conformity assessment, General requirements for proficiency testing. 2010.

[47] Angel, J., Lauridsen, T.,Feidenhans'l, R., Nielsen, M. S., De Chiffre, L. Using grating based X-ray contrast modalities for metrology. Dubrovnik, Croatia : Proceedings of the Euspen International Conference, 2014.

[48] Bartscher, M., Hilpert, U., Goebbels, J., Weidemann, G. Enhancement and Proof of Accuracy of Industrial Computed Tomography (CT) Measurements. CIRP Annals - Manufacturing Technology, Volume 56, Issue 1, 2007. pp. 495-498.

[49] ISO-286-2. Geometrical product specifications (GPS) - ISO code system for tolerances on linear sizes - Part 2: Tables of standard tolerance classes and limit deviations for holes and shafts. 2010.

[50] Yang, G. M., Coquille, J. C., Fontaine, J. F., Lambertin, M. Influence of roughness on characteristics of tight interference fit of a shaft and a hub. International Journal of Solids and Structures, Volume 38, Issues 42-43, 2001. pp. 7691-7701.

[51] Angel, J., De Chiffre, L., Larsen, E., Rasmussen, J., Sobiecki, R. CIA-CT comparison - Reference Measurements. Department of Mechanical Engineering, Technical University of Denmark, 2013.

[52] Angel, J., De Chiffre, L. CIA-CT comparison, Inter laboratory comparison on Industrial Computed Tomography, Final Report. Department of Mechanical Engineering, Technical University of Denmark, 2013.

[53] Müller, P., Hiller, J., Cantatore, A., Bartscher, M., De Chiffre, L. Investigation on the influence of image quality in X-ray CT metrology. Wels, Austria : Paper presented at Conference on Industrial Computed Tomography, 2012.

[54] Montgomery, D. C. Design and Analysis of Experiments (7th Edition). John Wiley & Sons, 2009.

[55] Carmignato, S. Accuracy of industrial computed tomography measurements: experimental results from an international comparison. Annals of the CIRP, 61/1, 2012. pp. 491-494.

[56] Hansen, H. N., De Chiffre, L. An industrial comparison of coordinate measuring machines in Scandinavia with focus on uncertainty statements. Prec. Eng., 23, 1999. pp. 185-195.

[57] De Chiffre, L., Hansen, H. N., Morace, R. E. CIRP Interlaboratory Comparison of Coordinate Measuring Machines using an Optomechanical Hole Plate. DTU, 2004. Publication no. IPL.141.04 (MM04.40).

[58] Angel, J., Cantatore, A., De Chiffre, L. CIA-CT audit - Inter laboratory comparison of industrial CT scanners, Final Report. Department of Mechanical Engineering, Technical University of Denmark, 2012.

[59] Angel, J., Cantatore, A., De Chiffre, L. Preliminary results of a proficiency testing of industrial CT scanners using small polymer items. Stockholm, Sweden : Proceedings of the Euspen International Conference, 2012. pp. 162-165.

[60] Johnson, R. A. Probability and statistics for engineers. Miller & Freund's, Seventh Edition, 2005. ISBN 0-13-143745-3.

[61] ISO/TS-23165. Geometrical product specifications (GPS) -- Guidelines for the evaluation of coordinate measuring machine (CMM) test uncertainty. 2006.

[62] Pfeiffer, F., Bech, M., Bunk, O., Donath, T., Henrich, B., David, P. K. C. X-ray dark-field and phase-contrast imaging using a grating interferometer. Journal of Applied Physics 105 102006, 2009.

[63] Bech, M., Jensen, T. H., Feidenhans'l, R., Bunk, O., David, C., Pfeiffer, F. Soft-tissue phase-contrast tomography with an X-ray tube source. IOP Publishing Ltd, 2009.

[64] Jensen, T. H., Bech, M., Bunk, O., Donath, T., David, C., Feidenhans'l, R., Pfeiffer, F. Directional X-ray dark-field imaging. IOP Publishing, Phys. Med Biol. 55, 2010. pp. 3317-3323.

[65] Palmgen, G. Nu får vi bedre røntgenbilleder. Illustreret Videnskab no. 13, 2008.

[66] Pfeiffer, F., Weitkamp, T., Bunk, O., David, C. Phase retrieval and differential phase-contrast imaging with low-brilliance X-ray sources. Nat. Phys. 2, 2006. pp. 258–261.

[67] Bech, M. X-ray imaging with a grating interferometer. Ph.D. thesis, NBI, 2009.

[68] Lorefice, S. Traceability and uncertainty analysis in volume measurements. Measurement 42, 2009. pp. 1510-1515.

[69] ISO/IEC-17025. General requirements for the competence of testing and calibration laboratories. 2005.

[70] Czichos, H., Saito, T., Smith, L. Handbook of Materials Measurement Methods. Springer, 2006. pp. 702-704.

[71] Carmignato, S., Savio, E. Traceable volume measurements using coordinate measuring systems. CIRP Annals - Manufacturing Technology 60, 2011. pp. 519-522.

[72] Waring, C. S. R., Bax, J. S., Samarabandu, A., Holdsworth, D. W., Fenster, A., Lacefield, J. C. Traceable micro-CT scaling accuracy phantom for applications requiring exact measurement of distances or volumes. Medical Physics 39, 2012. pp. 6023-6027.

[73] CAPINTEC-INC. http://www.capintec.com/index.php?option=com_virtuemart&view=category&virtuemart_category_id=35. 27-02-2014.

[74] Angel, J., Christensen, L. B., Cantatore, A., De Chiffre, L. Inter laboratory comparison on Computed Tomography for industrial applications in the slaughterhouses: CIA-CT comparison. DTU Mechanical Engineering, 2014. pp. 76.

[75] DIN-EN-725-7-(1996-01). Determination Of The Absolute Density. 1996.

[76] CIA-CT Newsletter no. 2. May 2010.

[77] Erbou, S. G. H. Modeling the Biological Diversity of Pig Carcasses. DTU Informatics, Technical University of Denmark, Lyngby, Denmark, 2009. Ph.D. thesis.

[78] Hansen, M. F. The virtual knife. DTU Informatics, Technical University of Denmark, Lyngby, Denmark, 2009. Ph.D. thesis.

[79] OPUS+on-line-CT. Udvide OPUS+ databasen til udbytte beregninger og validering af modeller. DMRI, Version 3, 2010. Project no.: 1378562.

[80] http://www.danishcrown.dk/B2B/Svinekoed-eksport/Produktkatalog.aspx. Danish Crown product catalogue, 06-02-2014.

[81] Caskey, C. F., Hlawitschka, M., Qin, S., Mahakian, L. M., Cardiff, R. D., Boone, J. M., Ferrara, K. W. An Open Environment CT-US Fusion for Tissue Segmentation during Interventional Guidance. PLoS ONE 6(11): e27372. doi:10.1371/journal.pone.0027372., 2011.

[82] Meyer, J., Nguyen, H. T. Multi-Dimensional Transfer Functions for Tissue Selection in Computed Tomography. ASME Conference Proceedings of BioMed, 3rd Frontiers in Biomedical Devices Conference, June 18-20, 2008.

[83] Jarvis, H. F. T. The thermal variation of the density of beef and the determination of its coefficient of cubical expansion. Journal of Food Technology, Volume 6, 1971. pp. 383-391.

[84] Coupland, J. N., McClements, D. J. Physical properties of liquid edible oils. Journal of the American Oil Chemists' Society, Volume 74, Issue 12, 1997. pp. 1559-1564.

[85] Lang, S. B. Thermal Expansion Coefficients and the Primary and Secondary Pyroelectric Coefficients of Animal Bone. Nature, Volume 224, Issue 5221, 1969. s. 798-799.

Own references

[1] **Islam, A., Hansen, H. N., Marhöfer, D. M., Angel, J., Dormann, B., Bondo, M.** (2012). *Two-component micro injection moulding for hearing aid applications*. International Journal of Advanced Manufacturing Technology, Vol. 62, No. 5-8, 2012, pp. 605-615.

[2] **Angel, J., Cantatore, A., De Chiffre, L.** (2012). *Preliminary results of a proficiency testing of industrial CT scanners using small polymer items*. Proceedings of the Euspen International Conference. 2012. Stockholm, Sweden, pp. 162-165.

[3] **Angel, J., Cantatore, A., De Chiffre, L.** (2012) *CIA-CT audit - Inter laboratory comparison of industrial CT scanners, Final Report*. DTU Mechanical Engineering, 2012. 52 pp. Report.

[4] **Cantatore, A., Angel, J., De Chiffre, L.** (2012). *Material investigation for manufacturing of reference step gauges for CT scanning verification*. Proceedings of the Euspen International Conference. 2012. Stockholm, Sweden, pp. 129-132.

[5] **Christensen, L. B., Angel, J.** (2013). *Inter-laboratory comparison of medical computed tomography (CT) scanners for industrial applications in the slaughterhouses*. Farm Animal IMaging FAIM II. 2013. Kaposvár, Hungary, pp. 27-32. ISBN 978-0-9570709-9-8.

[6] **Angel, J., De Chiffre, L., Larsen, E., Rasmussen, J., Sobiecki, R.** (2013). *Inter laboratory comparison on Industrial Computed Tomography : CIA-CT comparison. Reference Measurements*. DTU Mechanical Engineering, 2013. 86 pp. (CIA-CT Reference Measurements; No. 01). Report.

[7] **Angel, J., De Chiffre, L.** (2013). *Inter laboratory comparison on Industrial Computed Tomography : CIA-CT comparison. Final Report*. DTU Mechanical Engineering, 2013. 75 pp. (CIA-CT Final Report; No. 01). Report.

[8] **Angel, J., De Chiffre, L., Larsen, E., Rasmussen, J.** (2013). *Inter laboratory comparison on Industrial Computed Tomography : CIA-CT comparison. Technical Protocol*. DTU Mechanical Engineering, 2013. 12 pp. (CIA-CT Technical Protocol; No. 01). Report.

[9] **Tan, Y., Kiekens, K., Welkenhuyzen, F., Angel, J., De Chiffre, L., Kruth, J. P., Dewulf, W.** (2013). *Simulation-aided investigation of beam hardening induced errors in CT dimensional metrology*. The International Symposium of Measurement Technology and Intelligent Instruments. 2013. Aachen, Germany, pp. 1-7.

[10] **Tan, Y., Kiekens, K., Welkenhuyzen, F., Angel, J., De Chiffre, L., Kruth, J. P., Dewulf, W.** (2014). *Simulation-aided investigation of beam hardening induced errors in CT dimensional metrology*. Measurement Science and Technology 25, 2014, 10 pp.

[11] **Angel, J., Lauridsen, T., Feidenhans'l, R., Nielsen, M. S., De Chiffre, L.** (2014). *Using grating based X-ray contrast modalities for metrology*. Proceedings of the Euspen International Conference. 2014. Dubrovnik, Croatia, pp. 157-160.

[12] **Angel, J., Christensen, L. B., Cantatore, A., De Chiffre, L.** (2014). *Inter laboratory comparison on Computed Tomography for industrial applications in the slaughterhouses: CIA-CT comparison.* DTU Mechanical Engineering, 2014. 76 pp. Report.

[13] **Angel, J., De Chiffre, L.** (2014). *Comparison on Computed Tomography using industrial items.* Annals of the CIRP 63. 2014. pp. 473-476.

Appendix

This appendix contains a test report of the step gauges.

TEST REPORT

Calibrated object	Step gauge
Manufacturer	DTU Mekanik
Calibration period	November 2011 – October 2012
Operator	Jakob Rasmussen
Instrument	Coordinate measuring machine (CMM) Zeiss OMC 850, $MPE_{U3} = (3+L/250)$ µm (L in mm), Brock & Mikkelsen Certificate S012371, calibrated on 26.07.2007
Probe configuration	Diameter 0.8 mm and 20 mm long stylus
Length standard	Grade I steel blocks were used as length references to generate traceability, DTI Certificate 128.3852, calibrated on 24.07.1995
Environmental temperature	20.0±1.0°C

1. Calibrated object

The calibrated object features bidirectional and unidirectional lengths, see Figure 1. Five polyetheretherketone PEEK step gauges (PEEK SG: #1 to #5), five phenylenesulphide PPS step gauges (PPS SG: #6 to #10), two aluminium step gauges (Aluminium SG: #1, #2) and two steel step gauges (Steel SG: #1, #2) were manufactured using milling. Roughness measurements on the vertical planes on the grooves were carried out and the roughness lie in the range Ra = 0.2-1.0 µm for all four material types. Material characteristics are summarized in in Table 1.

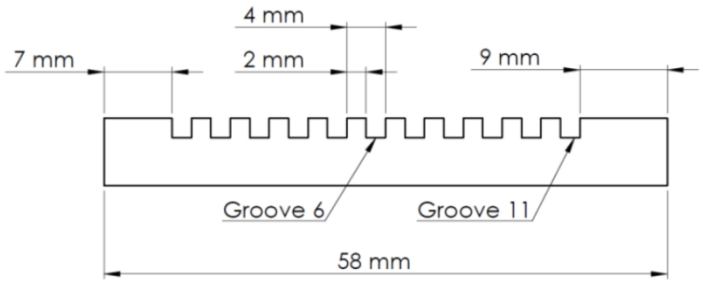

Figure 1. Step gauge with nominal dimensions.

Table 1. Material characteristics of the step gauges.

Material	Supplier	Grade	Density [g/cm³]	Thermal expansion coefficient [10^{-6} K^{-1}]
PEEK	Nordisk Plast A/S	PEEK Natur	1.310	50.0
PPS	Röchling High Performance Plastics	PPS GF 40	1.650	30.0
Aluminium	Alumeco A/S	AW 2011	2.830	22.9
Steel	Uddeholm A/S	UHB 11	7.800	11.0

2. Calibration procedure, coordinate system and alignment

The definition of the coordinate system for the step gauge is performed using a "3-2-1 alignment". Plane Z is created through least square fitting of four teeth areas positioned on the top of the step gauge teeth between groove 4 and 8. Line X (plane Y) is defined as a symmetry line by using least square fitting of the two most extreme areas along the step gauge longitudinal length. These lines are created by the best fitting approach. Plane X is on the left side of the sixth groove and is created through a least square fitting. The reference axis is defined as follows (see Figure 2). The measurement strategy of incremental lengths are computed indirectly as the distance between the center points of the corresponding groove planes obtained through a least square fitting of 8 points acquired on each groove side, as shown in Figure 2. All distances are defined as the distance from a random side to the left side of groove 6 resulting in a total of ten unidirectional (ranging from 2 to 20 mm with 4 mm intervals) and ten bidirectional incremental distances (ranging from 4 to 22 mm with 4 mm intervals). Some of the distances have identical lengths. Figure 3 can be used for identification of the unidirectional (U1 to U10) and bidirectional (B1 to B10) distances.

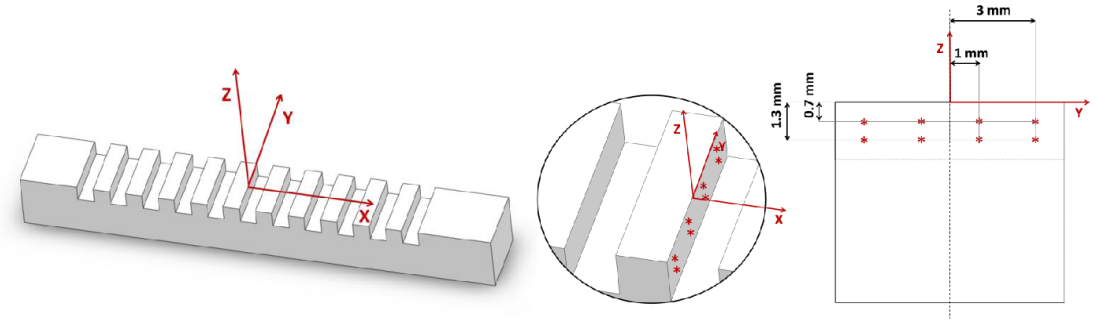

Figure 2. Left: definition of the reference system. Right: Measurement points example on the left side of groove 6.

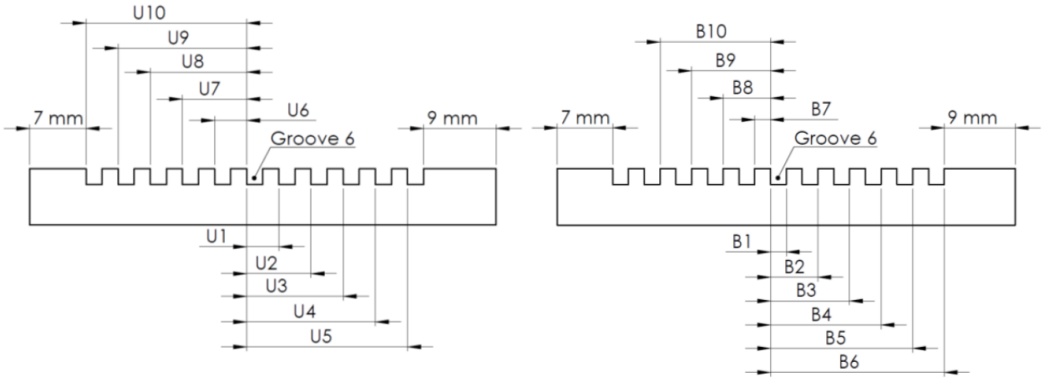

Figure 3. Identification of the unidirectional (left) and bidirectional (right) distances.

3. Calibration uncertainty

Calibration uncertainty resulted from five main contributors: 1) reference artefact u_r, 2) MPE u_m, 3) workpiece form error u_w, 4) temperature effects u_e, and 5) reproducibility u_p where the parts were repositioned and measured again five times. The temperature contribution was divided into three sub categories: 4.1) temperature difference for instrument $u_{e(1)}$, 4.2) temperature difference for artefact $u_{e(2)}$, and 4.3) deviation from the standard reference temperature $u_{e(3)}$. The model in

equation (1) is used for uncertainty estimation. Calibration uncertainties were assessed at a confidence level of 95%, corresponding to k=2.

$$U = k \cdot \sqrt{u_r^{\,2} + u_m^{\,2} + u_w^{\,2} + u_{e(1)}^{\,2} + u_{e(2)}^{\,2} + u_{e(3)}^{\,2} + u_p^{\,2}} \quad (1)$$

Table 2. Measurement results for PEEK step gauges. Values are in mm.

ID	#1		#2		#3		#4		#5	
	Y	U	Y	U	Y	U	Y	U	Y	U
U1	3.9970	0.0044	3.9955	0.0044	4.0003	0.0046	3.9952	0.0046	3.9966	0.0051
U2	7.9940	0.0045	7.9915	0.0047	7.9965	0.0047	7.9927	0.0036	7.9937	0.0046
U3	11.9916	0.0052	11.9870	0.0045	11.9922	0.0040	11.9886	0.0044	11.9900	0.0052
U4	15.9892	0.0038	15.9854	0.0056	15.9894	0.0048	15.9832	0.0053	15.9882	0.0047
U5	19.9838	0.0039	19.9801	0.0058	19.9853	0.0049	19.9820	0.0054	19.9826	0.0047
U6	3.9962	0.0045	3.9976	0.0050	3.9947	0.0048	3.9983	0.0046	3.9963	0.0053
U7	7.9948	0.0076	7.9966	0.0065	7.9916	0.0044	7.9943	0.0048	7.9930	0.0062
U8	11.9910	0.0039	11.9924	0.0050	11.9894	0.0043	11.9924	0.0037	11.9908	0.0063
U9	15.9875	0.0033	15.9905	0.0047	15.9856	0.0041	15.9888	0.0040	15.9879	0.0046
U10	19.9879	0.0049	19.9889	0.0053	19.9845	0.0047	19.9867	0.0035	19.9866	0.0046
B1	1.9966	0.0034	1.9935	0.0038	1.9988	0.0040	1.9959	0.0050	1.9968	0.0047
B2	5.9945	0.0035	5.9908	0.0036	5.9962	0.0037	5.9934	0.0041	5.9948	0.0040
B3	9.9921	0.0036	9.9880	0.0036	9.9937	0.0050	9.9893	0.0033	9.9925	0.0039
B4	13.9885	0.0040	13.9854	0.0043	13.9894	0.0039	13.9859	0.0034	13.9891	0.0045
B5	17.9853	0.0048	17.9823	0.0041	17.9874	0.0038	17.9818	0.0043	17.9860	0.0048
B6	21.9844	0.0052	21.9804	0.0039	21.9838	0.0044	21.9804	0.0038	21.9851	0.0046
B7	1.9988	0.0043	2.0005	0.0040	1.9970	0.0037	1.9998	0.0034	1.9978	0.0046
B8	5.9966	0.0039	5.9961	0.0037	5.9934	0.0042	5.9956	0.0040	5.9950	0.0044
B9	9.9924	0.0043	9.9926	0.0037	9.9905	0.0039	9.9926	0.0036	9.9918	0.0041
B10	13.9898	0.0047	13.9895	0.0047	13.9873	0.0042	13.9889	0.0040	13.9888	0.0041

Table 3. Measurement results for PPS step gauges. Values are in mm.

ID	#6		#7		#8		#9		#10	
	Y	U	Y	U	Y	U	Y	U	Y	U
U1	3.9997	0.0024	3.9967	0.0030	3.9997	0.0027	3.9965	0.0023	3.9910	0.0028
U2	7.9992	0.0024	7.9934	0.0028	7.9975	0.0027	7.9916	0.0029	7.9829	0.0028
U3	11.9987	0.0025	11.9909	0.0031	11.9971	0.0030	11.9877	0.0025	11.9743	0.0027
U4	16.0006	0.0033	15.9868	0.0032	15.9959	0.0029	15.9839	0.0028	15.9665	0.0031
U5	20.0003	0.0034	19.9842	0.0030	19.9951	0.0029	19.9805	0.0029	19.9616	0.0032
U6	3.9995	0.0027	3.9983	0.0030	3.9989	0.0029	3.9961	0.0024	3.9923	0.0030
U7	8.0011	0.0026	7.9965	0.0028	7.9975	0.0026	7.9911	0.0025	7.9840	0.0028
U8	12.0000	0.0028	11.9952	0.0029	11.9974	0.0030	11.9880	0.0025	11.9760	0.0029
U9	15.9992	0.0026	15.9944	0.0029	15.9962	0.0029	15.9845	0.0027	15.9701	0.0034
U10	20.0007	0.0027	19.9928	0.0029	19.9957	0.0028	19.9803	0.0027	19.9615	0.0029
B1	2.0007	0.0034	1.9984	0.0030	2.0016	0.0030	1.9981	0.0031	1.9941	0.0032
B2	6.0016	0.0026	5.9964	0.0027	6.0008	0.0028	5.9959	0.0027	5.9861	0.0029
B3	10.0024	0.0030	9.9930	0.0029	9.9996	0.0031	9.9917	0.0030	9.9785	0.0034
B4	14.0020	0.0031	13.9900	0.0029	13.9989	0.0038	13.9881	0.0029	13.9724	0.0028
B5	18.0042	0.0032	17.9875	0.0030	17.9989	0.0030	17.9861	0.0031	17.9660	0.0030
B6	22.0048	0.0035	21.9853	0.0033	21.9980	0.0030	21.9835	0.0034	21.9632	0.0032
B7	1.9959	0.0033	1.9979	0.0033	1.9963	0.0028	1.9946	0.0031	1.9954	0.0031
B8	5.9970	0.0036	5.9942	0.0031	5.9950	0.0031	5.9904	0.0032	5.9871	0.0033
B9	9.9967	0.0035	9.9924	0.0033	9.9941	0.0030	9.9863	0.0032	9.9769	0.0034
B10	13.9953	0.0036	13.9906	0.0034	13.9927	0.0034	13.9809	0.0033	13.9693	0.0031

Table 4. Measurement results for aluminium step gauges. Values are in mm.

ID	#1		#2	
	Y	U	Y	U
U1	4.0010	0.0022	4.0007	0.0023
U2	8.0021	0.0023	8.0024	0.0027
U3	12.0037	0.0022	12.0038	0.0026
U4	16.0056	0.0023	16.0047	0.0027
U5	20.0081	0.0024	20.0064	0.0028
U6	4.0022	0.0024	4.0023	0.0029
U7	8.0033	0.0023	8.0030	0.0032
U8	12.0043	0.0023	12.0040	0.0028
U9	16.0051	0.0022	16.0052	0.0029
U10	20.0066	0.0027	20.0061	0.0027
B1	2.0008	0.0022	2.0008	0.0026
B2	6.0030	0.0021	6.0028	0.0026
B3	10.0044	0.0021	10.0047	0.0024
B4	14.0064	0.0022	14.0064	0.0028
B5	18.0086	0.0023	18.0074	0.0026
B6	22.0108	0.0022	22.0085	0.0027
B7	1.9992	0.0022	1.9989	0.0026
B8	5.9995	0.0024	5.9996	0.0025
B9	10.0009	0.0021	10.0009	0.0026
B10	14.0015	0.0022	14.0018	0.0028

Table 5. Measurement results for steel step gauges. Values are in mm.

ID	#1		#2	
	Y	U	Y	U
U1	4.0000	0.0021	3.9999	0.0022
U2	8.0005	0.0027	8.0002	0.0028
U3	12.0013	0.0021	12.0012	0.0024
U4	16.0025	0.0043	16.0019	0.0027
U5	20.0021	0.0038	20.0032	0.0027
U6	4.0000	0.0022	4.0004	0.0023
U7	8.0000	0.0023	8.0006	0.0025
U8	12.0004	0.0022	12.0012	0.0024
U9	15.9998	0.0022	16.0010	0.0028
U10	19.9998	0.0024	20.0007	0.0025
B1	2.0019	0.0025	1.9981	0.0041
B2	6.0025	0.0034	5.9988	0.0039
B3	10.0019	0.0024	10.0000	0.0038
B4	14.0025	0.0022	14.0012	0.0040
B5	18.0034	0.0025	18.0027	0.0039
B6	22.0039	0.0026	22.0034	0.0041
B7	1.9979	0.0028	2.0012	0.0039
B8	5.9978	0.0036	6.0014	0.0041
B9	9.9985	0.0027	10.0013	0.0038
B10	13.9984	0.0030	14.0018	0.0038